UCLA
UCLA Electronic Theses and Dissertations

Title

Development of a Novel Animal Model and Small Molecule Therapeutics for Metastatic Kidney Cancer

Permalink

https://escholarship.org/uc/item/0pr4j29j

Author

Ishihara, Moe

Publication Date

2023

Peer reviewed|Thesis/dissertation

eScholarship.org Powered by the California Digital Library
University of California

UNIVERSITY OF CALIFORNIA

Los Angeles

Development of a Novel Animal Model and Small Molecule Therapeutics for Metastatic Kidney Cancer

A dissertation submitted in partial satisfaction of the

requirements for the degree Doctor of Philosophy

in Molecular and Medical Pharmacology

by

Moe Ishihara

2023

© Copyright by

Moe Ishihara

2023

ABSTRACT OF THE DISSERTATION

Development of a Novel Animal Model and

Small Molecule Therapeutics for Metastatic Kidney Cancer

by

Moe Ishihara

Doctor of Philosophy in Molecular and Medical Pharmacology

University of California, Los Angeles, 2023

Professor Lily Wu, Chair

Metastasis occurs in one-third of clear cell renal cell carcinoma (ccRCC) patients and accounts for the majority of ccRCC-related deaths. Unfortunately, no therapy is available for this lethal disease because the molecular mechanism of metastasis is not fully understood. Although it has been known for 25 years that the loss of function of the VHL tumor suppressor gene is pathognomonic of RCC, its involvement in malignant progression remains elusive. Using a CRISPR/ Cas9 gene editing system and a mouse orthotopic implantation model, we previously found that the intratumoral heterogeneity of VHL expression is essential in ccRCC metastasis. Specifically, the VHL(-) cell population serves as the metastatic driver. Therefore, in this study, we sought to develop 1) a novel animal model of cooperative ccRCC metastasis and 2) small molecules with selective toxicity against the VHL(-) cells. For the first aim, we have utilized the chicken chorioallantoic membrane (CAM) model to establish a novel, cost- and labor-efficient animal model of cooperative metastasis, which almost perfectly recapitulated the characteristic phenomena observed in the

mouse orthotopic implantation model. Using this model, we have also further explored exosome's involvement in cooperative metastasis.

For the second part of the project, we hypothesize that targeting the metastatic driver population, VHL(-), will effectively inhibit metastases. We have utilized high-throughput screening (HTS) for this purpose. A ratiometric black-box approach was employed to identify selective modulators of cell growth and survival of murine VHL(-) ccRCC cell lines with little to no effect on VHL(+) cells. Statins, the commonly used cholesterol-lowering drugs, showed up as hits. Dosage curves confirmed this result, and animal studies suggest its efficacy against ccRCC metastasis. The mechanism of action (MOA) is currently under investigation, but data implies that it may be distinct from statin's primary role as cholesterol-lowering. Strikingly, other metastatic cancer subtypes, such as triple-negative breast cancer (TNBC) and neuroendocrine prostate cancer (NEPC), were found to be more sensitive to statin treatment compared to their less aggressive counterparts. By investigating this further, we can potentially develop a pan-cancer small-molecule inhibitor of metastasis based on the FDA-approved, cheap, and widely available statins.

The dissertation of Moe Ishihara is approved.

Stuart Conway

Robert D. Damoiseaux

Orian Shirihai

Brian M. Shuch

Ting-Ting Wu

Lily Wu, Committee Chair

University of California, Los Angeles

2023

Dedicated to my family.

TABLE OF CONTENTS

Abstract of Dissertation……. ii

Committee Page……. iv

Dedication Page……. v

Acronyms and Abbreviations…… viii

List of Figures…… ix

List of Supplementary Figures and Tables…… x

Acknowledgments……. xi

Vita…… xiv

Chapter 1. Introduction…… 1

1.1. ccRCC Statistics, Biology, And Clinical Obstacles…… 1

1.2. Dissertation Overview…… 3

1.3. References…….. 6

Chapter 2. Mouse- and Patient-Derived Chorioallantoic Membrane (CAM) Xenografts for Studying Metastatic Renal Cell Carcinoma…… 8

2.1. Introduction…… 8

2.2. Cooperative Metastatic Model in Murine RCC……. 11

2.3. CAM Metastatic Model……. 12

2.4. Tumor Passaging from CAM to Mouse……. 15

2.5. CAM PDX……. 15

2.6. Cooperative Metastatic Model in Human RCC…… 16

2.7. Discussion……. 18

2.8. References……. 27

Chapter 3. Broader Applications of the CAM Model…….. 33

3.1. Introduction…… 33

3.2. Non-RCC Urological Cancers …….. 35

3.3. Exosome Studies…… 35

3.4. Discussion……. 37

3.5. References…….. 43

Chapter 4. Small Molecule Approach to Find Novel Therapeutics against Metastatic RCC…… 45

4.1. Introduction…… 45

4.2. Materials and Methods…….. 46

4.3. Results…… 48

4.4. Discussion…….. 55

4.5. Supporting Materials…….. 70

4.6. References…….. 84

Chapter 5. Conclusion and Future Prospects……... 88

ACRONYMS AND ABBREVIATIONS

RCC	Renal cell carcinoma
ccRCC	Clear cell RCC
SEER	National Cancer Institute's Surveillance, Epidemiology, and End Results Program
VHL	von Hippel-Lindau (gene)
pVHL	VHL protein
HIF	Hypoxia-inducible factor
EMT	Epithelia-to-mesenchymal transition
CRISPR	Clustered regularly interspaced short palindromic repeats
GFP	Green fluorescent protein
RFP	Red fluorescent protein
CAM	Chorioallantoic membrane
PDX	Patient-derived xenograft
BLI	Bioluminescence imaging
HTS	High-throughput screening
CDD	Collaborative Drug Discovery
FDA	US Food and Drug Administration
HMG-CoA	3-hydroxyl-3-methylglutaryl-CoA
HMGCR	HMG-CoA reductase
TNBC	Triple-negative breast cancer
NEPC	Neuroendocrine prostate caner
CRPC	Castration-resistant prostate cancer
SAR	Structure-activity relationship

LIST OF FIGURES

Fig. 1	ccRCC cooperative metastasis model mediated by VHL heterogeneity…….	4
Fig. 2.1	CRISPR-mediated knockout of VHL induces HIF pathways and EMT phenotype in RENCA cells……...	19
Fig. 2.2	VHL-loss-mediated metastatic RCC model in the mouse kidney……	20
Fig. 2.3	CAM metastatic model for murine RCC……..	21
Fig. 2.4	Tumor passaging from CAM to mouse……	22
Fig. 2.5	The CAM model successfully grafted patients' tumors without altering morphology or heterogeneity……	23
Fig. 2.6	Cooperative metastatic model and VHL heterogeneity in human RCC……	24
Fig. 2.7	Preliminary data for more CAM PDX applications…….	25
Fig. 3.1	Representative tumor development from prostate cancer cell lines…….	39
Fig. 3.2	Representative tumor development from bladder cancer…….	40
Fig. 3.3	VHL(-) exosomes are internalized into VHL(+) cells…….	41
Fig. 3.4	VHL(+)-exo induces distant metastases of VHL(+) tumors in an animal model……	42
Fig. 4.1	HTS setup and results……..	59
Fig. 4.2	MOA of Statins Cytotoxicity……...	61
Fig. 4.3	HIF, EMT, and statin sensitivity in pan-tissue metastatic cancer……	63
Fig. 4.4	Bioinformatical analyses to find common genes in statin-sensitive lines……...	65
Fig. 4.5	SAR-based analyses of statins' cytotoxicity……	66
Fig. 4.6	Therapeutic studies in two animal models……..	68
Fig. 4.7	Schematic of working hypothesis about MOA……	69
Fig. 5	Future directions……..	90

LIST OF SUPPLEMENTARY FIGURES AND TABLES

Suppl. Fig. S1	Detailed cell line information……	70
Suppl. Fig. S2	HTS optimization……..	72
Suppl. Fig. S3	Detailed HTS analysis……...	74
Suppl. Fig. S4	Optimization and validation of MOA of statins' cytotoxicity……	77
Suppl. Fig. S5	Additional TNBC/NEPC data and preliminary results on the relationship between HMGCR and hypoxia…….	78
Suppl. Fig. S6	GSEA analyses with Reactome gene sets…….	79
Suppl. Fig. S7	Additional cytotoxicity data of fluvastatin derivatives and enantiomers……..	80
Suppl. Table	The HTS had dozens of compounds targeting the mevalonate pathway……	81

ACKNOWLEDGEMENTS

First and foremost, I sincerely thank my mentor, Dr. Lily Wu, for providing an incredibly supportive environment to grow as a scientist and person. In her lab, I was free to explore the scientific questions that attracted me the most and conduct independent research on exciting and impactful topics. At the same time, Lily has been always available when needed and provided thoughtful and practical advice. In addition to deep insights into biology, Lily has amazing optimism, enthusiasm, and leadership skills, and I always look up to her for that from the day I first met her at my interview to the Pharmacology program in 2017. These traits of her shines both in and out of the lab, from the weekly lab meetings to numerous house parties at Lily's place with various delicious foods, and the six years of my graduate training spent in her lab were benefitted tremendously by all these interactions.

I would also like to extend my gratitude to current and previous Wu Lab members: Dr. Junhui Hu, Dr. Allison Sharrow, Dr. Shu Lian, Dr. Ping Tan, Rongwei Zhao, Xiaoyu Zhang, YongHyeon Choi, Dr. Zhenhua Liu, Dr. Zhicheng Zhang, Kailey Flora, Shannon Shams, and Dr. Qingming Kong for all the insightful discussions, precious advice, and unwavering help that have enriched my research significantly. I want to thank Celine Cano-Ruiz, Maia Jackson, Aimee Wu, Elizabeth Bowen, Kriti Shukla, Elise Tahti, Raven Blakemore, Tala Ayoub, Kaveeya Reghu, Julian Huang, Anthony Wang, and Aakriti Dura for their technical assistance that produced this work. Working with all of you talented and hardworking undergraduate students was such a pleasure and made me a better mentor. Margarita Calderon, our lab manager, was my mother away from home. I don't know anyone who is nicer, sweeter, and stronger than her. Thank you so much for always being sunshine of the lab. Your smile has made so many bad days tolerable. Also thank you, Graham, Lily's dog buddy and our lab mascot, for providing me with a free pet therapy every day. Your presence was a big part of my motivation to come to the lab.

This dissertation could not have been completed without many collaborators: Min Sub Lee (Steve Bensinger Lab) for cholesterol measurements; Dr. Fuyuhiko Tamanoi for CAM setup; Ewa Koziolek

(Claudio Scafoglio Lab) for CAM imaging; Dr. Glen Brodie (Stuart Conway Lab) for fluvastatin derivatives; Dr. Michelle Luo (Dennis Slamon Lab) for breast cancer cell lines; and Dr. Shiqin Liu, Dr. Alifiani Hartono, and Chung Lee (Tanya Stoyanova Lab) for prostate cancer cell lines and breast cancer subcutaneous implantation models. So as the core facilities, with special thanks to: Dr. Shili Xu & Mikayla Tamboline (Molecular Imaging Technology Center); Iris Williams & Min Zhou (Flow Cytometry Core); Ko Kiehle (Translational Pathology Core Laboratory - TPCL); Constance Yuen, Brandon Han, Aida Vargas (Molecular Screening Shared Resources – MSSR); and David Tokuda (Division of Laboratory Animal Medicine – DLAM). I would also like to thank my two rotation mentors and their lab members: Drs. Thomas Graeber and Robert Prins. Exposing myself in various disciplines in pharmacology was undoubtedly beneficial in forming this dissertation.

The committee members, Drs. Robert Damoiseaux, Stuart Conway, Brian Shuch, Orian Shirihai, and Ting-Ting Wu, have been exceptional resources to enrich the dissertation. They always asked great questions and suggested the right direction to go. They were also either active collaborators or an integral part of the Pharmacology PhD Program, so I greatly appreciated that. Pharmacology leadership, staff, and admins, especially Dr. Steven Cannon, Emily Fitch, and Bernadette Omote, were amazing. Thank you all for making this dissertation possible. Suzan Farag and Jared Retamoza played essential roles in making smooth execution of the dissertation project by taking care of ordering and budgeting.

All my talented, fun, kind, and hardworking friends. I was so fortunate to befriend with all and make countless unforgettable memories of travels, camping, road trips to national parks, live music, movie nights, restaurant/cafe hunts, ultimate frisbee, snowboarding, bouldering, home parties, and discussions about life. I never expected to be able to make so many friends in LA, needless to say having/enjoying life outside of the lab with them. Some were from the same background and share the culture and language, making me feel like I was back home. Some were pursuing the same goal of obtaining a PhD, making me feel I was not alone in this oftentimes tough journey of being a PhD student. Thank you so much to all of you, and I hope to continue making memories with everyone.

Last but certainly not least, my family in Japan. Financially and emotionally, it must be a tough decision to send off a daughter to a US college. We couldn't spend much time in the past ten years, and our weekly video calls also didn't go well many times due to time difference, my tight schedule or emotional insecurity. I feel sorry for all these, but I'm also so grateful for your unconditional support that make it possible to pursue my childhood dream – to be a researcher, which was inspired by my parents to begin with. Thank you for believing in me and being my allies and friends when needed the most.

Chapter 2 is reprinted (adapted) with permission from Ishihara, M., Hu, J., Wong, A., Cano-Ruiz, C., Wu, L. *Mouse- and Patient-Derived CAM Xenografts for Studying Metastatic Renal Cell Carcinoma.* In ENZ: Chick Chorioallantoic Membrane Model and Precision Cancer Therapy, 2019;46:59-80. PMID: 31727277, copyright (2019) Elsevier Inc. Prof. Lily Wu was the PI. All authors were involved in the data collection, results discussion, and manuscript review.

Chapter 3 is partially reprinted (adapted) with permission from: 1) Sharrow, A.C., Ishihara, M., Hu, J., Kim, I.H., Wu, L. *Using the Chick Chorioallantoic Membrane In Vivo Model to Study Gynecological and Urological Cancers.* Journal of Visualized Experiments, 2020;155:e60651. doi:10.3791/60651, copyright (2020) MyJoVE Corporation.; and 2) Flora, K.*, Ishihara, M.*, Zhang, Z., Bowen, E.S., Wu, A., Ayoub, T., Cano-Ruiz, C., Huang, J.T., Jackson, M., Reghu, K., Ayoub, Y., Zhu, Y., Tseng, H.R., Zhou, Z.H., Hu, J., Wu, L. *Exosomes from Von Hippel-Lindau-Null Cancer Cells Promote Metastasis in Renal Cell Carcinoma.* International Journal of Molecular Sciences, 2023;24:17307 doi:10.3390/ijms242417307, copyright (2023) MDPI. *Equal contribution. Prof. Lily was the PI. All authors were involved in the data collection, results discussion, and manuscript review.

The research presented in this dissertation was supported by 1) Japan Student Services Organization (JASSO)'s Graduate Scholarship; 2) Tobacco-Related Disease Research Program (TRDRP)'s Pre-doctoral Award; 3) UCLA Graduate Division's Dissertation Year Fellowship (DYF) and Dr. Ursula Mandel Fellowship; and 4) UCLA Graduate Programs in Bioscience.

VITA

2017 – 2023	Graduate Student Researcher with Prof. Lily Wu Molecular and Medical Pharmacology, PhD Program University of California, Los Angeles
2022	Teaching Assistant with Prof. Hung D. Pham Life Sciences 107, Fall 2022 University of California, Los Angeles
2013 – 2017	Bachelor of Science in Molecular, Cell and Developmental Biology; Bioinformatics minor *Magna Cum Laude* & Departmental Honors University of California, Los Angeles
2015 – 2017	Undergraduate Student Researcher with Prof. Harley I. Kornblum Molecular and Medical Pharmacology University of California, Los Angeles

Peer-Reviewed Publications

1. Hu J, **Ishihara M**, Chin AI, Wu L. *Establishment of Xenografts of Urological Cancers on Chicken Chorioallantoic Membrane (CAM) to Study Metastasis.* Precision Clinical Medicine, 2019;2(3):140–151. PMCID: PMC6770283.
2. **Ishihara M**, Hu J, Wong A, Cano-Ruiz C, Wu L. *Mouse- and Patient-Derived CAM Xenografts for Studying Metastatic Renal Cell Carcinoma.* In ENZ: Chick Chorioallantoic Membrane Model and Precision Cancer Therapy, 2019;46:59-80. PMID: 31727277.
3. Sharrow AC, **Ishihara M**, Hu J, Kim IH, Wu L. *Using the Chick Chorioallantoic Membrane In Vivo Model to Study Gynecological and Urological Cancers.* Journal of Visualized Experiments, 2020;155:e60651. doi:10.3791/60651.
4. **Ishihara M**, Hu J, Zhang X, [...], Wu L. *Comparing Metastatic Clear Cell Renal Cell Carcinoma Model Established in Mouse Kidney and on Chicken Chorioallantoic Membrane*. Journal of Visualized Experiments, 2020;156:e60314. doi:10.3791/60314.
5. Zhang Z, Hu J, **Ishihara M**, […] Wu L. *The miRNA-21-5p Payload in Exosomes from M2 Macrophages Drives Tumor Cell Aggression via PTEN/Akt Signaling in Renal Cell Carcinoma.* International Journal of Molecular Sciences, 2022;23(6): 3005.
6. Hu J, Tan P, **Ishihara M**, [...], Wu L. *Tumor Heterogeneity in VHL Drives Metastasis in Clear Cell Renal Cell Carcinoma.* Signal Transduction & Targeted Therapy, 2023;8(155).

7. Flora K*, **Ishihara M***, […] Wu L. *Exosomes from VHL-Null Cancer Cells Promote Metastasis in Renal Cell Carcinoma.* International Journal of Molecular Sciences, 2023;24: 17307. *Equal contribution.

Awards and Grants

1. Japan Student Services Organization (JASSO): Graduate Scholarship, 2019/9 – 2022/8
2. Tobacco-Related Disease Research Program (TRDRP): Pre-doctoral Award, 2020/7 –2024/6
3. UCLA Graduate Division Fellowships: Dissertation Year Fellowship (DYF) and Dr. Ursula Mandel Fellowship, 2022/9 – 2023/12
4. UCLA Graduate Programs in Bioscience: Fellowship Intensive Program, 2020/10 – 2022/10
5. UCLA JCCC Annual Retreat: Trainee Poster Award 2nd place, 2023/5
6. UCLA Graduate Programs in Bioscience: Travel Grant, 2023/7

Meeting Proceedings

1. **Ishihara M**, Hu J, Cano-Ruiz C, Wang A and Wu L. *Using the Chicken Chorioallantoic Membrane in vivo Model to Study Metastatic Kidney Cancer: A Novel Drug Screening Approach with More Sustainable PDXs*. AACR Annual Meeting, June 2020, Virtual.
2. **Ishihara M**, Hu J, Cano-Ruiz C, Shukla K, and Wu L. *Statins inhibit the Collaborative Metastasis Mediated by VHL Heterogeneity in Clear Cell Renal Cell Carcinoma*. The Molecular Biology Society of Japan (MBSJ) Annual Meeting, Dec 2021, Virtual.
3. **Ishihara M**, Hu J, Cano-Ruiz C, […], and Wu L. *Statins inhibit the collaborative metastasis mediated by VHL heterogeneity in clear cell renal cell carcinoma (ccRCC).* 12th AACR-JCA Joint Conference, Dec 2022, Maui, HI
4. **Ishihara M**, Hu J, Cano-Ruiz C, […], and Wu L. *Statins inhibit the collaborative metastasis mediated by VHL heterogeneity in clear cell renal cell carcinoma (ccRCC) via a non-cholesterol pathway.* AACR Annual Meeting, Apr 2023, Orlando, FL.
5. **Ishihara M**, Hu J, Cano-Ruiz C, […], and Wu L. *Statins inhibit the collaborative metastasis mediated by VHL heterogeneity in clear cell renal cell carcinoma (ccRCC) via a non-cholesterol pathway.* Kidney Cancer Research Summit (KCRS) 23, Jul 2023, Boston, MA

Chapter 1. Introduction

1.1. ccRCC STATISTICS, BIOLOGY, AND CLINICAL OBSTACLES

The challenges of metastatic ccRCC: Renal cell carcinoma (RCC) is the 7th most common cancer in the United States. There are an estimated 74,000 new cases every year, and more than 14,000 of those patients succumb to the disease [1]. The clear-cell histological subtype (ccRCC) is the most common, accounting for approximately 80% of RCC cases. Patients with localized malignancy are treated with nephrectomy and have a favorable 5-year survival rate of 73% [2]. However, even after successful excision, some patients experience a recurrence of the disease locally in the same kidney or nearby organs or metastases in distant organs. 25-30% of patients presenting with localized tumors will eventually develop metastasis, with the lungs being the most common site of metastatic dissemination [3-6]. Once metastases develop, patient outcome worsens dramatically, with a median survival time of 13 months and a 5-year survival rate of only 11% due to a lack of effective therapies [2]. Recent advances in checkpoint inhibitors show some promise and have been FDA-approved for the treatment of metastatic RCC [7], but the complete response rate is still below 10% with significant treatment-related side effects [8]. Therefore, a better understanding of the metastatic mechanism is needed in order to improve patient outcomes.

The precise oncogenic role of VHL and HIFαs in ccRCC remains elusive: A ground-breaking gene mapping study in 1993 identified the culprit gene in the von Hippel-Lindau (VHL) disease, a rare autosomal dominant cancer syndrome manifested by renal, CNS, adrenal, and pancreatic tumors [9]. Somatic mutations or deletion of the VHL tumor suppressor gene are also present in over 70% of the sporadic, non-familial ccRCC cases [10-13]. Seminal research in the following two decades has unraveled the VHL protein's essential function as an E3 ubiquitin ligase that targets the degradation of the alpha subunit of hypoxia-inducible transcription factors (HIFαs) in an oxygen-dependent manner [14,15]. Under hypoxia or in ccRCC with the loss of VHL function, HIFαs elude recognition by VHL, dimerize with HIFβ, and transcriptionally activate 100–200 hypoxia-responsive genes. The constitutive activation of the HIF pathway through the loss of VHL function implicated this pathway as an oncogenic driver and therapeutic

target [16]. However, despite intensive investigative efforts, the precise oncogenic mechanism of VHL loss is not fully understood. The traditional transgenesis approach has also failed to clarify the oncogenic role of VHL. Numerous mouse models of renal tubule targeted deletion of the VHL gene have failed to generate renal lesions beyond preneoplastic cysts, even when combined with deletion of other tumor suppressor genes such as PTEN or p53 [17,18].

EMT and cooperative model of metastasis: Recently, our group created a new VHL(-)cell line via CRISPR/Cas9-mediated knockout of the VHL gene in a murine VHL(+) ccRCC cell line (RENCA) [19, 20]. As previously reported in VHL knock-down studies [21, 22], VHL-KO cells go through epithelial-mesenchymal transition (EMT) indicated by morphological changes, slowed growth, enhanced migration, and upregulated EMT markers. EMT is an embryonic program that allows polarized epithelial cells to migrate during development. It has been identified as a process that carcinomas adapt in order to spread to other parts of the body [23, 24]. However, the direct causal relationship between EMT and metastasis *in vivo* has not been demonstrated. Two recent prominent studies suggested that EMT is not necessary for metastatic spread but plays a role in chemoresistance [25, 26]. Our work also supports an alternative conclusion on the relationship between EMT and metastasis. As shown in Fig. 1A, our murine model of orthotopic implantation showed that EMT+ VHL(-) cells alone grew poorly *in vivo* and were incapable of producing metastasis, whereas the non-EMT VHL(+) cells developed renal tumors readily but infrequently metastasized to the lung. Strikingly, mice implanted with a 1:1 mixture of VHL(-) and VHL (+) cells rapidly established a renal tumor and rampantly metastasized to the lungs [20]. More interestingly, the metastasized lesions mainly comprised VHL(+) non-EMT cells (Fig. 1B). The same phenomenon of cell composition shift was observed in a patient sample, where their primary tumor showed a high degree of VHL heterogeneity, while the lung biopsy showed predominantly VHL(+) metastatic population (Fig. 1C). This unexpected finding indicates a new paradigm-shifting cooperative metastatic mechanism is at play. In other words, ccRCC relies on the metastatic crosstalk between the two distinct tumor cell populations [27], where VHL (-) cells are the metastatic drivers as they induce the growth and aggression of VHL (+) cells through intercellular communication (Fig. 1D).

1.2. DISSERTATION OVERVIEW

To further explore cooperative metastasis in clinical samples, we sought to establish ccRCC patient-derived xenografts (PDXs). However, the low survival and growth rate made it difficult to establish the ccRCC PDX model in mice subcutaneously or orthotopically. The chicken chorioallantoic membrane (CAM) model is a time- and cost-efficient, sustainable alternative to the traditional mouse model [28]. CAM provides a rich nutrient supply for tumors to seed, grow, and disseminate fast. To use this alternative animal model for PDXs, we showed it faithfully recapitulated our orthotopic implantation model and retained the VHL heterogeneity of clinical samples in Chapter 2.

Chapter 3 demonstrates CAM's many more applications beyond ccRCC PDX. This chapter explores the usage of CAM in non-RCC cancer engraftments and exosome studies. First, we have successfully engrafted gynecological (ovarian) and urological cancers (prostate and bladder) of both mouse and human origin in the CAM. Of those, the results of urological cancers are shown here, including gross CAM pictures, bioluminescent imaging (BLI), and histological analyses. In the second part of the chapter, we show how CAM has accelerated the mechanistic study of the RCC cooperative metastasis. We have explored how exosomes, multifunctional extracellular cargos, are involved in the intratumoral pro-metastatic crosstalk between VHL(+) and VHL(-) cells. The *in ovo* study using CAM is excerpted here, showing how the model strongly supported their hypothesis by providing a rapid animal system. Some unpublished imaging, immune incorporation, and PDX propagation data are also shown.

Chapter 4 aimed to develop a drug capable of selectively inhibiting VHL (-) metastatic driver cells, representing a new class of therapeutic agents that could offer long-term survival for patients with metastatic ccRCC. A high-throughput screening (HTS) was conducted to find small molecules that selectively inhibit the growth and survival of VHL (-) cells. Statins came out as the sole hits, but not all statins had the same level of cytotoxicity. Dosage curves confirmed this result, and animal studies suggest its efficacy against KC metastasis. The mechanism of action (MOA) is currently under investigation, but data implies that it may be distinct from statin's primary role as cholesterol-lowering. By investigating this

further, we could potentially develop a novel small-molecule inhibitor of ccRCC metastasis based on the FDA-approved, cheap, and widely available statins.

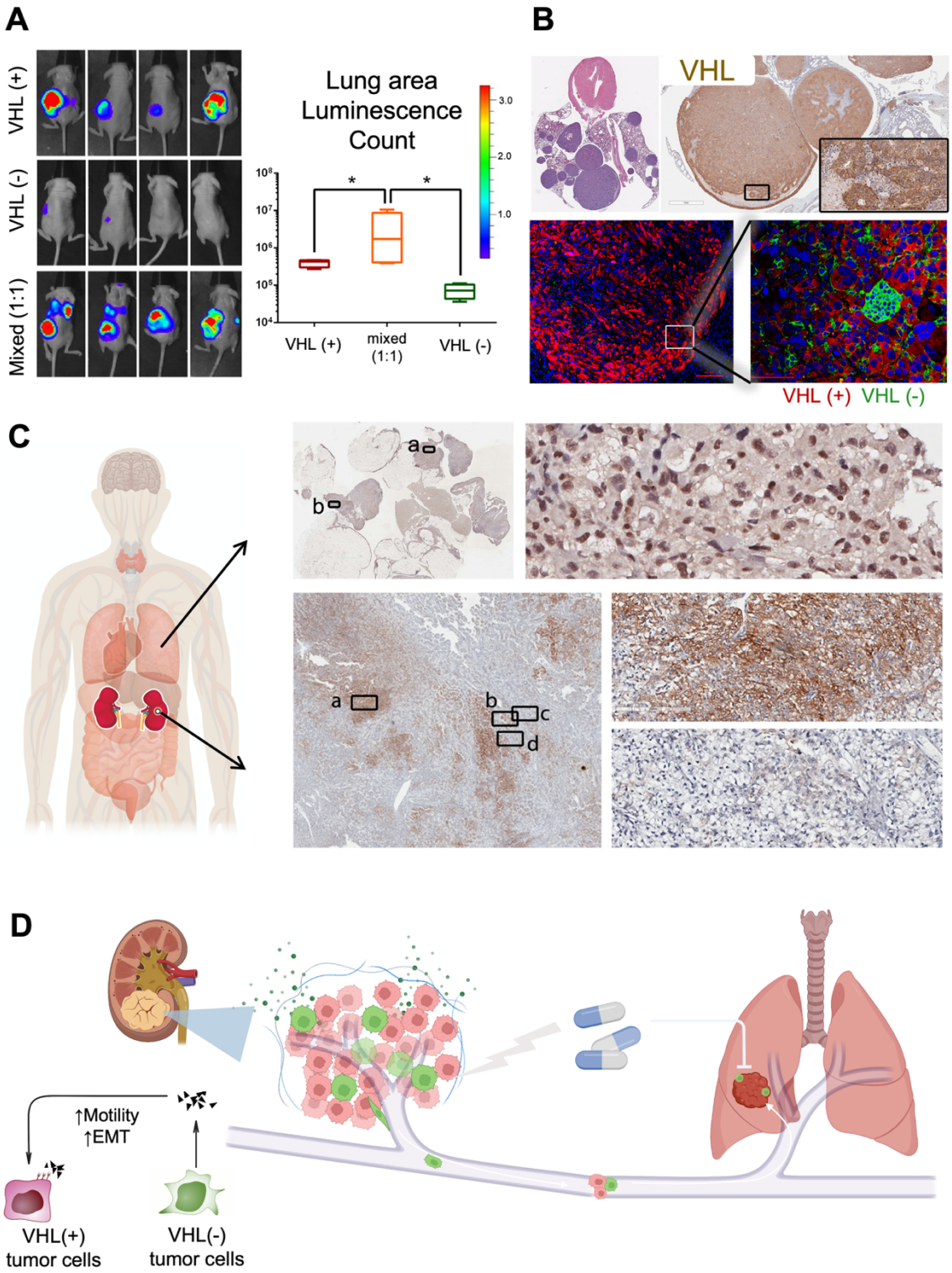


Fig. 1 ccRCC cooperative metastasis model mediated by VHL heterogeneity. (A) Bioluminescence imaging (BLI) of the RENCA orthotopic implantation model four weeks after implantation (left) and quantification of lung area luminescence count (right). (B) Lung sections of the mixed tumor. Top left: H&E; top right: immunohistochemistry (IHC) against VHL; bottom: immunofluorescence with RFP (VHL+) and GFP (VHL-). (C) A clinical sample from case #22, the most aggressive metastatic ccRCC, in which the patient succumbed one year after diagnosis. IHC against VHL is shown with boxed areas magnified on the right. Top: lung metastasis biopsy; bottom: primary kidney tumor. The human anatomy schematic was adapted from https://projects.sfchronicle.com/2020/virus-organs-graphic/. (D) Schematic summary of our working model, in which VHL heterogeneity in the primary tumor is essential, and VHL (-) is the metastatic driver. Thus, disrupting VHL (-) could prevent metastasis.

1.3. REFERENCES

1. http://seer.cancer.gov/statfacts/html/kidrp.html

2. Cohen, H. T. & McGovern, F. J. Renal-cell carcinoma. *The New England Journal of Medicine.* **353** (23), 2477-2490, (2005).

3. Frank, I. *et al.* An outcome prediction model for patients with clear cell renal cell carcinoma treated with radical nephrectomy based on tumor stage, size, grade and necrosis: the SSIGN score. *The Journal of urology.* **168** (6), 2395-2400, (2002).

4. Meskawi, M. *et al.* A review of integrated staging systems for renal cell carcinoma. *European urology.* **62** (2), 303-314, (2012).

5. Patard, J. J. *et al.* Use of the University of California Los Angeles integrated staging system to predict survival in renal cell carcinoma: an international multicenter study. *Journal of clinical oncology : official journal of the American Society of Clinical Oncology.* **22** (16), 3316-3322, (2004).

6. Wolff, I. *et al.* Do we need new high-risk criteria for surgically treated renal cancer patients to improve the outcome of future clinical trials in the adjuvant setting? Results of a comprehensive analysis based on the multicenter CORONA database. *European journal of surgical oncology : the journal of the European Society of Surgical Oncology and the British Association of Surgical Oncology.* **42** (5), 744-750, (2016).

7. Labriola, M. K. *et al.* Immunotherapy Is Changing First-Line Treatment of Metastatic Renal-Cell Carcinoma. *Clinical genitourinary cancer.* **17** (3), e513-e521, (2019).

8. Motzer, R. J. *et al.* Nivolumab plus Ipilimumab versus Sunitinib in Advanced Renal-Cell Carcinoma. *The New England Journal of Medicine.* **378** (14), 1277-1290, (2018).

9. Latif, F. *et al.* Identification of the von Hippel-Lindau disease tumor suppressor gene. *Science (New York, NY).* **260** (5112), 1317-1320, (1993).

10. Foster, K. *et al.* Somatic mutations of the von Hippel-Lindau disease tumour suppressor gene in non-familial clear cell renal carcinoma. *Human Molecular Genetics.* **3**, (1994).

11. Gossage, L., Eisen, T. & Maher, E. R. VHL, the story of a tumour suppressor gene. *Nature reviews Cancer.* **15** (1), 55-64, (2015).

12. Sato, Y. *et al.* Integrated molecular analysis of clear-cell renal cell carcinoma. *Nature Genetics.* **45** (8), 860-867, (2013).

13. Young, A. C. *et al.* Analysis of VHL Gene Alterations and their Relationship to Clinical Parameters in Sporadic Conventional Renal Cell Carcinoma. *Clinical Cancer Research.* **15** (24), 7582-7592, (2009).

14. Jaakkola, P. *et al.* Targeting of HIF-alpha to the von Hippel-Lindau ubiquitylation complex by O2-regulated prolyl hydroxylation. *Science (New York, NY).* **292** (5516), 468-472, (2001).

15. Ivan, M. *et al.* HIFalpha targeted for VHL-mediated destruction by proline hydroxylation: implications for O2 sensing. *Science (New York, NY).* **292** (5516), 464-468, (2001).

16. Motzer, R. J. & Bukowski, R. M. Targeted therapy for metastatic renal cell carcinoma. *Journal of clinical oncology : official journal of the American Society of Clinical Oncology.* **24** (35), 5601-5608, (2006).

17. Hsu, T. Complex cellular functions of the von Hippel-Lindau tumor suppressor gene: insights from model organisms. *Oncogene.* **31** (18), 2247-2257, (2012).

18. Albers, J. *et al.* Combined mutation of Vhl and Trp53 causes renal cysts and tumours in mice. *EMBO Molecular Medicine.* **5** (6), 949-964, (2013).

19. Schokrpur, S. *et al.* CRISPR-Mediated VHL Knockout Generates an Improved Model for Metastatic Renal Cell Carcinoma. *Scientific Reports.* **6** 29032, (2016).

20. Hu, J. *et al.* A Non-integrating Lentiviral Approach Overcomes Cas9-Induced Immune Rejection to Establish an Immunocompetent Metastatic Renal Cancer Model. *Molecular Therapy Methods & Clinical Development.* **9** 203-210, (2018).

21. Thomas, G. V. *et al.* Hypoxia-inducible factor determines sensitivity to inhibitors of mTOR in kidney cancer. *Nat Med.* **12** (1), 122-127, (2006).

22. Pantuck, A. J., An, J., Liu, H. & Rettig, M. B. NF-kappaB-dependent plasticity of the epithelial to mesenchymal transition induced by Von Hippel-Lindau inactivation in renal cell carcinomas. *Cancer Res.* **70** (2), 752-761, (2010).

23. Thiery, J. P. Epithelial-mesenchymal transitions in tumour progression. *Nature reviews Cancer.* **2** (6), 442-454, (2002).

24. Kalluri, R. & Weinberg, R. A. The basics of epithelial-mesenchymal transition. *The Journal of clinical investigation.* **119** (6), 1420-1428, (2009).

25. Fischer, K. R. *et al.* Epithelial-to-mesenchymal transition is not required for lung metastasis but contributes to chemoresistance. *Nature.* **527** (7579), 472-476, (2015).

26. Zheng, X. *et al.* Epithelial-to-mesenchymal transition is dispensable for metastasis but induces chemoresistance in pancreatic cancer. *Nature.* **527** (7579), 525-530, (2015).

27. Hu, J. *et al.* Tumor heterogeneity in VHL drives metastasis in clear cell renal cell carcinoma. *Signal Transduct. Target. Ther.* **8**, 155 (2023).

28. Liu, M. *et al.* The Histone Methyltransferase EZH2 Mediates Tumor Progression on the Chick Chorioallantoic Membrane Assay, a Novel Model of Head and Neck Squamous Cell Carcinoma. *Transl. Oncol.* **6**, 273–281 (2013).

Chapter 2. Mouse- and Patient-Derived Chorioallantoic Membrane (CAM) Xenografts for Studying Metastatic Renal Cell Carcinoma

Reprinted (adapted) with permission from Ishihara, M., Hu, J., Wong, A., Cano-Ruiz, C., Wu, L. *Mouse- and Patient-Derived CAM Xenografts for Studying Metastatic Renal Cell Carcinoma.* In ENZ: Chick Chorioallantoic Membrane Model and Precision Cancer Therapy, 2019;46:59-80. PMID: 31727277, copyright (2019) Elsevier Inc.

ABSTRACT

Renal cell carcinoma is the seventh most common cancer in the United States, and its metastatic form has a very poor prognosis due to a lack of effective treatment and thorough understanding on metastatic mechanism. This chapter will demonstrate a novel concept that intratumoral heterogeneity is essential for metastasis in renal cell carcinoma. We will first introduce the in vitro system and the mouse model that led to the finding of the cooperative mechanism for metastasis. Then, the results from the CAM model illustrate the cooperative interactions that lead to metastasis also occur in this model. We believe that the CAM model, as a unique and sustainable system, can open up new opportunities to study the metastatic disease.

2.1. INTRODUCTION

Kidney cancer annually accounts for 74,000 newly diagnosed malignances and more than 14,000 deaths in the United States (http://seer.cancer.gov/statfacts/html/kidrp.html). Renal cell carcinoma (RCC), a subtype of kidney cancer, is the 7th most common cancer in the United States, and makes up about >90% of kidney cancers overall [1,2]. Amongst a large number of histological and molecular subtypes of RCC, the clear cell subtype (ccRCC) is the most common, comprising of approximately 75-80% of RCC cases, and accounts for most RCC-related deaths [2].

Diagnosis of RCC hinges upon the observation of gross or microscopic hematuria [1]. The symptom of hematuria is usually further assessed by computed tomographic (CT) scan of the genitourinary tract and/or cystoscopy, depending on the age of the patient. Typical radiological features of ccRCC include exophytic growth, heterogeneous morphology caused by necrosis or hemorrhage, and high uptake of contrast agents [3]. The prevalence of RCC has risen in previous decades, most likely due to the steady improvement of radiological technology such as CT imaging or ultrasonography, which has increased incidental findings of RCC in imaging analyses performed for another purpose. It is also possible that RCC incidence is increasing due to environmental or carcinogens exposures, which are known risk factors for this cancer [4,5].

RCC is derived from the renal tubular epithelium [6]. Thus, patients with localized malignancy usually undergo primary treatment of nephrectomy (partial or radical) [7], ablation [8], or active surveillance [9], with a favorable 5-year survival rate of 73% [1]. However, even after successful excision, some patients could experience a recurrence of the disease locally in the same kidney or nearby organs, or metastasize to distant organs. For 25-30% of patients presenting localized tumors will eventually develop metastasis, with lungs being the most common site of metastatic dissemination [10-13]. RCC also spreads to bone, liver and lymph nodes [14]. Once metastases develop, patient outcome worsens dramatically, with a median survival time of 13 months and a 5-year survival rate of only 11% due to a lack of effective therapy [1]. Recent advances in the checkpoint inhibitors show some promise and have been approved by the FDA for treatment of metastatic RCC [15] with initially nivolumab [16], followed by a combination of nivolumab and ipilimumab [17]. Nevertheless, further understanding of the metastatic mechanism is necessary for an improved outcome.

One of the pathological signatures of ccRCC is the loss of function of the von Hippel-Lindau (VHL) protein, a tumor suppressor discovered in 1993 [18-22]. The VHL gene was identified through the study of the VHL disease, which is a rare familial cancer syndrome consisting mainly of hemangioblastomas and ccRCC. Remarkably, a majority of the sporadic ccRCC cases also contains defects within the VHL gene [23]. However, the precise oncogenic mechanism of VHL loss remains elusive. Despite numerous

attempts at VHL knockout targeting renal epithelia, researchers can only observe the preneoplastic cystic lesions in mice [24,25], even when combining with the knockout of other tumor suppressors such as PTEN and p53 [26]. Notably, VHL expression status cannot predict the outcome of ccRCC patients, neither [27]. These findings support the idea that VHL loss alone is insufficient for tumorigenesis or oncogenic development leading to distant metastasis [28].

The downstream pathway of VHL has been studied extensively. VHL protein plays an essential role in oxygen sensing by regulating the alpha subunit of the heterodimeric transcription factor hypoxia-inducible factor, which includes HIF-1α and HIF-2α (referred here as HIFαs) [29,30]. Under normoxia, VHL protein directly binds to HIFαs, leading to their ubiquitination and degradation via proteasome. The loss of VHL results in the accumulation of HIFαs and the upregulation of the overall hypoxia transcription apparatus, which consists of more than 100 genes [31,32]. Some common HIF-regulated genes include transforming growth factor α (TGF-α), vascular endothelial growth factor (VEGF), and glucose transporter 1 (Glut-1) [33]. Without VHL, RCC cells activate such genes even under normoxia, leading to heightened angiogenesis. Both HIF-1α and HIF-2α are the direct downstream target of VHL, and thus they can serve a causal role in ccRCC oncogenesis. These two HIFα isoforms appear to play different roles in ccRCC tumor cells [34,35]. Current literature suggests HIF-2α as the oncogenic driver and HIF-1α as the tumor suppressor [36]. However, our work implicates that HIF-1α is growth suppressive but promotes epithelial to mesenchymal transition (EMT) and metastatic driving actions [37].

In this chapter, we will demonstrate a novel concept that heterogeneity in VHL status is essential for ccRCC metastasis. Our group and others have observed that VHL loss leads to EMT [37-40], which has been considered as a key indicator of metastasis. Surprisingly, our study later found that EMT cells contribute to metastasis *indirectly* as a driver that assists the growth and migration of non-EMT VHL-positive cells [37,41]. We will first introduce the *in vitro* system and the mouse model that led to the finding of the VHL/HIF-mediated cooperative mechanism of metastatic ccRCC. Then, we will show how the CAM model can accelerate and enrich the study by allowing further investigation on the cooperative interactions in human ccRCC. Given the numerous advantages discussed in other chapters as well as in this chapter,

CAM model is highly suited to create patient-derived xenografts (PDX) of ccRCC, enabling further research on the metastatic mechanism and novel therapeutic strategies against it.

2.2. COOPERATIVE METASTATIC MODEL IN MURINE RCC

In this section, we will briefly go over the novel concept of the cooperative model in metastatic ccRCC, where the two cell populations with distinct VHL status cooperate to cause distant metastasis to the lung. It was first suggested in *in vitro*, strengthened in orthotopic implantation model in mouse, and further analyzed *in vitro* and in the CAM system.

2.2.1. CRISPR-mediated VHL-KO RCC model

Recently, our group created a new VHL-knockout (VHL-KO) cell line using CRISPR/Cas9-mediated deletion of VHL gene in murine VHL-positive ccRCC cell line (RENCA; referred here as VHL-WT) [37,41]. Lentiviral-delivered CRISPR effectively knocked out VHL and induced the expression of HIF-1α in normoxia (Fig. 2.1A). VHL loss activated the hypoxia program and upregulated the HIF responsive genes such as Glut-1, PGK1, LDHA and NDRG1 (Fig. 2.1B). VHL-KO cells significantly slowed growth (Fig. 2.1C), but exhibited increased motility and invasion shown in scratch assay (Fig. 2.1D) and transwell migration/invasion assay (Fig. 2.1E). In addition, those VHL-KO cells seemed to go through EMT, as suggested by mesenchymal morphology (Fig. 2.1F) and molecular changes such as decreases in E-cadherin and increases in N-cadherin, α-SMA and MMP-9 (Fig. 2.1G). Therefore, knockout of VHL leads to high motility and EMT, but do these *in vitro* characteristics mean metastasis *in vivo*?

2.2.2. Metastatic model in the mouse kidney

The answer was no. After clonally selecting VHL-WT and VHL-KO cells, we orthotopically implanted either cell line into the renal capsule of 5-week-old female NU/J nude mice. Interestingly, primary tumors from VHL-KO group grew very poorly compared to VHL-WT tumors with no increase in lung metastasis, as monitored by firefly luciferase (FL)-based *in vivo* bioluminescence imaging (BLI) (Fig.

2.2A). Next, we asked whether the mixed population of VHL-WT and VHL-KO cells had metastatic potential by implanting VHL-WT cells alone or 1:4 mixtures of VHL-WT and VHL-KO cells into the subcapsular space of the left kidney in 4-week-old female BALB/C mice. After 6 weeks of implantation, primary tumors from both groups displayed robust growth, while only the mixed population showed rampant metastasis to the lung, as observed with FL-BLI (Fig. 2.2B) and confirmed with immunohistochemistry (IHC) (Fig. 2.2C). Surprisingly, the metastasized lesion was mainly composed of VHL-WT, or more epithelial cells (data not shown).

In order to explain this phenomenon, we went back to the *in vitro* assay to study the cooperative effect of VHL-WT and -KO cells. We observed that VHL-KO cells helped VHL-WT cells to grow and migrate faster through both direct cell-cell communication and secreted factor (data not shown). The knockout of HIF-1α, a direct downstream target of VHL, abrogated the assisted growth and migration, further affirming the contribution of VHL loss in cooperative metastasis model (data not shown). As such, our preclinical data using murine ccRCC cells suggest that (i) VHL-KO EMT cells are the metastatic drivers, (ii) VHL-KO cells induce mobility of non-EMT VHL-WT cells through cell-cell interactions and soluble factors, (iii) the cooperation can occur at primary tumors, in circulation and at the metastatic site. To validate the cooperative model in clinical ccRCC, we need to study signal crosstalk in patient tumors by establishing PDXs. This led us to utilize the chick CAM system due to its unique advantages discussed in the next section.

2.3. CAM METASTATIC MODEL

2.3.1. CAM history and advantages over mouse model

The chicken embryo CAM is an *in vivo* model that has been used to study cancer biology and progression through implantation of tumors and cancerous cell lines [42]. Before hatching, the CAM serves as a highly vascularized gas-exchange organ due to its large surface area and close proximity to membranes resting on the shell [43]. Overall, the development of the chick embryo lasts a total of 21 days, allowing a maximum of 11 days for implanted tumor or cells to grow until the CAM is destroyed. Although the time

of growth seems short, tumors nourished with preexisting vessels grow quickly, achieving successful engraftment [42].

Another important advantage of the CAM model is the innate immunodeficient state of the chicken embryo during development. This lack of immune response allows successful transplantations of a number of diverse species and tissues. The immune system consisting of B cells and T cells begins to form 2 weeks into its development, as well as the presence of monocytes and macrophages [44-46]. By day 18, the chicken embryo evolves to become immunocompetent [44]. Due to a little chance of rejection of transplantations, the CAM has a long history of usage in the study of tumor growth and metastasis [42].

Metastasis is a series of temporally- and spatially-linked events. Tumor progression in the CAM model has given great insights into all the metastatic steps including local dissociation, intravasation into blood vessels, survival in the circulation, extravasation out of circulation, and seeding in distant organs [47-50]. According to the experimental CAM model, tumor cells injected through the allantoic vein propagate through the circulation with an 80% survival rate and successful extravasation, as shown by migration to preexisting blood vessels [51]. Successful metastasis can be visualized by the formation of smaller tumors spreading from the site of transplantation or injection to the lower CAM and other distant organs [52].

As such, the CAM system has great advantages in terms of time-, labor-, and cost-efficiency. Compared to the traditional mouse model specifically, the visible engraftment of tumors in the CAM is far more rapid (3-11 days vs. 3-6 weeks), and the cost of fertilized eggs is much less expensive (~$1 vs. over $100 for a SCID mouse). It is important to note that the CAM model is not likely to replace the traditional mouse model because of the significant physiological differences between birds and mammals. Nonetheless, the CAM model could serve as a sustainable and accelerated animal model that can work in harmony with the mouse model. Aiming for the long-term goal of establishing CAM PDX, the model was first evaluated for its ability to retain the ccRCC biology observed in the mouse model such as growth and metastatic behavior.

2.3.2. CAM metastatic model for murine RENCA cells

After 7 days of pre-incubation at 37 °C and 55-65% humidity, the CAM of fertilized eggs was dropped to open a window. On embryonic developmental day 10, the same groups of cells used in the mouse orthotopic model were implanted on CAM (RENCA VHL-WT cells alone, VHL-KO cells alone, or 1:1 mix of the two; all at the concentration of 2 x 10^6 cells/egg). Tumor growth was recorded every other day starting on tumor day 3 (or developmental day 13). On developmental day 19, tumors were harvested for gross picture and histological analyses. Chicken blood was also collected to detect circulating tumor cells (CTC) by flow cytometry as a measurement of metastasis. In concordance with the mouse model, the CAM system successfully maintained the growth and metastatic behavior of the RENCA tumors. First, primary tumors from both VHL-WT and mix tumor group grew well to a size of about 1 cm, while VHL-KO tumors grew poorly (Fig. 2.3A and B). The RENCA tumor growth characteristic of VHL-WT, mixed and VHL-KO cells replicates that observed in mice. Furthermore, histology shows high degree of similarity in cellular morphology and structure between the mouse and CAM tumor, except for the stroma and blood components derived from the chicken (please see Figure 2.4B). Most importantly, the CTC counts were significantly higher for the mix tumors than the VHL-WT (Fig. 2.3C and D). These results show that the metastatic behavior we observed in the mouse model is recapitulated in the CAM model, further supporting the contribution of VHL heterogeneity to the metastatic process.

2.3.3. Lung metastasis observed in hatched chicken

The later steps of metastasis such as extravasation and seeding in distant organs are harder to observe in the CAM model due to the short growth period before hatching and the disparate physiology of uninflated chicken embryo lung. To overcome these limitations, we obtained an approval from the Institutional Animal Care and Use Committee (IACUC) to extend the analyses of distant metastases for 2 weeks in hatched chickens. As shown in Fig. 2.3E, this extension enabled the cancer cells to establish micrometastatic nodules (pointed by arrowheads) near the pulmonary artery in the chicken lung (marked with #), as visualized by H&E stains. A majority of the metastatic lesions consisted of HA-tagged VHL-WT cells, whereas flag-tagged VHL-KO cells were difficult to locate. This finding was very consistent with

what we observed in the mouse model (data not shown). Thus, metastasis analyses in hatched chicken provide unique histological information such as structural morphology, which cannot be assessed using qPCR or flow cytometry.

2.4. TUMOR PASSAGING FROM CAM TO MOUSE

In order to overcome the short growth period of CAM, some researchers have passaged the CAM tumor from one egg to another, for up to 3 successful serial passages [53,54]. As an alternative method to extend the growth period, we transplanted the RENCA tumors formed in CAM to a nude mouse.

On day 20 of chicken embryonic development, we harvested the RENCA tumor from the CAM and transplanted to the axilla subcutaneous tissue of a 1-year-old female nude mouse. One side received the VHL-WT tumor and the other received the mixed tumor (Fig. 2.4A). After 3 weeks of transplantation, the tumors were excised. As shown in Fig. 2.4B, the CAM tumors survived and engrafted to the mouse tissue. The gross morphology shown by H&E and VHL stains shows high resemblance between the CAM tumor before and after the transplantation, excluding the chicken stroma and blood components replaced by the mouse counterparts (Fig. 2.4B, arrows). In fact, these tumors were comparable with those grown just in the mouse (Fig. 2.2C, kidney H&E), showing that the CAM system does not alter the pathophysiology of the tumor. These results demonstrated the usefulness of the CAM system as an intermediate model between one animal to the other. Because the CAM has an abundant supply of blood and nutrient to support the growth, it might be especially beneficial to support the initial growth of patient samples and relay them to mouse PDXs.

2.5. CAM PDX

2.5.1. History of CAM PDX

PDXs have been primarily established in mice as a model that maintains the biological structure and other characteristics of patient tumors. PDXs in mice have faithfully recapitulated pathophysiology, intratumoral heterogeneity, and treatment response of patient tumors [55]. For ccRCC, a recent study

documented successful establishment of PDX that recapitulated the patient's reported clinical response to targeted therapies [56-58]. This allows further investigation into the oncological mechanism and development of precision medicine. Regardless of the establishment of PDXs in mouse models, the CAM model offers new advantages such as lower cost and higher efficiency compared to the mouse model [42]. In the CAM PDX, studies reported successful engraftment of tumors with increased similarity to the patient tumor, higher levels of vascularization, as well as successful metastasis in circulation [59,60]. Although CAM PDXs have their own limitations such as short time frame and evolving chicken immune system, the model has high potential of being an efficient, clinically relevant approach.

2.5.2. Successful establishment of CAM ccRCC PDX in our lab

There are some literature reporting successful establishment of CAM PDXs for ccRCC [57,58]. To further characterize the VHL mutation status and molecular program involved, we also sought to establish CAM PDXs from primary tumors collected at our urological surgery department. Over the past 3 years, 26 cases have been examined, with the first 16 cases being paraffin-embedded samples and the remaining 10 being freshly harvested tumor specimens collected from surgeries performed by a single surgeon. We generated CAM PDXs from small chunks of those 10 cases with a very high success rate of 70% (data not shown). The implanted chunks became embedded in the CAM with ample tumor vasculature (Fig. 2.5A), and its morphology resembled well the original patient tumor (Fig. 2.5B). Importantly, we observed that CAM PDXs were able to preserve the intratumoral VHL heterogeneity that exists in patients' tumors (Fig. 2.5C). Thus, we believe that CAM PDXs can serve as a valuable tool to investigate the critical crosstalk on growth and metastasis, and to test novel therapies. Currently, we are actively investigating these approaches.

2.6. COOPERATIVE METASTATIC MODEL IN HUMAN RCC

So far, we presented results from animal models that illustrate the relationship between intratumoral heterogeneity and a cooperative mechanism of metastasis. In this last section of the chapter, we will briefly

address the relevance of the new idea posed by our cooperative model to human disease, in human RCC cell line and clinical cases.

2.6.1. CRISPR-mediated VHL-KO in human RCC cell line

The key findings of the cooperative metastasis model were demonstrated in the RENCA cell line, a widely used RCC cell line derived from murine renal epithelium [61]. We asked whether VHL knockout in human ccRCC cell line would also exhibit the EMT phenotype of slowed growth, high motility and increased mesenchymal morphology that were observed in the murine RENCA cells. To answer this question, we applied the same CRISPR/Cas9 system used in RENCA cells to knockout the VHL gene in the human ACHN cell line, which is widely used human RCC cell line with wild-type expression of VHL protein [62]. Consistent with the findings in the RENCA model, VHL-KO in ACHN cells (AC-VHL-KO) exhibited mesenchymal morphology (Fig. 2.6A, right) with lower E-cadherin and higher N-cadherin and MMP-9 expression measured by RT-PCR (Fig. 2.6B). These cells had elevated levels of HIF1α protein and decreased proliferation compared to the AC-VHL-WT control line (data not shown). Remarkably, the *in vivo* cooperative metastatic behavior was also recapitulated in this ACHN model. Tumors from AC-VHL-WT alone and 1:1 mix of AC-VHL-WT and AC-VHL-KO groups both grew well after intrarenal implantation. However, only the animal bearing 1:1 mixed tumor showed multiple small metastases in lung, which was assessed by gross tissue inspection (Fig. 2.6C) and detailed histology (Fig. 2.6D). Thus, for both murine and human cell lines, poorly proliferative VHL-KO cells drive metastasis by promoting the growth and motility of VHL-WT cells.

2.6.2. Intratumoral heterogeneity of VHL expression in patient tumors

A number of previous literature has documented the heterogeneous genomic landscape of ccRCC [63-65]. This results in heterogeneity in gene expression, which can be further linked to disease progression and metastasis [63,66,67]. Although the loss-of-function mutation of VHL protein has been reported to occur in up to 90% of cases [19], thus making VHL loss a truncal mutation of ccRCC [63,68], it remains unclear how uniformly VHL is deleted in individual cells throughout the entire tumor. In order for the cooperative

mechanism to be operating in clinical disease, we would expect a heterogeneity of VHL expression to exist within a single tumor. In other words, both VHL-positive and VHL-negative cancer cells will be present in a tumor. To address this point, we studied expression of VHL protein in large tissue sections of 26 primary tumors collected in the process previously mentioned in section 5.2. IHC analyses showed that all 26 cases exhibited various levels of VHL protein, with VHL positive cells ranging from 10% to 90% in each tumor (data not shown). In other words, none of the cases sustained a uniform loss of VHL protein throughout the entire tumor. The VHL expression was highly heterogeneous, with VHL-positive cells immediately juxtaposed with VHL-negative cells, as shown in a representative IHC stain (Fig. 2.6E). Collectively, the histological analyses revealed that expression of VHL protein displays intercellular heterogeneity within individual human ccRCC tumors, creating a scenario where *in vivo* cooperative crosstalk can occur. Since CAM PDXs can preserve the intratumoral heterogeneity of patients' tumors (Fig. 2.5C), we believe that they will provide a very valuable system to interrogate the cooperative metastatic crosstalk in clinical ccRCC.

2.7. DISCUSSION

Our preclinical data shown in this chapter strongly support that tumor heterogeneity contributes to an aggressive phenotype. Specifically, interaction between cells with distinct VHL status might be an essential promoter of metastasis. Thus, it is important to further verify this novel concept in clinical cases. We have already achieved a critical objective in establishing CAM PDXs, which maintain the heterogeneity and architecture observed in patient tumors. The next step would be to verify the new molecular mechanism of metastasis in the CAM PDXs. Furthermore, we are attempting PET/CT imaging, PDX propagation in CAM, and incorporation of autologous immune cells to build even more clinically relevant models (Fig. 2.7). If successful, these humanized CAM PDXs can serve as renewable sources of tumor specimen and as an extremely valuable resource to test and personalize therapeutic strategy for ccRCC patients in the future. This work was funded by the UCLA JCCC seed grant, UCLA 3R grant, UCLA CTSI and UC TRDRP (LW).

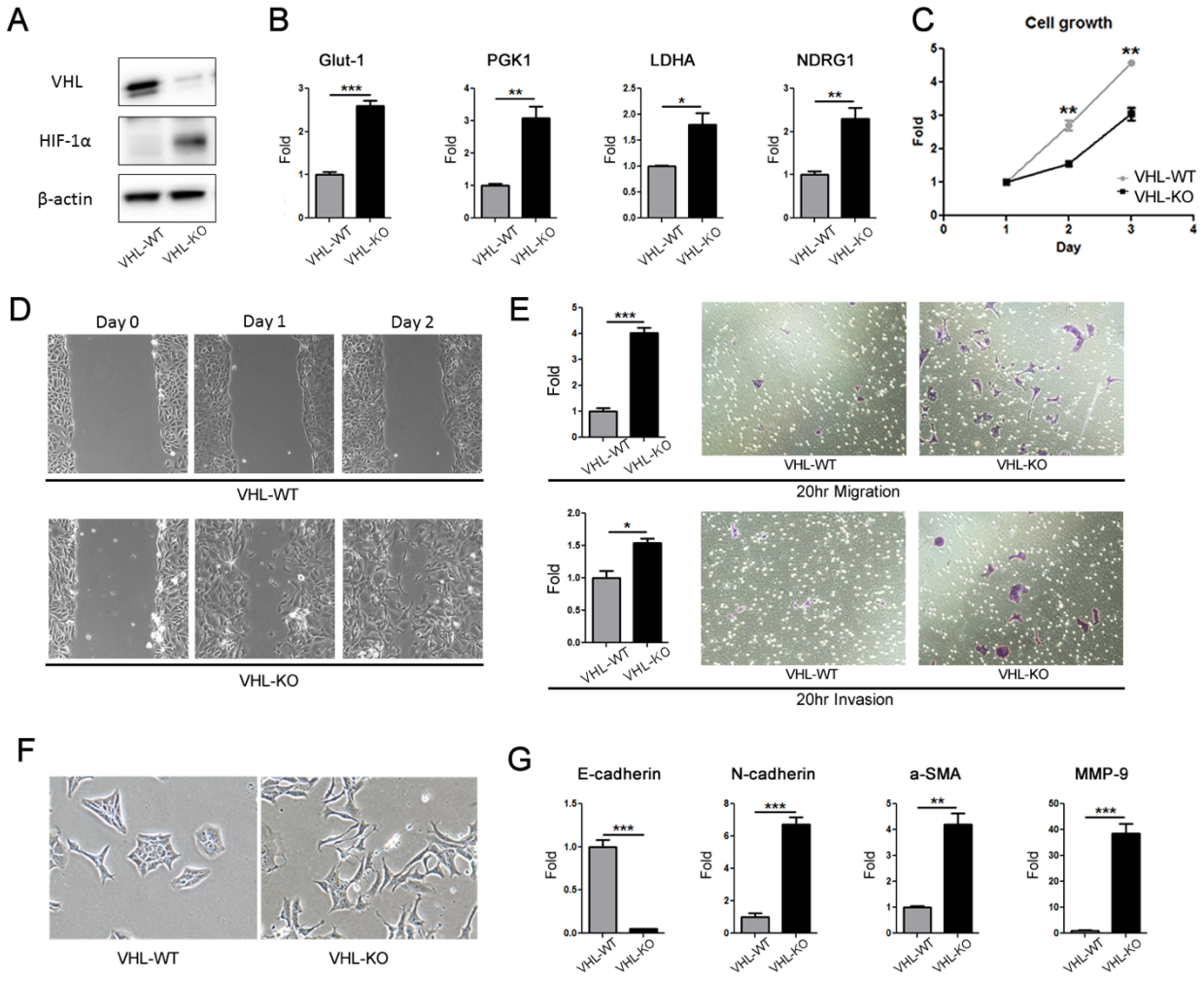


Fig. 2.1 CRISPR-mediated knockout of VHL induces HIF pathways and EMT phenotype in RENCA cells. (A) Western blot for murine VHL, HIF-1α and β-actin in VHL-WT and VHL-KO cells. (B) Gene expression analyzed by RT-PCR for Glut-1, PGK1, LDHA and NDRG1. (C) Growth curve of VHL-WT versus VHL-KO cells. (D) Representative images of VHL-WT (top) and VHL-KO (bottom) cells in a scratch assay on Days 0, 1 and 2 after scratching. (E) Quantification and representative images of VHL-WT and VHL-KO cells' migration (top) and invasion (bottom). (F) Phase contrast 10X images of VHL-WT and VHL-KO cells. (G) Gene expression analyzed by RT-PCR for E-cadherin, N-cadherin, α-SMA and MMP-9. n = 3 for RT-PCR and proliferation assay, *denotes $P < 0.05$, **denotes $P < 0.01$, ***denotes $P < 0.001$. *Adapted and modified from Schokrpur, S., et al. CRISPR-Mediated VHL Knockout Generates an Improved Model for Metastatic Renal Cell Carcinoma. Sci. Rep. 6 (2016) 29032 [37].*

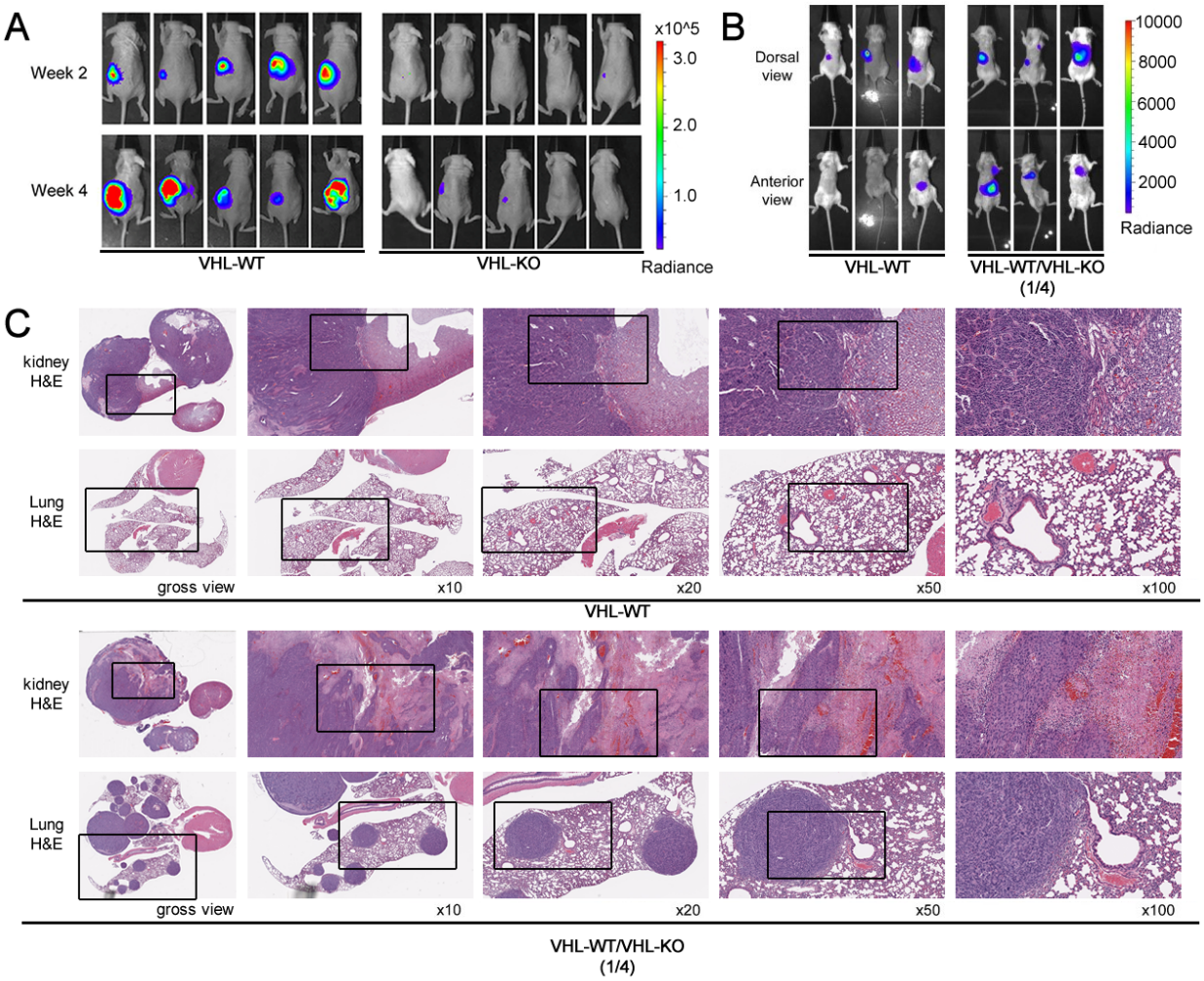


Fig. 2.2 VHL-loss-mediated metastatic RCC model in the mouse kidney. (A) FL-BLI were taken 2 and 4 weeks after the orthotopic implantation of either VHL-WT (left) or VHL-KO (right) cells in the renal subcapsular space in nude mice. (B) FL-BLI were taken 6 weeks after the orthotopic implantation of either VHL-WT cells alone (left) or 1:4 ratio of VHL-WT and VHL-KO cells (right) in the renal subcapsular space of BALB/c mice. (C) H&E stain of harvested organs, including the primary kidney tumor and contralateral normal kidney, as well as lung and heart from both groups, were shown. *Adapted from Hu, J., et al. A Non-integrating Lentiviral Approach Overcomes Cas9-Induced Immune Rejection to Establish an Immunocompetent Metastatic Renal Cancer Model. Mol. Ther. Methods Clin. Dev. 9 (2018) 203-210 [41].*

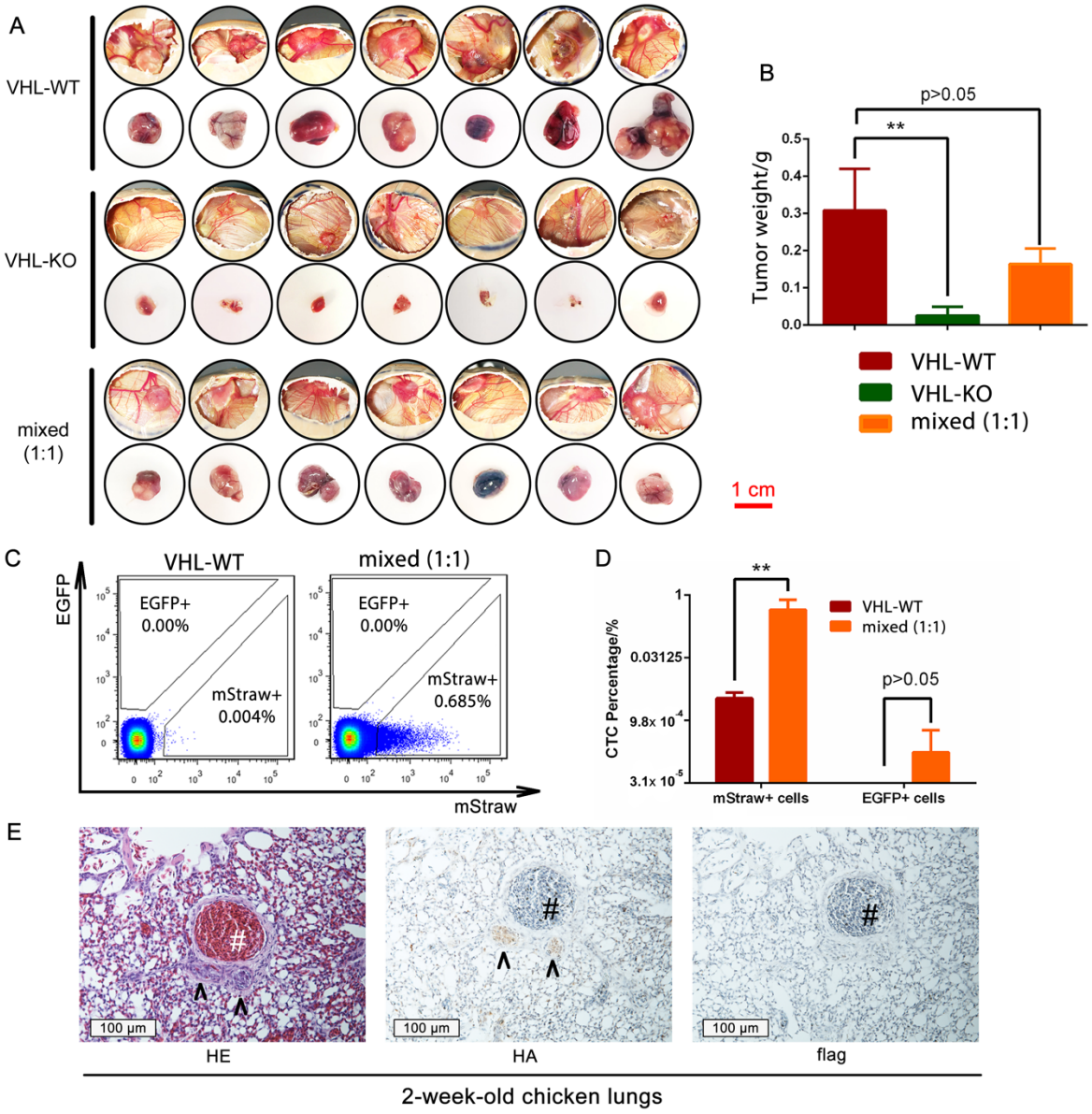


Fig. 2.3 CAM metastatic model for murine RCC. (A) Representative images of RENCA tumors implanted and grown on CAM. There were 3 tumor groups: VHL-WT alone (top), VHL-KO alone (middle), and 1:1 mixture of VHL-WT and VHL-KO (bottom). Pictures were taken on developmental day 20 (10 days after implantation) before and after the excision of the tumors (top and bottom, respectively, for each tumor group). (B) Weight of each tumor was measured after excision. (C) Representative flow analysis for detecting mStrawberry+ and EGFP+ cells circulating in blood for VHL-WT (left) and 1:1 mixed groups (right). (D) Quantification of the flow analysis. (E) IHC stains of the lung from 2-week-old chick bearing

metastatic tumor during its embryonic stage. From left, 20X images show H&E, HA, and flag stains. #: chicken pulmonary artery; arrowhead: metastatic nodules. n =7 for tumor weight analysis and n = 3 for CTC counts, **denotes P < 0.01, mStraw denotes mStrawberry. *Adapted from Hu, J., et al. Establishment of xenografts of urological cancers on chicken chorioallantoic membrane (CAM) to study metastasis. Precis. Clin. Med. 2 (2019) 140-151 [69].*

Figure 4

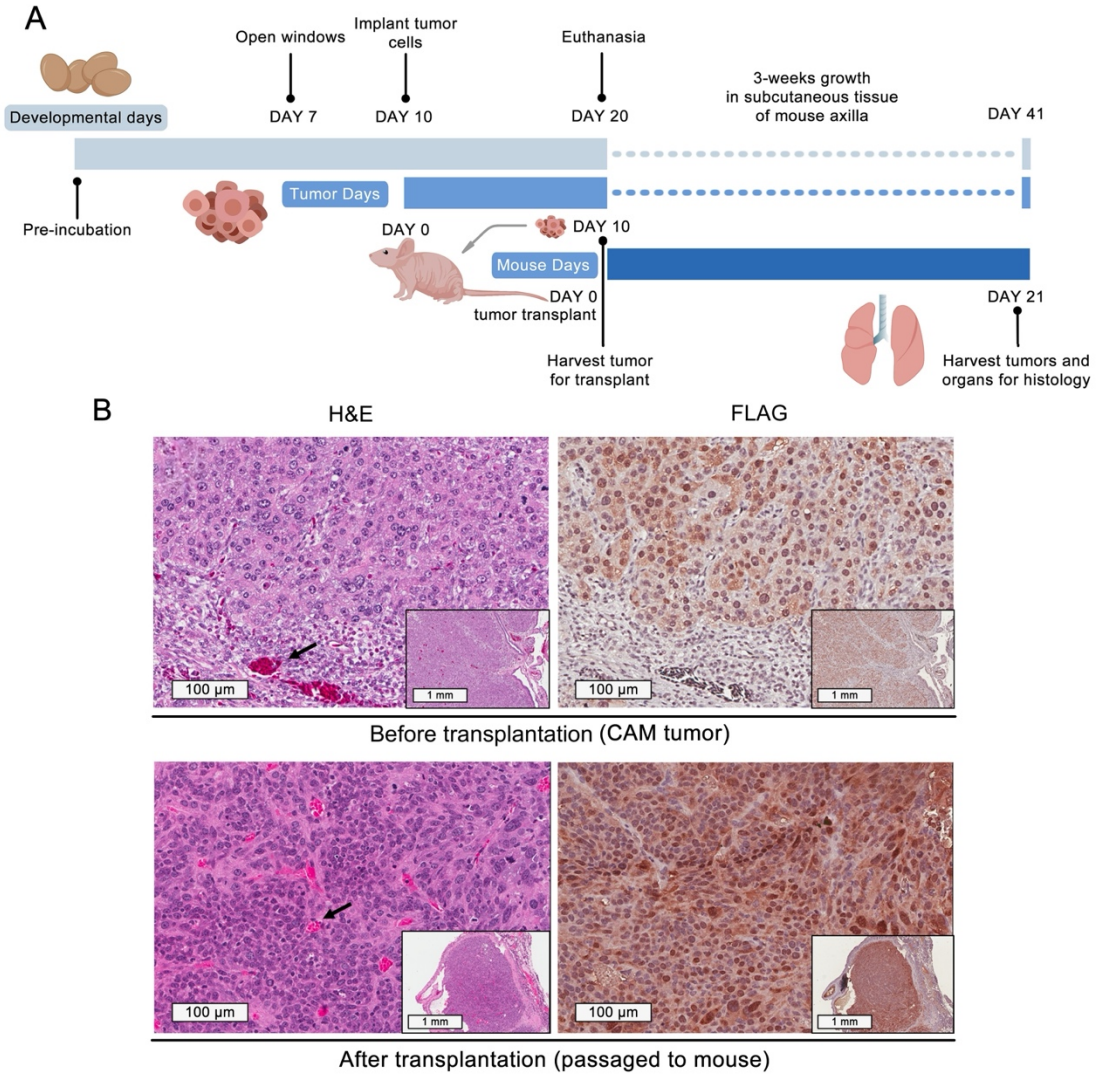


Fig. 2.4 Tumor passaging from CAM to mouse. (A) Schematic representation and timeline of tumor passaging from CAM to mouse. The image was created with BioRender. (B) Representative images of

H&E and FLAG stains of a CAM RENCA tumor before the passaging (top; harvested from CAM) and after the passaging (bottom; harvested from the axilla subcutaneous tissue of a nude mouse). All images were taken at 4X and 20X magnification. Arrows point out the red blood cells of chicken (nucleated) and mouse (non-nucleated), respectively. *Panel A was adapted and modified from Hu, J., et al. Establishment of xenografts of urological cancers on chicken chorioallantoic membrane (CAM) to study metastasis. Precis. Clin. Med. 2 (2019) 140-151 [69].*

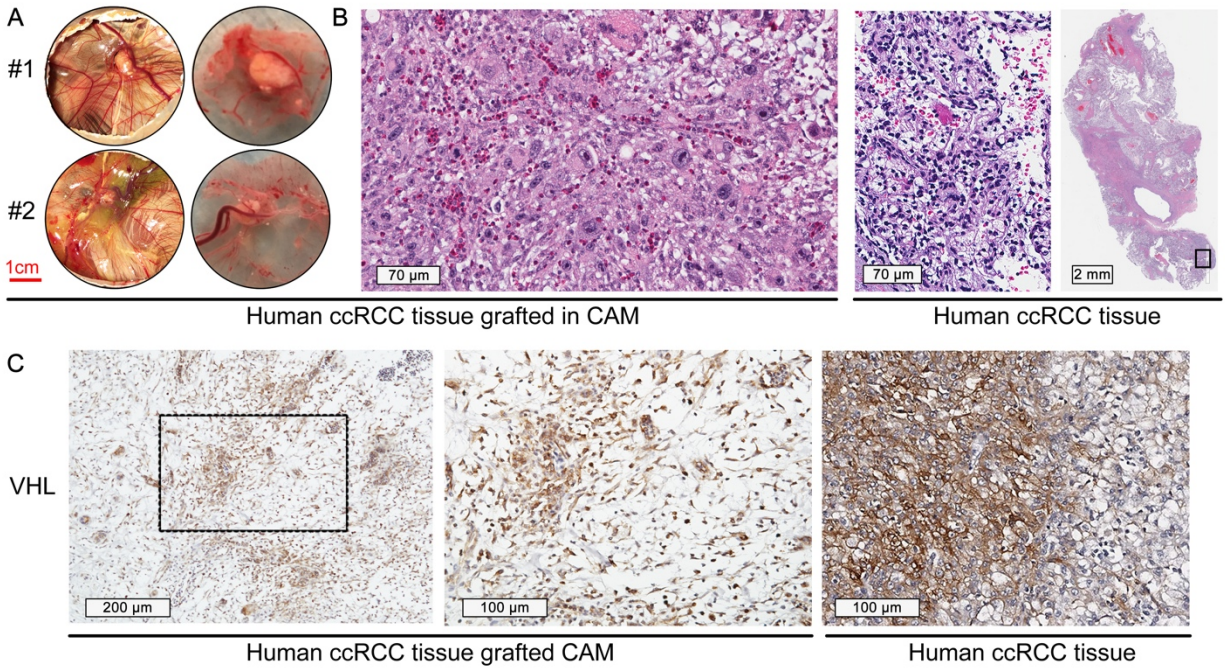


Fig. 2.5 The CAM model successfully grafted patients' tumors without altering morphology or heterogeneity. (A) Two representative cases of patient's ccRCC tumors were shown to grow well on CAM with ample vascularization. Pictures were taken before (left) and after (right) the excision of the tumors. (B) Representative images of H&E stain of a CAM PDX (left, 30X) and an original patient's tumor (middle, 20X; right, 1.5X) showed that the CAM PDX maintained the original tumor morphology. (C) Representative images of IHC staining against human VHL in a CAM PDX (left, 10X; middle 20X) and another original patient's tumor (right, 20X) showed that the CAM PDX maintained the VHL heterogeneity of patient's tumor. *Panels A and B were adapted from Hu, J., et al. Establishment of xenografts of*

urological cancers on chicken chorioallantoic membrane (CAM) to study metastasis Precis. Clin. Med. 2 (2019) 140-151 [69].

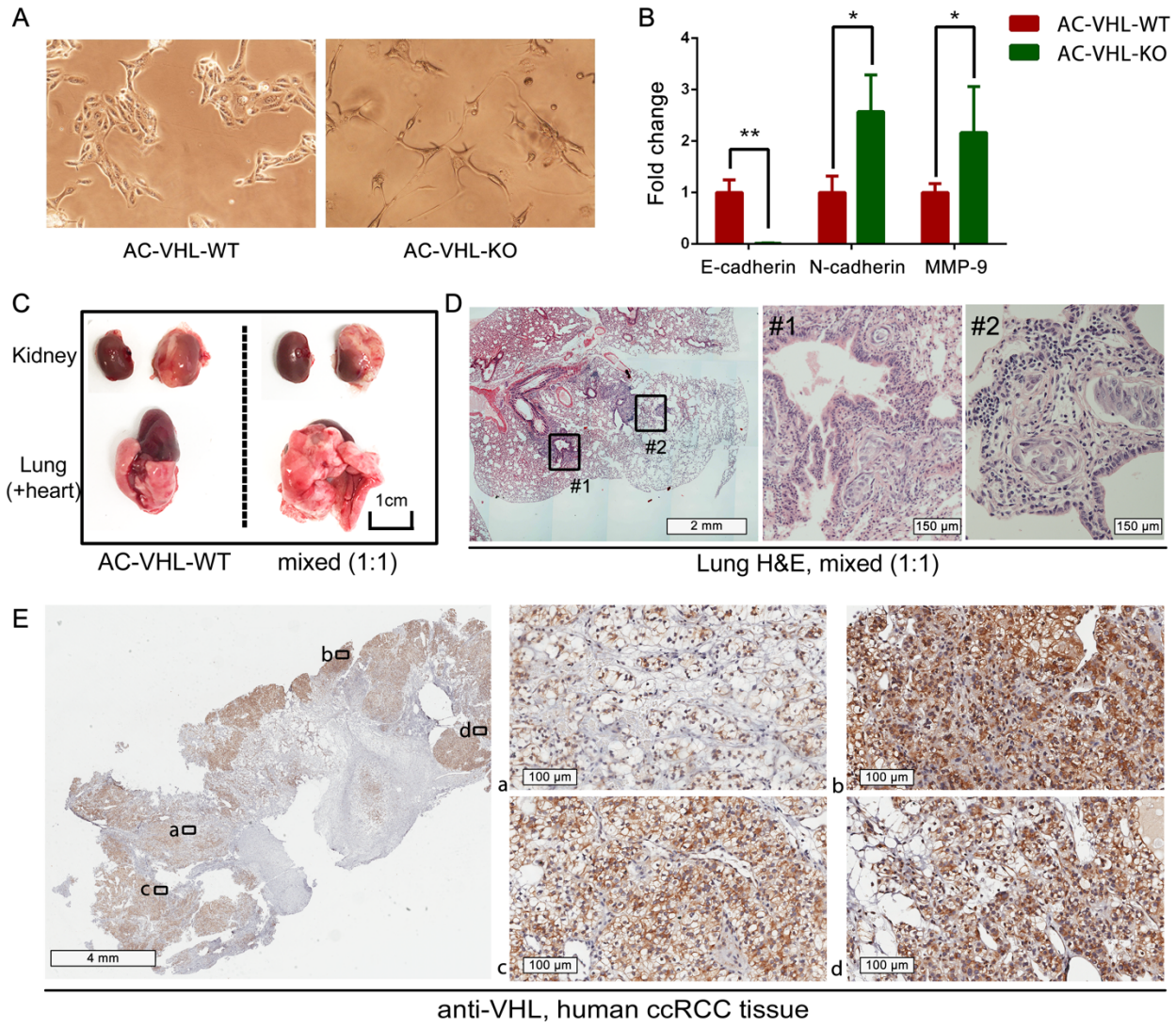


Fig. 2.6 Cooperative metastatic model and VHL heterogeneity in human RCC. (A) Phase contrast 10X images of AC-VHL-WT and AC-VHL-KO cells. (B) Gene expression analyzed by RT-PCR for E-cadherin, N-cadherin and MMP-9. (C) Representative gross images of harvested organs, including the primary kidney tumor and contralateral normal kidney, as well as lung and heart, from the two tumor groups established in Nu mice: AC-VHL-WT alone (left) and 1:1 mix of AC-VHL-WT and AC-VHL-KO (right). (D) H&E stain of harvested lung from the 1:1 mixed tumor group. Representative images at magnification of 4X (left) and 20X (middle and right) showed multiple small metastatic lesions. (E) IHC for human VHL in a

representative case of patient ccRCC showed an extensive intratumoral heterogeneity with interspersed VHL-positive and VHL-negative areas throughout the tumor. Images were taken unmagnified (left) and at 20X (right; a-d). This is the same tumor section as Fig. 2.5B. n = 3 for RT-PCR, *denotes P < 0.05, **denotes P < 0.01. *Adapted from Hu, J., et al. Signal Transduct. Target Ther. 8 (1) (2023) 155 [70].*

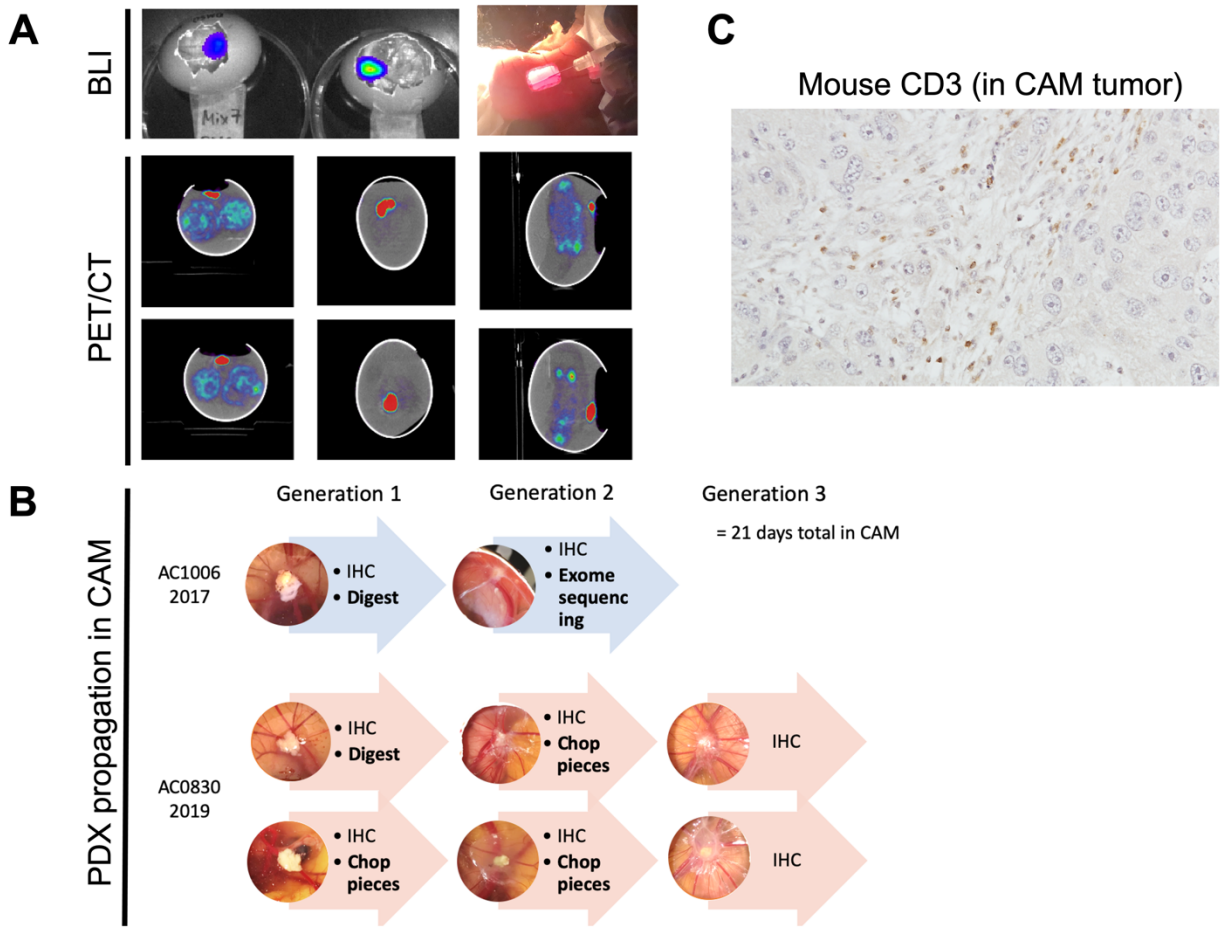


Fig. 2.7 Preliminary data for more CAM PDX applications. (A) Representative images of bioluminescence images (BLI), intravenous (i.v.) injection, and PET/CT scan of CAM, which can be beneficial for imaging of PDX without luminescence of fluorescent labeling. (B) Schema of PDX propagation in CAM up to 3 generations, totaling 21 days in CAM. Two PDXs were tried both in the forms of chunks and/or digested cells. After each generation, CAM PDXs were collected for IHC, then chopped or digested for the next generation. Exosome sequencing was conducted for AC10062017 after the second generation to confirm

that the genetic signature was unaltered from the original patient tumor by CAM propagations. (C) A histological image of a CAM tumor injected with murine splenocytes is shown at 10x magnification. The histological section was stained for murine CD3. Splenocytes were isolated from a BALB/c mouse and injected i.v. to CAM as shown in panel (A) after tumor was established. Both tumor cells (blue staining with enlarged nucleus) and injected CD3 cells (small brown staining) can be observed, showing autologous immune incorporation is possible in CAM model.

2.8. REFERENCES

1. H. T. Cohen,F. J. McGovern, Renal-cell carcinoma, N Engl J Med. 353 (2005) 2477-2490.

2. J. J. Hsieh, M. P. Purdue, S. Signoretti, C. Swanton, L. Albiges, M. Schmidinger, D. Y. Heng, J. Larkin,V. Ficarra, Renal cell carcinoma, Nature Reviews. Disease Primers. 3 (2017) 17009.

3. C. A. Karlo, P. L. Di Paolo, J. Chaim, A. A. Hakimi, I. Ostrovnaya, P. Russo, H. Hricak, R. Motzer, J. J. Hsieh,O. Akin, Radiogenomics of clear cell renal cell carcinoma: associations between CT imaging features and mutations, Radiology. 270 (2014) 464-471.

4. W. H. Chow, L. M. Dong,S. S. Devesa, Epidemiology and risk factors for kidney cancer, Nat Rev Urol. 7 (2010) 245-257.

5. B. Ljungberg, S. C. Campbell, H. Y. Choi, D. Jacqmin, J. E. Lee, S. Weikert,L. A. Kiemeney, The epidemiology of renal cell carcinoma, Eur Urol. 60 (2011) 615-621.

6. A. Jemal, F. Bray, M. M. Center, J. Ferlay, E. Ward,D. Forman, Global cancer statistics, CA Cancer J Clin. 61 (2011) 69-90.

7. B. Ljungberg, K. Bensalah, S. Canfield, S. Dabestani, F. Hofmann, M. Hora, M. A. Kuczyk, T. Lam, L. Marconi, A. S. Merseburger, P. Mulders, T. Powles, M. Staehler, A. Volpe,A. Bex, EAU guidelines on renal cell carcinoma: 2014 update, Eur Urol. 67 (2015) 913-924.

8. R. El Dib, N. J. Touma,A. Kapoor, Cryoablation vs radiofrequency ablation for the treatment of renal cell carcinoma: a meta-analysis of case series studies, BJU Int. 110 (2012) 510-516.

9. P. M. Pierorazio, M. H. Johnson, M. W. Ball, M. A. Gorin, B. J. Trock, P. Chang, A. A. Wagner, J. M. McKiernan,M. E. Allaf, Five-year analysis of a multi-institutional prospective clinical trial of delayed intervention and surveillance for small renal masses: the DISSRM registry, Eur Urol. 68 (2015) 408-415.

10. I. Frank, M. L. Blute, J. C. Cheville, C. M. Lohse, A. L. Weaver,H. Zincke, An outcome prediction model for patients with clear cell renal cell carcinoma treated with radical nephrectomy based on tumor stage, size, grade and necrosis: the SSIGN score, J Urol. 168 (2002) 2395-2400.

11. J. J. Patard, H. L. Kim, J. S. Lam, F. J. Dorey, A. J. Pantuck, A. Zisman, V. Ficarra, K. R. Han, L. Cindolo, A. De La Taille, J. Tostain, W. Artibani, C. P. Dinney, C. G. Wood, D. A. Swanson, C. C. Abbou, B. Lobel, P. F. Mulders, D. K. Chopin, R. A. Figlin,A. S. Belldegrun, Use of the University of California Los Angeles integrated staging system to predict survival in renal cell carcinoma: an international multicenter study, J Clin Oncol. 22 (2004) 3316-3322.

12. I. Wolff, M. May, B. Hoschke, R. Zigeuner, L. Cindolo, G. Hutterer, L. Schips, O. De Cobelli, B. Rocco, C. De Nunzio, A. Tubaro, I. Coman, B. Feciche, M. Truss, O. Dalpiaz, R. S. Figenshau, K. Madison, M. Sanchez-Chapado, M. D. Santiago Martin, L. Salzano, G. Lotrecchiano, S. F. Shariat, M. Hohenfellner, R. Waidelich, C. Stief, K. Miller, S. Pahernik, S. Brookman-May, Corona Project Members of the,Group the European Association of Urology Young Academic Urologists Renal Cancer, Do we need new high-risk criteria for surgically treated renal cancer patients to improve the outcome of future clinical trials in the adjuvant setting? Results of a comprehensive analysis based on the multicenter CORONA database, Eur J Surg Oncol. 42 (2016) 744-750.

13. M. Meskawi, M. Sun, Q. D. Trinh, M. Bianchi, J. Hansen, Z. Tian, M. Rink, S. Ismail, S. F. Shariat,

F. Montorsi, P. Perrotte,P. I. Karakiewicz, A review of integrated staging systems for renal cell carcinoma, Eur Urol. 62 (2012) 303-314.

14. M. Bianchi, M. Sun, C. Jeldres, S. F. Shariat, Q. D. Trinh, A. Briganti, Z. Tian, J. Schmitges, M. Graefen, P. Perrotte, M. Menon, F. Montorsi,P. I. Karakiewicz, Distribution of metastatic sites in renal cell carcinoma: a population-based analysis, Ann Oncol. 23 (2012) 973-980.

15. M. K. Labriola, K. A. Batich, J. Zhu, M. A. McNamara, M. R. Harrison, A. J. Armstrong, D. J. George,T. Zhang, Immunotherapy Is Changing First-Line Treatment of Metastatic Renal-Cell Carcinoma, Clin Genitourin Cancer. 17 (2019) e513-e521.

16. R. J. Motzer, B. Escudier, D. F. McDermott, S. George, H. J. Hammers, S. Srinivas, S. S. Tykodi, J. A. Sosman, G. Procopio, E. R. Plimack, D. Castellano, T. K. Choueiri, H. Gurney, F. Donskov, P. Bono, J. Wagstaff, T. C. Gauler, T. Ueda, Y. Tomita, F. A. Schutz, C. Kollmannsberger, J. Larkin, A. Ravaud, J. S. Simon, L. A. Xu, I. M. Waxman, P. Sharma,Investigators CheckMate, Nivolumab versus Everolimus in Advanced Renal-Cell Carcinoma, N Engl J Med. 373 (2015) 1803-1813.

17. R. J. Motzer, N. M. Tannir, D. F. McDermott, O. Aren Frontera, B. Melichar, T. K. Choueiri, E. R. Plimack, P. Barthelemy, C. Porta, S. George, T. Powles, F. Donskov, V. Neiman, C. K. Kollmannsberger, P. Salman, H. Gurney, R. Hawkins, A. Ravaud, M. O. Grimm, S. Bracarda, C. H. Barrios, Y. Tomita, D. Castellano, B. I. Rini, A. C. Chen, S. Mekan, M. B. McHenry, M. Wind-Rotolo, J. Doan, P. Sharma, H. J. Hammers, B. Escudier,Investigators CheckMate, Nivolumab plus Ipilimumab versus Sunitinib in Advanced Renal-Cell Carcinoma, N Engl J Med. 378 (2018) 1277-1290.

18. Keith Foster, Amanda Prowse, Anke van den Berg, Stewart Fleming, Miriam M.F. Hulsbeek, Paul Crossey, Frances Richards, Paul Cairns, Nabeel A. Affara, Malcolm Ferguson-Smith, Charles H.Cm. Buys,Eamonn Maher, Somatic mutations of the von Hippel-Lindau disease tumour suppressor gene in non-familial clear cell renal carcinoma, Hum Mol Genet. 3 (1994).

19. L. Gossage, T. Eisen,E. R. Maher, VHL, the story of a tumour suppressor gene, Nature Reviews. Cancer. 15 (2015) 55-64.

20. Y. Sato, T. Yoshizato, Y. Shiraishi, S. Maekawa, Y. Okuno, T. Kamura, T. Shimamura, A. Sato-Otsubo, G. Nagae, H. Suzuki, Y. Nagata, K. Yoshida, A. Kon, Y. Suzuki, K. Chiba, H. Tanaka, A. Niida, A. Fujimoto, T. Tsunoda, T. Morikawa, D. Maeda, H. Kume, S. Sugano, M. Fukayama, H. Aburatani, M. Sanada, S. Miyano, Y. Homma,S. Ogawa, Integrated molecular analysis of clear-cell renal cell carcinoma, Nature Genetics. 45 (2013) 860-867.

21. A. C. Young, R. A. Craven, D. Cohen, C. Taylor, C. Booth, P. Harnden, D. A. Cairns, D. Astuti, W. Gregory, E. R. Maher, M. A. Knowles, A. Joyce, P. J. Selby,R. E. Banks, Analysis of VHL Gene Alterations and their Relationship to Clinical Parameters in Sporadic Conventional Renal Cell Carcinoma, Clinical Cancer Research. 15 (2009) 7582-7592.

22. F. Latif, K. Tory, J. Gnarra, M. Yao, F. M. Duh, M. L. Orcutt, T. Stackhouse, I. Kuzmin, W. Modi, L. Geil,et al., Identification of the von Hippel-Lindau disease tumor suppressor gene, Science. 260 (1993) 1317-1320.

23. W. Y. Kim,W. G. Kaelin, Role of VHL gene mutation in human cancer, J Clin Oncol. 22 (2004) 4991-5004.

24. T. Hsu, Complex cellular functions of the von Hippel-Lindau tumor suppressor gene: insights from

model organisms, Oncogene. 31 (2012) 2247-2257.

25. P. P. Kapitsinou,V. H. Haase, The VHL tumor suppressor and HIF: insights from genetic studies in mice, Cell Death Differ. 15 (2008) 650-659.

26. J. Albers, M. Rajski, D. Schönenberger, S. Harlander, P. Schraml, A. von Teichman, S. Georgiev, P. J. Wild, H. Moch, W. Krek,I. J. Frew, Combined mutation of Vhl and Trp53 causes renal cysts and tumours in mice, EMBO Mol Med. 5 (2013) 949-964.

27. T. K. Choueiri, A. P. Fay, R. Gagnon, Y. Lin, B. Bahamon, V. Brown, J. E. Rosenberg, T. E. Hutson, K. L. Baker-Neblett, C. Carpenter, Y. Liu, L. Pandite,S. Signoretti, The role of aberrant VHL/HIF pathway elements in predicting clinical outcome to pazopanib therapy in patients with metastatic clear-cell renal cell carcinoma, Clin Cancer Res. 19 (2013) 5218-5226.

28. E. Y. Wei,J. J. Hsieh, A river model to map convergent cancer evolution and guide therapy in RCC, Nat Rev Urol. 12 (2015) 706-712.

29. N. Masson,P. J. Ratcliffe, Hypoxia signaling pathways in cancer metabolism: the importance of co-selecting interconnected physiological pathways, Cancer Metab. 2 (2014) 3.

30. G. L. Semenza, HIF-1 mediates metabolic responses to intratumoral hypoxia and oncogenic mutations, J Clin Invest. 123 (2013) 3664-3671.

31. G. L. Semenza, Hypoxia-inducible factor 1: oxygen homeostasis and disease pathophysiology, Trends Mol Med. 7 (2001) 345-350.

32. R. H. Wenger, D. P. Stiehl,G. Camenisch, Integration of oxygen signaling at the consensus HRE, Sci STKE. 2005 (2005) re12.

33. A. A. Hakimi, E. Reznik, C. H. Lee, C. J. Creighton, A. R. Brannon, A. Luna, B. A. Aksoy, E. M. Liu, R. Shen, W. Lee, Y. Chen, S. M. Stirdivant, P. Russo, Y. B. Chen, S. K. Tickoo, V. E. Reuter, E. H. Cheng, C. Sander,J. J. Hsieh, An Integrated Metabolic Atlas of Clear Cell Renal Cell Carcinoma, Cancer Cell. 29 (2016) 104-116.

34. Cheng-Jun Hu, Li-Yi Wang, Lewis A. Chodosh, Brian Keith,M. Celeste Simon, Differential Roles of Hypoxia-Inducible Factor 1α (HIF-1α) and HIF-2α in Hypoxic Gene Regulation, Molecular and Cellular Biology. 23 (2003) 9361-9374.

35. R. R. Raval, K. W. Lau, M. G. Tran, H. M. Sowter, S. J. Mandriota, J. L. Li, C. W. Pugh, P. H. Maxwell, A. L. Harris,P. J. Ratcliffe, Contrasting properties of hypoxia-inducible factor 1 (HIF-1) and HIF-2 in von Hippel-Lindau-associated renal cell carcinoma, Mol Cell Biol. 25 (2005) 5675-5686.

36. Chuan Shen, Rameen Beroukhim, Steven E. Schumacher, Jing Zhou, Michelle Chang, Sabina Signoretti,William G. Kaelin, Genetic and Functional Studies Implicate HIF1α as a 14q Kidney Cancer Suppressor Gene, Cancer Discovery. 1 (2011) 222-235.

37. S. Schokrpur, J. Hu, D. L. Moughon, P. Liu, L. C. Lin, K. Hermann, S. Mangul, W. Guan, M. Pellegrini, H. Xu,L. Wu, CRISPR-Mediated VHL Knockout Generates an Improved Model for Metastatic Renal Cell Carcinoma, Scientific Reports. 6 (2016) 29032.

38. S. Zhang, X. Zhou, B. Wang, K. Zhang, S. Liu, K. Yue, L. Zhang,X. Wang, Loss of VHL expression contributes to epithelial-mesenchymal transition in oral squamous cell carcinoma, Oral Oncol. 50

(2014) 809-817.

39. Q. Zhou, T. Chen, J. C. Ibe, J. U. Raj,G. Zhou, Knockdown of von Hippel-Lindau protein decreases lung cancer cell proliferation and colonization, FEBS Lett. 586 (2012) 1510-1515.

40. A. J. Pantuck, J. An, H. Liu,M. B. Rettig, NF-kappaB-dependent plasticity of the epithelial to mesenchymal transition induced by Von Hippel-Lindau inactivation in renal cell carcinomas, Cancer Res. 70 (2010) 752-761.

41. J. Hu, S. Schokrpur, M. Archang, K. Hermann, A. C. Sharrow, P. Khanna, J. Novak, S. Signoretti, R. S. Bhatt, B. S. Knudsen, H. Xu,L. Wu, A Non-integrating Lentiviral Approach Overcomes Cas9-Induced Immune Rejection to Establish an Immunocompetent Metastatic Renal Cancer Model, Molecular Therapy. Methods & Clinical Development. 9 (2018) 203-210.

42. D. Ribatti, The chick embryo chorioallantoic membrane as a model for tumor biology, Experimental Cell Research. 328 (2014) 314-324.

43. Alexis Lawrence Romanoff, *The avian embryo; structural and functional development* (New York,: Macmillan, 1960), pp. xvi, 1305 p.

44. W. Leene, M. J. Duyzings,C. van Steeg, Lymphoid stem cell identification in the developing thymus and bursa of Fabricius of the chick, Z Zellforsch Mikrosk Anat. 136 (1973) 521-533.

45. J. B. Solomon, 'Lymphocytopoiesis and ontogeny of defined immunity in birds.', in *Foetal and neonatal immunology* (Amsterdam,: North-Holland Pub. Co., 1971), pp. xv, 381 p. with illus.

46. E. M. Janse,S. H. Jeurissen, Ontogeny and function of two non-lymphoid cell populations in the chicken embryo, Immunobiology. 182 (1991) 472-481.

47. R. Auerbach, L. Kubai,Y. Sidky, Angiogenesis induction by tumors, embryonic tissues, and lymphocytes, Cancer Res. 36 (1976) 3435-3440.

48. T. Shioda, L. L. Munn, M. H. Fenner, R. K. Jain,K. J. Isselbacher, Early events of metastasis in the microcirculation involve changes in gene expression of cancer cells. Tracking mRNA levels of metastasizing cancer cells in the chick embryo chorioallantoic membrane, Am J Pathol. 150 (1997) 2099-2112.

49. J. J. Harris, The human tumor grown in the egg, Ann N Y Acad Sci. 76 (1958) 764-769; discussion 769-774.

50. A. F. Chambers, E. E. Schmidt, I. C. MacDonald, V. L. Morris,A. C. Groom, Early steps in hematogenous metastasis of B16F1 melanoma cells in chick embryos studied by high-resolution intravital videomicroscopy, J Natl Cancer Inst. 84 (1992) 797-803.

51. R. Auerbach, L. Kubai, D. Knighton,J. Folkman, A simple procedure for the long-term cultivation of chicken embryos, Dev Biol. 41 (1974) 391-394.

52. A. Zijlstra, R. Mellor, G. Panzarella, R. T. Aimes, J. D. Hooper, N. D. Marchenko,J. P. Quigley, A quantitative analysis of rate-limiting steps in the metastatic cascade using human-specific real-time polymerase chain reaction, Cancer Res. 62 (2002) 7083-7092.

53. M. S. Ismail, U. Torsten, C. Dressler, J. E. Diederichs, S. Huske, H. Weitzel,H. P. Berlien, Photodynamic Therapy of Malignant Ovarian Tumours Cultivated on CAM, Lasers Med Sci. 14

(1999) 91-96.

54. N. Kaufman, T. D. Kinney, E. J. Mason,L. C. Prieto, Jr., Maintenance of human neoplasm on the chick chorioallantoic membrane, Am J Pathol. 32 (1956) 271-285.

55. L. C. DeBord, R. R. Pathak, M. Villaneuva, H. C. Liu, D. A. Harrington, W. Yu, M. T. Lewis,A. G. Sikora, The chick chorioallantoic membrane (CAM) as a versatile patient-derived xenograft (PDX) platform for precision medicine and preclinical research, Am J Cancer Res. 8 (2018) 1642-1660.

56. Y. Dong, B. J. Manley, M. F. Becerra, A. Redzematovic, J. Casuscelli, D. M. Tennenbaum, E. Reznik, S. Han, N. Benfante, Y. B. Chen, M. E. Arcila, O. Aras, M. H. Voss, D. R. Feldman, R. J. Motzer, N. Fabbri, J. H. Healey, P. J. Boland, M. Chawla, J. C. Durack, C. H. Lee, J. A. Coleman, P. Russo, A. A. Hakimi, E. H. Cheng,J. J. Hsieh, Tumor Xenografts of Human Clear Cell Renal Cell Carcinoma But Not Corresponding Cell Lines Recapitulate Clinical Response to Sunitinib: Feasibility of Using Biopsy Samples, Eur Urol Focus. 3 (2017) 590-598.

57. P. Fergelot, J. C. Bernhard, F. Soulet, W. W. Kilarski, C. Leon, N. Courtois, C. Deminiere, J. M. Herbert, P. Antczak, F. Falciani, N. Rioux-Leclercq, J. J. Patard, J. M. Ferriere, A. Ravaud, M. Hagedorn,A. Bikfalvi, The experimental renal cell carcinoma model in the chick embryo, Angiogenesis. 16 (2013) 181-194.

58. O. Ferician, A. M. Cimpean, S. Avram,M. Raica, Endostatin Effects on Tumor Cells and Vascular Network of Human Renal Cell Carcinoma Implanted on Chick Embryo Chorioallantoic Membrane, Anticancer Res. 35 (2015) 6521-6528.

59. M. Klingenberg, J. Becker, S. Eberth, D. Kube,J. Wilting, The chick chorioallantoic membrane as an in vivo xenograft model for Burkitt lymphoma, BMC Cancer. 14 (2014) 339.

60. Z. Zuo, T. Syrovets, Y. Wu, S. Hafner, I. Vernikouskaya, W. Liu, G. Ma, T. Weil, T. Simmet,V. Rasche, The CAM cancer xenograft as a model for initial evaluation of MR labelled compounds, Sci Rep. 7 (2017) 46690.

61. L. A. Norian, T. P. Kresowik, H. M. Rosevear, B. R. James, T. R. Rosean, A. J. Lightfoot, T. A. Kucaba, C. Schwarz, C. J. Weydert, M. D. Henry,T. S. Griffith, Eradication of metastatic renal cell carcinoma after adenovirus-encoded TNF-related apoptosis-inducing ligand (TRAIL)/CpG immunotherapy, PLoS One. 7 (2012) e31085.

62. Donald J. Giard, Stuart A. Aaronson, Wade P. Parks, George J. Todaro, Paul Arnstein, John H. Kersey,Harvey Dosik, In Vitro Cultivation of Human Tumors: Establishment of Cell Lines Derived From a Series of Solid Tumors2, JNCI: Journal of the National Cancer Institute. 51 (1973) 1417-1423.

63. Marco Gerlinger, Andrew J. Rowan, Stuart Horswell, James Larkin, David Endesfelder, Eva Gronroos, Pierre Martinez, Nicholas Matthews, Aengus Stewart, Patrick Tarpey, Ignacio Varela, Benjamin Phillimore, Sharmin Begum, Neil Q. McDonald, Adam Butler, David Jones, Keiran Raine, Calli Latimer, Claudio R. Santos, Mahrokh Nohadani, Aron C. Eklund, Bradley Spencer-Dene, Graham Clark, Lisa Pickering, Gordon Stamp, Martin Gore, Zoltan Szallasi, Julian Downward, P. Andrew Futreal,Charles Swanton, Intratumor Heterogeneity and Branched Evolution Revealed by Multiregion Sequencing, New England Journal of Medicine. 366 (2012) 883-892.

64. M. Gerlinger, S. Horswell, J. Larkin, A. J. Rowan, M. P. Salm, I. Varela, R. Fisher, N. McGranahan,

N. Matthews, C. R. Santos, P. Martinez, B. Phillimore, S. Begum, A. Rabinowitz, B. Spencer-Dene, S. Gulati, P. A. Bates, G. Stamp, L. Pickering, M. Gore, D. L. Nicol, S. Hazell, P. A. Futreal, A. Stewart,C. Swanton, Genomic architecture and evolution of clear cell renal cell carcinomas defined by multiregion sequencing, Nat Genet. 46 (2014) 225-233.

65. A. Sankin, A. A. Hakimi, N. Mikkilineni, I. Ostrovnaya, M. T. Silk, Y. Liang, R. Mano, M. Chevinsky, R. J. Motzer, S. B. Solomon, E. H. Cheng, J. C. Durack, J. A. Coleman, P. Russo,J. J. Hsieh, The impact of genetic heterogeneity on biomarker development in kidney cancer assessed by multiregional sampling, Cancer Med. 3 (2014) 1485-1492.

66. S. Turajlic, H. Xu, K. Litchfield, A. Rowan, T. Chambers, J. I. Lopez, D. Nicol, T. O'Brien, J. Larkin, S. Horswell, M. Stares, L. Au, M. Jamal-Hanjani, B. Challacombe, A. Chandra, S. Hazell, C. Eichler-Jonsson, A. Soultati, S. Chowdhury, S. Rudman, J. Lynch, A. Fernando, G. Stamp, E. Nye, F. Jabbar, L. Spain, S. Lall, R. Guarch, M. Falzon, I. Proctor, L. Pickering, M. Gore, T. B. K. Watkins, S. Ward, A. Stewart, R. DiNatale, M. F. Becerra, E. Reznik, J. J. Hsieh, T. A. Richmond, G. F. Mayhew, S. M. Hill, C. D. McNally, C. Jones, H. Rosenbaum, S. Stanislaw, D. L. Burgess, N. R. Alexander,C. Swanton, Tracking Cancer Evolution Reveals Constrained Routes to Metastases: TRACERx Renal, Cell. 173 (2018) 581-594.e512.

67. D. Neelakantan, D. J. Drasin, H. L. Ford, Intratumoral heterogeneity: Clonal cooperation in epithelial-to-mesenchymal transition and metastasis, Cell Adh Migr. 9 (2015) 265-276.

68. T. J. Mitchell, S. Turajlic, A. Rowan, D. Nicol, J. H. R. Farmery, T. O'Brien, I. Martincorena, P. Tarpey, N. Angelopoulos, L. R. Yates, A. P. Butler, K. Raine, G. D. Stewart, B. Challacombe, A. Fernando, J. I. Lopez, S. Hazell, A. Chandra, S. Chowdhury, S. Rudman, A. Soultati, G. Stamp, N. Fotiadis, L. Pickering, L. Au, L. Spain, J. Lynch, M. Stares, J. Teague, F. Maura, D. C. Wedge, S. Horswell, T. Chambers, K. Litchfield, H. Xu, A. Stewart, R. Elaidi, S. Oudard, N. McGranahan, I. Csabai, M. Gore, P. A. Futreal, J. Larkin, A. G. Lynch, Z. Szallasi, C. Swanton, P. J. Campbell,T. RACERx Renal Consortium, Timing the Landmark Events in the Evolution of Clear Cell Renal Cell Cancer: TRACERx Renal, Cell. 173 (2018) 611-623 e617.

69. J. Hu, M. Ishihara, A. I. Chin, L. Wu. Establishment of xenografts of urological cancers on chicken chorioallantoic membrane (CAM) to study metastasis, Precis Clin Med. 2(3) (2019) 140-151.

70. J. Hu, P. Tan, M. Ishihara, N. A. Bayley, S. Schokrpur, J. G. Reynoso, Y. Zhang, R. J. Lim, C. Dumitras, L. Yang, S. M. Dubinett, P. S. Jat, J. Van Snick, J. Huang, A. I. Chin, R. M. Prins, T. G. Graeber, H. Xu, L. Wu. Tumor heterogeneity in VHL drives metastasis in clear cell renal cell carcinoma, Signal Transduct Target Ther. 8(1) (2023) 155.

Chapter 3. Broader Applications of the CAM Model

Partially reprinted (adapted) with permission from:

1. Sharrow, A.C., Ishihara, M., Hu, J., Kim, I.H., Wu, L. *Using the Chick Chorioallantoic Membrane In Vivo Model to Study Gynecological and Urological Cancers.* Journal of Visualized Experiments, 2020;155:e60651. doi:10.3791/60651, copyright (2020) MyJoVE Corporation.; and
2. Flora, K.*, Ishihara, M.*, Zhang, Z., Bowen, E.S., Wu, A., Ayoub, T., Cano-Ruiz, C., Huang, J.T., Jackson, M., Reghu, K., Ayoub, Y., Zhu, Y., Tseng, H.R., Zhou, Z.H., Hu, J., Wu, L. *Exosomes from Von Hippel-Lindau-Null Cancer Cells Promote Metastasis in Renal Cell Carcinoma.* International Journal of Molecular Sciences, 2023;24:17307 doi:10.3390/ijms242417307, copyright (2023) MDPI. *Equal contribution.

ABSTRACT

CAM has many more applications beyond RCC PDX. This chapter explores the usage of CAM in non-RCC cancer engraftments and exosome studies. First, we have successfully engrafted gynecological (ovarian) and urological cancers (prostate and bladder) of both mouse and human origin in the CAM. Of those, the results of urological cancers are shown here, including gross CAM pictures, bioluminescent imaging (BLI), and histological analyses. In the second part of the chapter, we show how CAM has accelerated the mechanistic study of the RCC cooperative metastasis. Flora and Ishihara et al. (under revision) have explored how exosomes, multifunctional extracellular cargos, are involved in the intratumoral pro-metastatic crosstalk between VHL(+) and VHL(-) cells. The *in ovo* study using CAM is excerpted here, showing how the model strongly supported their hypothesis by providing a rapid animal system.

3.1. INTRODUCTION

Urological cancers (kidney, prostate, and bladder cancers) constitute 19% of all cancer cases in the United States and 11% of cancer-related deaths [1]. Thus, a novel in vivo approach to study urological cancers could save a laboratory considerable time, labor, and money, even if this model is only applied to initial screening experiments. Additionally, the resulting acceleration of research findings could significantly impact the 177,000 individuals diagnosed with these cancers annually. Therefore, we sought to optimize the CAM model for the engraftment of urological cancers. Due to the immunocompromised status of the early chicken embryo [2], both mouse and human cells can be readily implanted. As such, we have successfully engrafted kidney, prostate, and bladder cancers. For each of these tumor types, the CAM readily accepts established murine and/or human tumor cell lines. Each of these cancer types and cell sources requires optimization, which we share here.

Exosomes are a type of extracellular vesicles secreted by a wide range of cell types that can act locally or disperse via circulation and act at distant sites [3–5]. Exosomes can carry distinct cargos containing cell- and environment-specific bioactive materials to transmit instructive signals between cells [3], altering gene expression and cellular pathways and functions in recipient cells. A large amount of evidence showed that exosomes produced by different cells in the tumor microenvironment, such as stroma, macrophages, and cancer cells themselves, can facilitate metastasis [6–9]. One of the explanations is that, in hypoxic environments like tumors, cells produce increased exosomes compared to cells in a normoxic environment [10]. Hypoxia-derived exosomes regulate the expression of genes associated with angiogenesis, epithelial-to-mesenchymal transition (EMT), and metastasis, adapting the cells to the hypoxic environment by promoting their motility, escape and survival of the unfavorable condition [10–11]. Due to the absence of a functioning pVHL to down-regulate the hypoxic response, VHL(-) cells are in a pseudo-hypoxic state and produce more exosomes than their counterparts [25]. As a result, exosomes originating from VHL(-) cells may act as a driver of metastasis in heterogeneous ccRCC tumors. Therefore, this study assessed the functional capabilities of exosomes from VHL(+) and VHL(-) cells to understand their contribution to the pro-metastatic cross communication in heterogeneous ccRCC tumors.

All of the experiments presented herein were reviewed and approved by the appropriate ethical committees at the University of California, Los Angeles (UCLA). The use of deidentified, primary human tumors has been approved by the UCLA Institutional Review Board (Protocol numbers 17-000037, 17-001169, and 11-001363). At UCLA, Animal Research Committee review is not required for experiments using chicken embryos; protocol approval is only required when the eggs will be hatched. However, best practices, such as the AVMA Guidelines for the Euthanasia of Animals, were used to handle chicken embryos ethically and to avoid pain as much as possible. Researchers are urged to verify the oversight requirements at their institution prior to initiating studies using CAM models.

3.2. NON-RCC UROLOGICAL CANCERS

Thus far, we have found this method of implantation to be successful for kidney, prostate, and bladder cancers. Each was optimized to identify specific conditions for implantation, although there may be flexibility. Multiple human and murine prostate cancer cell lines were tested for CAM engraftment (Fig. 3.1). Each grew well when 2 x 10^6 cells were implanted using the nonstick ring. Histological evaluation of the resulting tumors was consistent with expectations for each cell line. Additionally, implantation of cells stably marked with firefly luciferase permitted tumor identification with bioluminescence imaging (Fig. 3.1A).

Bladder cancer was established in the CAM model from established cell lines and pieces of primary human tissue (Fig. 3.2). Cell lines grew well when implanted with 2 x 10^6 cells without the nonstick ring (Fig. 3.2A, B), although implantation with the ring was successful. Primary human tumor may be implanted from pieces of tissue (Fig. 3.2C). The presented case originated from a patient with high grade, non-muscle-invasive, urothelial carcinoma. Implantation of digested cells has not yet been attempted due to ongoing tumor digestion optimization. Cancer cells of the resulting CAM tumors retained the morphology of the original tumor, but with an altered stromal component. Tumor growth was less than for renal cell carcinoma and prostate cancer, though still readily visible.

3.3. EXOSOME STUDY

Exosomes are extracellular vesicles that modulate essential physiological and pathological signals. This study investigates whether exosomes mediate the metastatic crosstalk between VHL(+) and VHL(-). Exosomes isolated from paired VHL(+) and VHL(-) cancer cell lines were assessed for physical, biochemical, and biological characteristics.

3.3.1. Exosome Uptake

First, we assessed the physical uptake of VHL(-) exosomes into the VHL(+) cells that initiates the pro-metastatic cross-communication. To ascertain the uptake process, VHL(-) exosomes were stained with PKH67. After a 24-hour incubation with the exosomes, two-dimensional images show exosomes within the boundary of the cell, as the green fluorescence (PKH67) is localized within the cytoplasm instead of at the cell membrane where red fluorescence staining of fibrous actin in the cytoskeleton is prevalent (data not shown). To confirm that exosomes are internalized and localized near the nucleus (DAPI, blue), three-dimensional imaging was performed (Fig. 3.3). Separation of z-axis layers into upper, middle, and lower x-y images show that the highest presence of green exosomes can be seen near the blue, DAPI-stained nucleus as when the red, F-actin-stained cytoskeleton is in primary view in the lower layer, there is much less green fluorescence than upper and middle layers (Fig. 3.3A). By selecting smaller sections of the original images, a clearer view of exosome internalization can be observed (Fig. 3.3B). Within the upper, middle, and lower x-y images through the z-dimension, one can see that peak green exosome fluorescence appears with peak blue nucleus fluorescence. Additionally, when rotated about the x-axis to view the z-dimension, this further corroborates that the exosome signal appears at the same dimension as the nucleus and within the boundaries of the red cytoskeleton. These images suggest that 24 hours is sufficient for the internalization of exosomes into the cell for both the RENCA and ACHN cell lines.

3.3.2. VHL(-) Exosomes Promote RCC Metastasis in Ovo

Next, we assessed the impact of exosome treatment on *in ovo* tumor growth and metastasis in a duck chorioallantoic membrane model (dCAM). The dCAM model has a short tumor growth window of two weeks after implantation, an adequate time for aggressive tumor cells to escape form the primary tumor and disseminate via circulation to distant organs and establish micro-metastases in the embryo (Fig. 3.4A). RC-VHL(+) cells were treated with no exosomes, RC-VHL(+) exosomes, or RC-VHL(-) exosomes, given three times throughout the remaining developmental window, from developmental day 14 to day 28. On the day of euthanasia, after 14 days of tumor growth, the average size of primary tumors and liver metastases were analyzed. Liver is the most vascularized organ of the embryo and have high potential as a metastatic site. This differs from clinical RCC in humans, where lung metastasis is the most common metastatic site [12,13]. This difference is because the embryonic lungs have not inflated and are less vascularized than the liver prior to hatching, consequently less likely to be a metastatic site [14].

The average weights of RC-VHL(+) CAM tumor after a 14-day incubation were 0.6 g, 0.5 g, and 0.75 g for the PBS, RC-VHL(+)-exo, and RC-VHL(-)-exo treatment groups, respectively, and did not reach a statistical significance (Fig. 3.4B). This result was consistent with the findings of in vitro proliferation assays (data not shown). The extent of murine RC cells metastasized to the liver was assessed by the ratio of murine to avian DNA using quantitative PCR (Fig. 3.4C). Both the control RC-VHL(+) cell-only group and the RC-VHL(+)-exo treatment group showed no detectable level of mouse β-actin DNA. Only the RC-VHL(-)-exo treated group showed a detectable level of mouse DNA in the duck embryo liver, significantly higher than the other two treatment groups. These results corroborate the *in vitro* data where exosomes from VHL(-) but not VHL(+) cells are able to induce more migratory and invasive behaviors of VHL(+) cells (data not shown). Moreover, the *in vitro* phenotypic changes directly contribute to metastatic function *in vivo*, leading to distant metastases and completing the full metastatic cascade in the animal model.

3.4. DISCUSSION

Tumor expansion and engraftment using the CAM model permits more rapid and directly observable tumor growth than existing *in vivo* animal models. The initial, immunocompromised state of

chicken embryos readily permits engraftment of human and murine tissue. Even with these strengths, the CAM model does have limitations. Although all the tumor types we presented engraft into the CAM model, they do so with varying degrees of growth. Tumor growth and speed would need to be assessed for a particular tumor type to determine if the CAM would be a suitable experimental model.

This study is also a follow-up of our prior study to ask whether exosomes produced by VHL(-) cells could also be driving metastatic progression in ccRCC. In summation, the answer to this inquiry is clearly positive. the functional capabilities of the exosomes produced by each cell type are distinctly different. Treating VHL(+) cells with VHL(-) exosomes leads to changes consistent with EMT, resulting in increased EMT markers such as N-cadherin, α-SMA, and MMP-9, and increased migration and invasiveness ability *in vitro* (data not shown) and metastasis to distant organs *in vivo*. This work clearly supports that exosomes can serve as a means of pro-metastatic cross-communicator between different cell populations to achieve cooperative metastasis in ccRCC.

Future applications of this model system depend on the hypothesis to be tested. For example, these tumor grafts could be used to test novel therapeutic approaches to reduce tumor size or deplete a subpopulation of the tumor. Co-implantation with cells from the host tumor microenvironment could permit studies of the influence of these cells on a variety of parameters, including tumor growth and treatment resistance. These applications have yet to be tested, but warrant further exploration.

The authors wish to thank Dr. Fuyuhiko Tamanoi and Binh Vu for the initial training on this method. Discussions with Dr. Eva Koziolek have been instrumental in optimizing this approach and have been very much appreciated. We also thank members from Dr. Hsian-Rong Tseng Lab (University of California, Los Angeles, CA, UCLA), Jing Wang and Wenxi Xia, for providing much support in DLS analysis and TEM imaging of exosomes. Additional TEM imaging was completed by Judith Su from Dr. Z Hong Zhou Lab (University of California, Los Angeles, CA, UCLA). This work would not have been possible without funding from the following sources: the Tobacco-Related Disease Research Program Postdoctoral Fellowship (27FT-0023, to ACS), the Department of Defense (DoD) Ovarian Cancer Research Program (W81XWH-17-1-0160), NCI/NIH (1R21CA216770), Tobacco-Related Disease Research Program High

Impact Pilot Award (27IR-0016), DoD Kidney Cancer Research Program (grant number W81XWH-20-1-0918 and HT94252310858), UCLA institutional support, including a JCCC Seed Grant (NCI/NIH P30CA016042) and a 3R Grant from Office of the Vice Chancellor for Research to LW, and the UCLA Clinical and Translational Science Institute (grant number UL1TR001881) to ZHZ and LW.

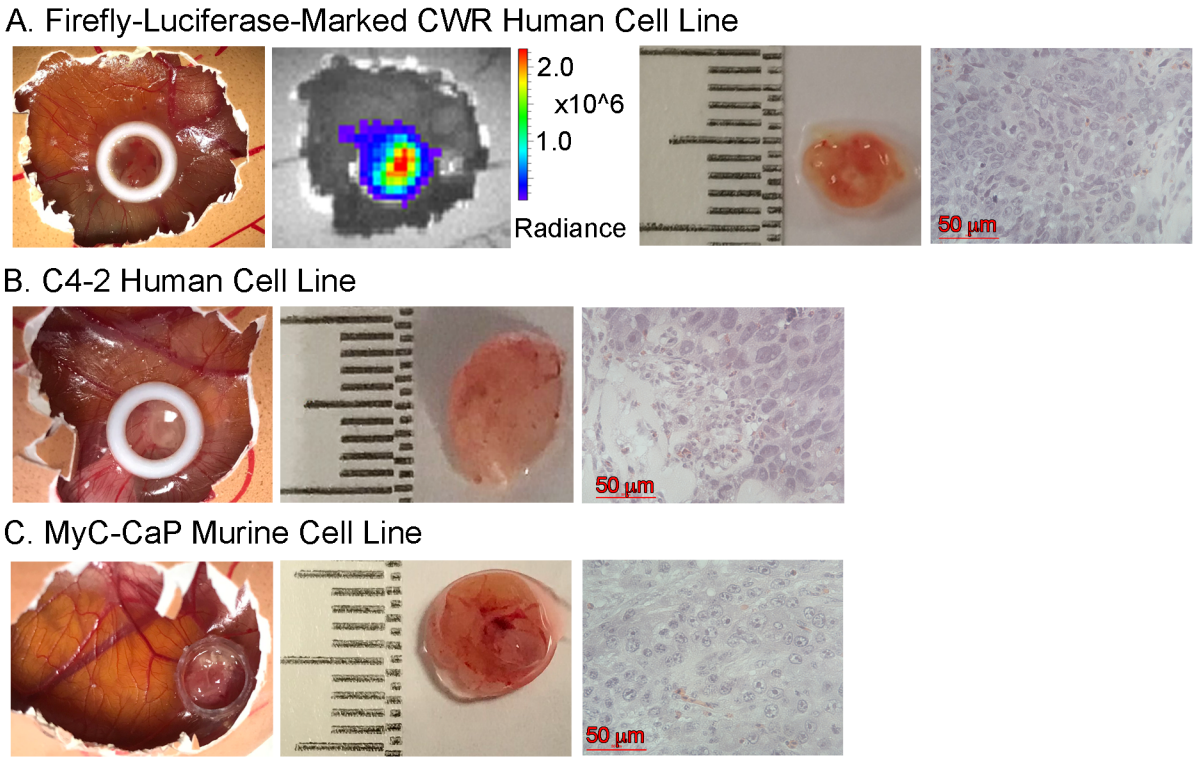


Figure 3.1 Representative tumor development from prostate cancer cell lines. Representative tumors and hematoxylin and eosin staining resulting from the implantation of the human prostate cancer cell lines (**A**) CWR and (**B**) C4-2 along with the murine cell line (**C**) MyC-CaP. Bioluminescence imaging of the resulting tumors from firefly luciferase marked CWR cells is shown in (**A**). The measurement scale adjacent to the excised tumors shows 1 mm markings.

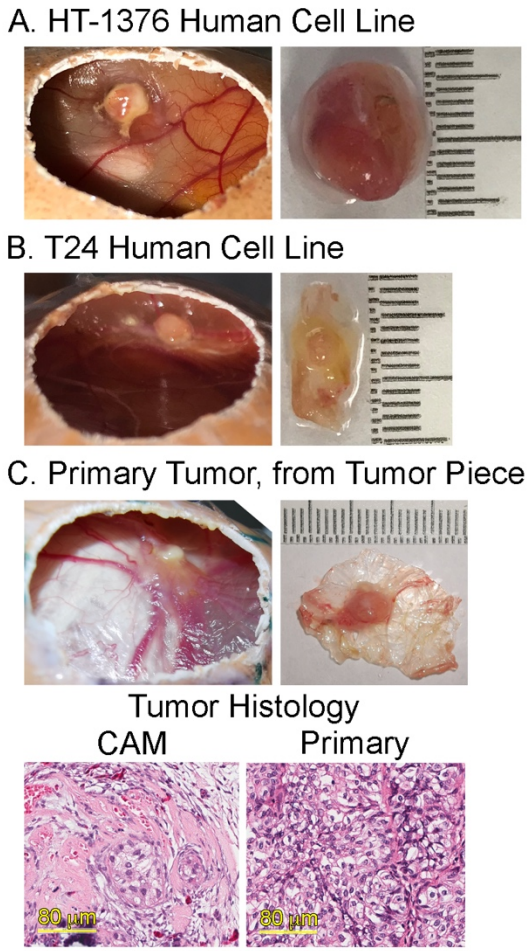


Fig. 3.2 Representative tumor development from bladder cancer. Representative tumors resulting from the implantation of the established human bladder cancer cell lines (**A**) HT-1376, (**B**) T24, and (**C**) primary human bladder tumor. In (**C**), hematoxylin and eosin staining of the resulting CAM tumor and the primary tumor are shown. The measurement scale adjacent to the excised tumors shows 1 mm markings.

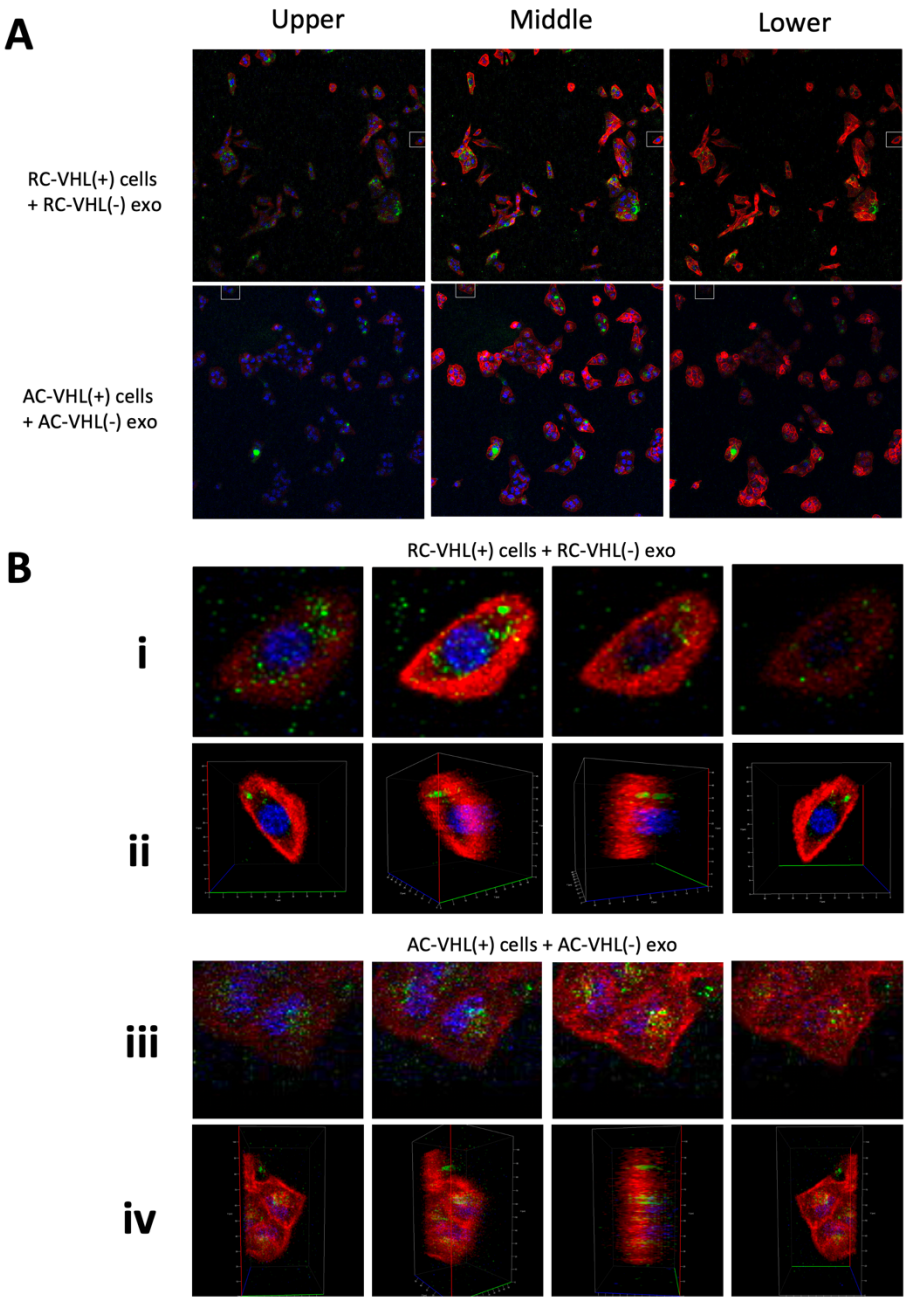


Fig. 3.3 VHL(-) exosomes are internalized into VHL(+) cells. Three-dimensional confocal imaging of (A) RC-VHL(+) cells with RC-VHL(-) exosomes and AC-VHL(+) cells with AC-VHL(-) exosomes shown as layers moving through z plane from upper to lower view. White boxes are used for closeups of small cell clusters in (B), in i and iii, layers of the z plane, and ii and iv, rotation about the x-axis. Confocal imaging was completed at 10x magnification.

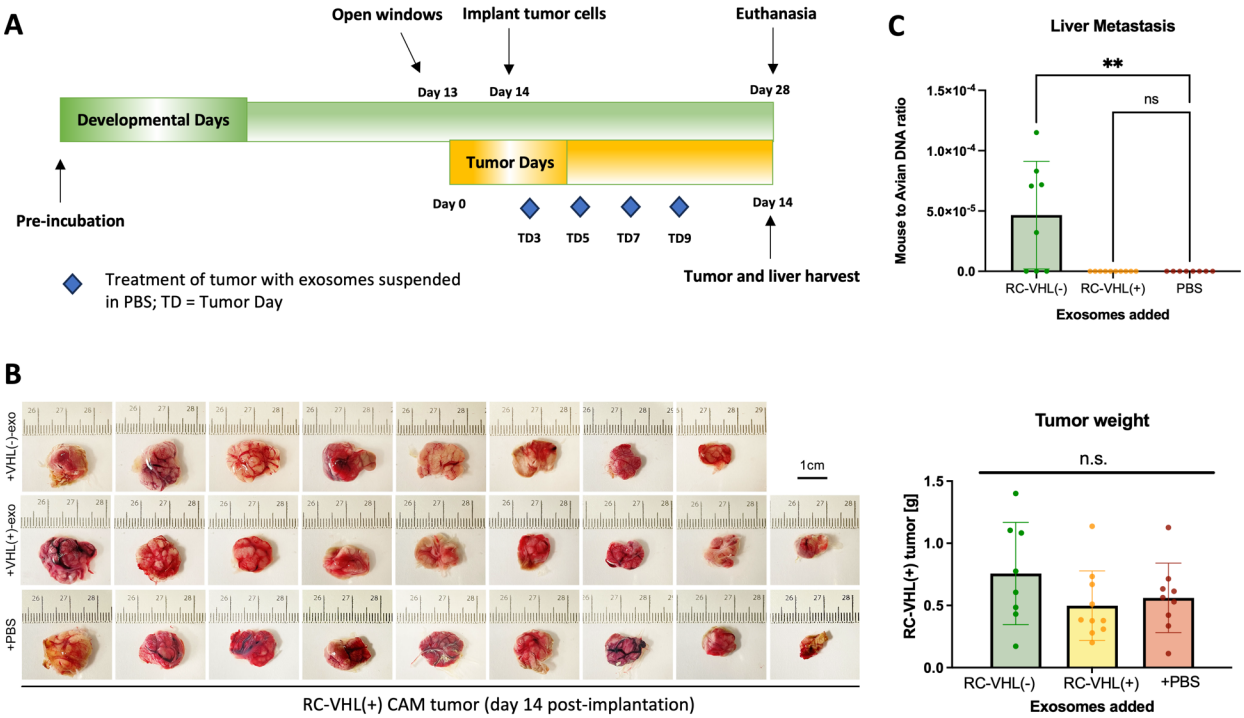


Fig. 3.4 VHL(+)-exo induces distant metastases of VHL(+) tumors in an animal model. (**A**) Schema of the dCAM model. (**B**) Gross pictures of RC-VHL(+) tumors formed in dCAM and their weight analysis. (**C**) qPCR analysis of dCAM livers measuring mouse to avian β-actin ratio, indicative of distant metastases. Statistical analysis was completed using (**A**) ordinary one-way ANOVA and (Dunnett's test (**$p < 0.01$, ns: not significant).

3.5. REFERENCES

1. Howlader, N. et al. SEER Cancer Statistics Review, 1975-2016. National Cancer Institute. Bethesda, MD, https://seer.cancer.gov/ csr/1975_2016/ based on November 2018 SEER data submission, posted to the SEER web site, April (2019).

2. Ribatti, D. The chick embryo chorioallantoic membrane as a model for tumor biology. Experimental Cell Research. 328 (2), 314-324 (2014).

3. Sun, Z.; Wang, L.; Dong, L.; Wang, X. Emerging Role of Exosome Signalling in Maintaining Cancer Stem Cell Dynamic Equi-librium. J. Cell. Mol. Med. 2018, 22, 3719–3728, doi:10.1111/jcmm.13676.

4. Maia, J.; Caja, S.; Moraes, M.C.S.; Couto, N.; Costa-Silva, B. Exosome-Based Cell-Cell Communication in the Tumor Microen-vironment. Front. Cell Dev. Biol. 2018, 6, 18, doi:10.3389/fcell.2018.00018.

5. Willms, E.; Cabañas, C.; Mäger, I.; Wood, M.J.A.; Vader, P. Extracellular Vesicle Heterogeneity: Subpopulations, Isolation Techniques, and Diverse Functions in Cancer Progression. Front. Immunol. 2018, 9, 738, doi:10.3389/fimmu.2018.00738.

6. Xu, R.; Rai, A.; Chen, M.; Suwakulsiri, W.; Greening, D.W.; Simpson, R.J. Extracellular Vesicles in Cancer — Implications for Future Improvements in Cancer Care. Nat. Rev. Clin. Oncol. 2018, 15, 617–638, doi:10.1038/s41571-018-0036-9.

7. Xie, Z.; Gao, Y.; Ho, C.; Li, L.; Jin, C.; Wang, X.; Zou, C.; Mao, Y.; Wang, X.; Li, Q.; et al. Exosome-Delivered CD44v6/C1QBP Complex Drives Pancreatic Cancer Liver Metastasis by Promoting Fibrotic Liver Microenvironment. Gut 2022, 71, 568–579, doi:10.1136/gutjnl-2020-323014.

8. Fang, T.; Lv, H.; Lv, G.; Li, T.; Wang, C.; Han, Q.; Yu, L.; Su, B.; Guo, L.; Huang, S.; et al. Tumor-Derived Exosomal MiR-1247-3p Induces Cancer-Associated Fibroblast Activation to Foster Lung Metastasis of Liver Cancer. Nat. Commun. 2018, 9, 191, doi:10.1038/s41467-017-02583-0.

9. Zhang, Z.; Hu, J.; Ishihara, M.; Sharrow, A.C.; Flora, K.; He, Y.; Wu, L. The MiRNA-21-5p Payload in Exosomes from M2 Macrophages Drives Tumor Cell Aggression via PTEN/Akt Signaling in Renal Cell Carcinoma. Int. J. Mol. Sci. 2022, 23, 3005, doi:10.3390/ijms23063005.

10. Shao, C.; Yang, F.; Miao, S.; Liu, W.; Wang, C.; Shu, Y.; Shen, H. Role of Hypoxia-Induced Exosomes in Tumor Biology. Mol. Cancer 2018, 17, 120, doi:10.1186/s12943-018-0869-y.

11. Bister, N.; Pistono, C.; Huremagic, B.; Jolkkonen, J.; Giugno, R.; Malm, T. Hypoxia and Extracellular Vesicles: A Review on Methods, Vesicular Cargo and Functions. J. Extracell. Vesicles 2020, 10, e12002, doi:10.1002/jev2.12002.

12. Dudani, S.; Velasco, G. de; Wells, J.C.; Gan, C.L.; Donskov, F.; Porta, C.; Fraccon, A.; Pasini, F.; Lee, J.L.; Hansen, A.; et al. Evaluation of Clear Cell, Papillary, and Chromophobe Renal Cell Carcinoma Metastasis Sites and Association With Survival. JAMA Netw. Open 2021, 4, e2021869, doi:10.1001/jamanetworkopen.2020.21869.

13. Xue, J.; Chen, W.; Xu, W.; Xu, Z.; Li, X.; Qi, F.; Wang, Z. Patterns of Distant Metastases in Patients with Clear Cell Renal Cell Carcinoma—A Population-based Analysis. Cancer Med. 2021, 10, 173–

187, doi:10.1002/cam4.3596.

14. Ishihara, M.; Hu, J.; Zhang, X.; Choi, Y.; Wong, A.; Cano-Ruiz, C.; Zhao, R.; Tan, P.; Tso, J.L.; Wu, L. Comparing Metastatic Clear Cell Renal Cell Carcinoma Model Established in Mouse Kidney and on Chicken Chorioallantoic Membrane. J. Vis. Exp. 2020, doi:10.3791/60314.

Chapter 4. Small Molecule Approach to Find Novel Therapeutics against Metastatic RCC

ABSTRACT

Loss of VHL is the unique hallmark of ccRCC, and our previous studies suggest that the VHL (-) cells induce metastasis-driving effects on VHL(+) cells. A high-throughput screening (HTS) was conducted to find small molecules that selectively inhibit the growth and survival of VHL (-) cells. Statins came out as the sole hits, but not all statins had the same level of cytotoxicity. Therefore, the first aim of this chapter is to discover the mechanism of action (MOA) that explains the VHL(+) vs. VHL(-) sensitivity difference, as well as the intra-statin efficacy difference. Among the components of the mevalonate pathway, the HMGCR/cholesterol arm was dispensable, whereas mevalonate and GGPP were not. HIF or EMT may explain the differential sensitivity of VHL(+) vs. VHL(-) RCC, TNBC vs. non-TNBC breast cancer, and NEPC vs. adenocarcinoma prostate cancer, suggesting statin's potential as the pan-cancer anti-metastatic reagent. Further validation is necessary, but sequencing suggested MYC targets, DNA repair, or E2F targets were upregulated in the statin-sensitive lines and may be crucial in MOA. From the medicinal chemistry perspective, the 3,5-dihydroxyheptenoic acid part of statins and stereochemistry were essential. Completion of this project will lead to the development of a novel, pan-cancer anti-metastatic reagent, which will tremendously improve the current poor prognosis of deadly tumors.

4.1. INTRODUCTION

High-throughput screening (HTS) is a common approach to finding new small-molecule therapeutics in the pharmaceutical industry. It was not common in the academic setting due to lack of resources, but institutions like Molecular Screening Shared Resources (MSSR) at UCLA introduced the approach and produced fruitful results [1]. Drug libraries can be divided into two categories: approved drugs with known pathways ("repurposing libraries") and novel compounds without established knowledge about their pathway. Each has pros and cons. The repurposing library is much smaller than the latter and thus limits the usefulness of HTS, but its known MOA helps investigate more about biology, while the hits

found through the novel compound library may take longer to find out the drug target and MOA. Therefore, the repurposing library was used to find small molecules that could specifically inhibit the metastatic driver, VHL(-) RCC cells, and thus suppress metastasis.

Transdifferentiation is a concept where tumors originating from different organ sites possessing various genomic or cellular characteristics diverge into a common type as they progress into more aggressive types. RCC is a relatively uncommon disease, but its metastatic mechanism (pseudo-hypoxia, EMT) could be shared across different cancer types. To test this and increase the potential clinical impact of this project, the HTS hits were tested in two other aggressive tumor types: triple-negative breast cancer (TNBC) and neuroendocrine prostate cancer (NEPC). Statins were most studied in breast cancer, including clinical trials, or it will produce more insight. TNBC is a genetic characteristic like VHL, while NEPC is mainly caused by treatment. Still, they shared the same phenotype, indicating the wide usage of statins in aggressive tumors caused by genetics or therapy.

4.2. MATERIALS AND METHODS

4.2.1. Cell line

VHL(+) and VHL(-) cells were generated previously [2,3]. Briefly, the original RENCA cell line was obtained from ATCC. Retroviral transfection was conducted to create RENCA-FL (firefly luciferase) [4,5]. Then, non-integrating CRISPR-Cas9 was employed to create RC (NIC1) = VHL-WT and RVN (NIC5) = VHL-KO lines using gRNA RLuc2 (Renilla luciferase, neg-control) and mVHL1 (mouse VHL plasmid 1), respectively. Cells underwent puromycin and clonal selection [3,6] (Suppl. Fig. S1A). VHL-WT and VHL-KO cells underwent another lentiviral transfection to be tagged with FLAG and RFP or GFP, respectively. These tags were connected to the N-terminus of the CMV promoter, making these tags ubiquitously expressed in the cells. Flow cytometry was used to sort RFP+ or GFP+ cells, establishing VHL(+) and VHL(-) cells, respectively (Suppl. Fig. S1B). The plasmids used for these transfections were obtained from Addgene (Suppl. Fig. S1C, D). The resulting cells have low expression of Cas9, allowing stable growth of these cells in immunocompetent mice, and sequencing results confirmed VHL knockout

in RVN(NIC5) = VHL(-) cells [3] (Suppl. Fig. S1E, F). A summary table of cell line information is available in [6]. HIF1, 2, and 1/2 CRISPR knockout on VHL(-) were done like above, except that only selection clonal selection was done but not antibiotic selection.

Three human RCC lines were from the following sources: RCC4 was a generous gift from Dr. Brian Shuch; 786O was obtained from ATCC; and #18 was from a patient tumor. All the prostate and breast cancer lines were a generous gift from Drs. Tanya Stoyanova and Dennis Slamon.

4.2.2. High-throughput screening (HTS) setup

The seeding cell number, DMSO concentration, and 2-DG (positive control) concentration were optimized via gradient testing (Suppl. Fig. S2). Total cell number of 3000/well mix population VHL(-): VHL(+) = 2:1, DMSO concentration of 0.5% (v/v), and 2-DG concentration of 1% (v/v) were used. To prepare the screening plates, 25μL of appropriate complete media was first distributed in columns 1-22 of 11 black-lid 384-well plates (Greiner Bio-One, #781091) using a MultiFlo Fx (BioTek). Using the same machine, columns 23-24 filled 25μL of complete media with 1% (v/v) 2-DG. These plates were next pinned by BioMek FX (Beckman Coulter) with 250 nL of the MSSR Repurposing Libraries containing 2,530 FDA-approved small molecules (LOPAC 1-4, NIHII 1-3, NPW 1-4; final concentration of drug = 5μM). 25L of cell-containing complete media was added to each well using MultiFlo Fx; then, cells were incubated for 48h at the normal cell culturing condition. On the day of imaging, the stock Hoechst 33342 at 1.25μg/mL (1000x) concentration was diluted to 7.5 ng/mL (6x) and added 10μL to each well containing 50μL cells + complete media + drug. After a 45-minute incubation, an automated imaging system (ImageXpress Confocal, Molecular Devices) was used to image for three fluorescent colors: TexasRed (VHL(+)), GFP (VHL(-)), and Hoechst (nucleus).

4.2.3. HTS validation and IC_{50} determination

HTS results were validated with MTS and hit-pick assays. MTS was done in 96-well plates with 4000 VHL(+) and 3000 VHL(-) cells plated separately with four doses of each drug (1.25, 2.5, 5, and 10μM)

for 48h. Hit-pick assays were done at MSSR using the same setting as described above for the HTS setup, except for each drug having triplicates instead of a single well and the cell number adjusted to 1500/well from 3000/well. IC_{50} determination followed hit-pick assays. 20-step titration ranging from 95.4pM to 50μM (each step = 1:1 dilution) was used for each hit validated in the above assays. In addition to MultiFlo Fx, Multidrop384 (Thermo LabSystems) was used as a liquid handler. Human cell lines were incubated between 72h and 6 days, depending on the cell line.

4.3. RESULTS

4.3.1. Statins are the only hits in the HTS

A ratiometric black-box approach was used to identify selective modulators of cell growth and survival of murine VHL(-) RCC cell lines without affecting VHL(+) cells (Fig. 3.1A). 2DG is used as the positive control because VHL(-) cells are more glycolytic and thus more sensitive to 2DG than VHL(+) counterparts. (Suppl. Fig. S2B) [7]. Out of 2,530 small molecules tested, the initial HTS data mining with CDD Vault revealed 33 compounds that selectively decreased %GFP, indicative of VHL(-)-specific inhibitors (Suppl. Fig. S3A; bottom black box). Of note, although this HTS assay was designed to find VHL(-)-specific inhibitors, the analysis parameters can be adjusted to discover other interesting compounds that can, for example, increase %GFP, promote the growth of either cell line, or show cytotoxicity for both cell lines (Suppl. Fig. S3A; top green, right blue, and left red boxes, respectively). Compounds that increased %GFP (Suppl. Fig. S3A; top green) were especially interesting, as they either showed either VHL(+)-specific toxicity or the "yellow dots" phenomenon represented in Suppl. Fig. S3A, sunitinib. These compounds were elaborated further in the Discussion section.

Of the 33 compounds found in CDD Vault, the majority were false positives that didn't satisfy the visual criteria of VHL(-)-specific toxicity (Suppl. Fig. S3B and Fig. 3.1B-D). Only nine compounds proceeded with hit picks (repeat of 5μM, 48hr incubation) (Suppl. Fig. S3C, Fig. 3.1C simvastatin, and Fig. 3.1D fluvastatin). Then, only seven proceeded with IC_{50} validation, where three of them were excluded due to no efficacy (tolazoline), general toxicity (cladribine), or compound unavailability (thimerosal) (Suppl.

Fig. S3D, E). Interestingly, STITCH pathway analyses predicted stronger connections among the seven hits that proceeded to IC_{50} validation than talampicillin or olopatadine, which were excluded before this step (Suppl. Fig. S3F). Four compounds left at the end were compactin (mevastatin), simvastatin, lovastatin, and fluvastatin, and their pathways are strongly interconnected (Suppl. Fig. S3F; green area), as they belong to the same drug family and target the same molecule, HMG-CoA reductase (HMGCR).

4.3.2. Not all statins work the same way

Statins are very common and affordable cholesterol-lowering drugs prescribed worldwide to prevent cardiovascular diseases in high-risk patients [8–10]. Binding to HMGCR, the rate-limiting step of cholesterol synthesis through the mevalonate pathway, statins can induce cholesterol uptake in cells, especially in hepatic cells, and help decrease blood cholesterol. There are two major classes of statins: fungal-derived and synthetic. Older statins (mevastatin, lovastatin, and pravastatin) are fungal-derived natural statins, simvastatin is semi-synthetic derived from lovastatin, and anything newer is fully synthetic (fluvastatin, cerivastatin, atorvastatin, rosuvastatin, and pitavastatin) [11]. Their chemical structures are quite variable, but due to their shared HMG-CoA-like structure first discovered in mevastatin, they're classified as one family. Out of all statins, everything except for mevastatin has been used in the clinic, but cerivastatin was voluntarily withdrawn in the 2000s due to severe side effects [12]. The most commonly used statins were atorvastatin (Lipitor from Pfizer) before the end of their market exclusivity [13], and in general, newer statins have better cholesterol-lowering ability [14].

Our HTS revealed that all hits were statins (mevastatin, lovastatin, simvastatin, and fluvastatin). Among the 2,530 compounds tested were also pravastatin and atorvastatin; however, these two statins did not suppress VHL(-) or VHL(+) cells (Fig. 3.1D). To determine the IC_{50} of all statins, 20-step titration ranging from 95.4pM to 50μM (each step = double concentration) was applied to the same well setting as the HTS. Remarkably, compared to the most potent fluvastatin (IC_{50} = 0.61μM), atorvastatin was about five times less effective (IC_{50} = 3.2μM), while rosuvastatin was 28 times less effective (IC_{50} = 17μM), respectively, against VHL(-) cells (Fig. 3.1E). Pravastatin was the least effective and didn't even reach 50%

inhibition within the tested range. Though VHL(+) cells were 3-4 times more resistant than VHL(-), the general rank order of statins was preserved, where fluvastatin and simvastatin were most effective (IC_{50} = 1.9 and 2.5μM), while atorvastatin, rosuvastatin, and pravastatin were least effective (IC_{50} = 12μM, 79μM, and not reached) (Suppl. Fig. S3G). This variation can be observed as early as at 24h using MTS assay (Suppl. Fig. S3H). This rank order was observed in three human cell lines: 786O, RCC4, and #18 (patient-derived primary cells), all lacking functional VHL (Fig. 3.1F). Thus, newer statins, such as atorvastatin and rosuvastatin, had less efficacy in VHL(-) inhibition despite improved cholesterol-lowering ability. This result suggests that statins' VHL(-) inhibition may be through a distinct pathway from their primary cholesterol-lowering mechanism, as the preceding literature implies [15].

4.3.3. MOA study reveals cholesterol is not relevant, but other mevalonate pathway arms may be

To elucidate the mechanism of action (MOA) of statins' cytotoxicity against VHL(-), we first asked if the HMGCR expression level is heightened in VHL(-) cells, thus making them more sensitive to HMGCR inhibition by statins. Both at protein and mRNA levels, however, HMGCR expression was lower in VHL(-) than in VHL(+) cells (Fig. 3.2A). In concert with this, HMGCR knockdown in VHL(-) didn't affect cell growth or statin sensitivity (Fig. 3.2B-D and Suppl. Fig. S4A). Of note, complete knockout of HMGCR was lethal, so a doxycycline-inducible HMGCR-knockdown line was generated from VHL (-) cells and used. Next, we asked if VHL (+)'s resistance to statins and the ineffectiveness of some statins was due to drug uptake. If that's the case, the synthetic cholesterol level would be stable upon statin treatment. Lipidomics data revealed a contradictory result where all statin treatments in VHL(+) cells significantly lowered synthetic cholesterol levels. On the other hand, VHL(-) showed unaltered or even higher cholesterol synthesis upon stain treatments, depending on which statin (Fig. 3.2E). This discrepancy was also overserved at the total cholesterol level, where VHL(+) was unaltered, whereas VHL(-) treated with fluvastatin and simvastatin had a higher total cholesterol (Suppl. Fig. S4B). Statin concentration may need to be adjusted because the cell number measurement suggested that the used concentration was already toxic to VHL(-) (Suppl. Fig. S4C).

Next, several rescue and synergy experiments were conducted. Squalene, the precursor of cholesterol in the mevalonate pathway, was added to VHL(-) treated with fluvastatin but did not rescue (Fig. 3.2F). The squalene concentration used here was much lower than those reported previously due to its toxicity to our cells [15] (Suppl. Fig. S4D). Similarly, adding rosuvastatin to fluvastatin treatment did not rescue VHL (-) cells from dying (Fig. 3.2G). Because rosuvastatin's affinity to HMGCR is 8-fold higher than fluvastatin [16], co-treatment with these two statins should prevent fluvastatin from binding HMGCR and thus save cells if HMGCR is the sole binding target. Rather, the two statins showed synergy and enhanced cytotoxicity against VHL(-), again suggesting the existence of a novel target of fluvastatin. The same observation was made with co-treatment with fluvastatin, atorvastatin, and rosuvastatin in VHL(-) but not in VHL(+), most likely because the drug concentration was too low (Suppl. Fig. S4E).

As the literature suggests, the mevalonate pathway has arms other than cholesterol [17]. Even though HMGCR and cholesterol were inferred dispensable above, other intermediates, such as mevalonate and GGPP, were not (Fig. 3.2H) as the preceding literature suggested [15]. Additionally, a clinically approved antiplatelet medicine, dipyridamole (DP), has been shown to synergize with statin by inhibiting the SREBP-mediated feedback loop of the mevalonate pathway [18]. In concordance with this, DP potentiates fluvastatin against VHL (+) cells, originally resistant to statins, to the same level as VHL(-), which also showed DP and fluvastatin synergy (Fig. 3.2I). Atorvastatin was also potentiated against VHL (-) cells, which were not very sensitive to atorvastatin treatment alone (Suppl. Fig. S4F compared to Fig. 3.1D, E atorvastatin). Therefore, the mevalonate/GGPP axis may mediate statins' cytotoxicity, where the SREBP feedback loop can also be involved, according to the DP synergy experiment. On the other hand, the HMGCR/cholesterol arm is most likely dispensable, and so are the other intermediates of the mevalonate pathway, except for the GGPP/RAS axis (Suppl. Table).

4.3.4. HIF or EMT may be the biomarker of statin sensitivity across different tumor types

In the previous section, the main focus was on the mevalonate pathway and intra-statin difference. In this section, we asked if and how the VHL pathway was related to statin sensitivity. The most prevalent

downstream molecules of VHL are HIF1 and HIF2. VHL (-) cells were utilized to generate HIF1, HIF2, or HIF1/2 knockout lines and tested for IC_{50}. The morphology of HIF1 and HIF1/2 knockout lines were distinctively epithelial compared to its parental line, VHL(-), which has the characteristic spindle shape of mesenchymal cells (Fig. 3.3A and Suppl. Fig. S1A, B). On the other hand, the HIF2 knockout retained the mesenchymal morphology, and the western blot showed a HIF1 level comparable to VHL(-) (Fig. 3.3A). Strikingly, these morphological changes corresponded to their statin sensitivity. HIF1 and HIF1/2 with epithelial look were much more resistant to statins than its parental VHL(-), just like VHL(+) with epithelial look were resistant to statins; in contrast, HIF2 knockout stayed statin-sensitive (Fig. 3.3B). These results suggest the involvement of either HIF1 or EMT.

Warita *et al.* examined the relationship between EMT and statin sensitivity and found mesenchymal cells with high vimentin and low E-cadherin expression were more sensitive to atorvastatin [19]. EMT and hypoxia are some of the hallmarks of aggressive transformation in solid tumors [20]. Combining with the HIF-knockout results above, we hypothesized that the idea of more aggressive, metastatic subtypes being statin-sensitive could be applied to cancer types other than kidney cancer. Both triple-negative breast cancer (TNBC) and neuroendocrine prostate cancer (NEPC) are known as the aggressive subtypes of breast cancer and prostate cancer, respectively, due to their high metastatic rate and drug resistance [21,22]. Although TNBC and NEPC were reported to be more sensitive to statins than their less aggressive counterparts, statins or cell lines used in these studies were not comprehensive or at a very high concentration [23–26]. The 8-statin library used for RCC was applied to eight breast cancer lines (5 TNBC vs. 3 non-TNBC) and seven prostate cancer lines (2 NEPC vs. 2 castrate-resistant prostate cancer CRPC vs. 3 adenocarcinomas) (Fig. 3.3C, D and Suppl. Fig. S5A, B). Both TNBC and NEPC were sensitive to statins with varying degrees depending on each statin, while non-TNBC and prostate adenocarcinoma were almost completely resistant regardless of statin type. The most effective statin in TNBC and NEPC was pitavastatin, followed by fluvastatin and simvastatin. CRPC's sensitivity was in between NEPC and adenocarcinoma, just like its clinical behavior [26].

To see if MOA is the same, TNBC's morphology and HMGCR/HIF expression was checked. TNBC had slightly more mesenchymal morphology than non-TNBC, but the difference was not as clear as VHL(-) vs. VHL(+) (Suppl. Fig. S5C and Suppl. Fig. S1A). HMGCR or HIF expression was not the determinate of statin sensitivity, except that MDA-MB-231, the most sensitive TNBC, had dramatically upregulated HIF1 at 1h timepoint in hypoxia (Suppl. Fig. S5D, E). Though preliminarily, on the other hand, both TNBC and RCC showed suppressed HMGCR mRNA expression in hypoxia for short-term (Suppl. Fig. S5F). This may explain the connection between HIF/EMT and statin sensitivity.

4.3.5. Bioinformatical analysis revealed several key pathways and genes

Among the TNBC and NEPC panels tested for statin sensitivity above, the LnCaP and LnCaP-trop2 pair was most relevant to the RCC result, as one genetic change (trop2 overexpression) transformed LnCaP2 from adenocarcinoma to NEPC (Fig. 3.3D, left column). To reveal if any pathways are shared among statin-sensitive cell lines, sequencing was conducted on RCC lines and the LnCaP and LnCaP-trop2 pairs. RNA sequencing was done on five RENCA lines: VHL(+), VHL(-), HIF1-KO VHL(-), HIF2-KO VHL(-), and HIF1/2-KO VHL(-). Proteomics was run on the LnCaP and LnCaP-trop2 pair and was compared to the RNA sequencing results of the RENCA lines. Appropriate normalizations were used to overcome RNA vs. protein sequencing and mouse vs. human comparisons. GSEA with Hallmark gene sets, which has 50 pathways in total, revealed four pathways commonly upregulated in the sensitive lines (Fig. 3.4A). Commonly upregulated genes within these pathways were also looked up: MYC_targets_V2 (nolc1), MYC_targets_V1 (nolc1, pcna, uba2, rrm1, dek), DNA_repair (alyref, pcna), and E2F_targets (nolc1, mcm3, pcna, dek, and mcm6). There were more shared pathways downregulated in the sensitive lines (xenobiotic_metabolism, oxidative_phosphorylation, adiogenesis, fatty_acid_metabolism, and mTORC1_signaling), but the number of shared genes within these pathways was less than the upregulated ones (Fig. 3.4B). GSEA with the Reactome gene sets, which has 1,615 pathways in total, revealed 25 upregulated and 16 downregulated pathways (Suppl. Fig. S6A, B). Genes found in both Hallmark and Reactome results were mcm3, alyref, rrm1 for the upregulated genes, and maoa and cat for the

downregulated genes. Volcano plots were also created to find shared upregulated or downregulated genes between the LnCap vs. LnCap-trop2 pair and the VHL(+) vs. VHL(-) pair without running GSEA first. Only one gene was shared between these comparisons for upregulated and downregulated category each: Gss and cct3. These two genes appeared in the GSEA analyses above, demonstrating the integrity and different strengths of various bioinformatical methods.

4.3.6. SAR-based approach to improve fluvastatin IC_{50}

Statin compounds all share two chemical components (Fig. 3.5A): the indole ring (blue) and the 3,5-dihydroxyheptenoic acid chain (red). Since statins were reported to bind the β2 integrin leukocyte function antigen-1 (LFA-1) through the indole ring and induce immune suppression [27], an LFA-1 inhibitor BMS-688521 was obtained and tested for its cytotoxicity against VHL(+) and VHL(-) RCC cells (Fig. 3.5B). Within the usual concentration range used for MTS (0 to 10μM), BMS-688521 did not affect either cell line. Because LFA-1's main functions in the immune system include adhesion and migration [28], BMS-688521 was tested to inhibit VHL(-)'s upregulating migration of VHL(+) [6] but did not produce a significant difference (Fig. 3.5C). Determining that the statin's indole ring/LFA-1 interaction was not involved in cytotoxicity or even the pro-metastatic intratumor communication, the 3,5-dihydroxyheptenoic acid chain was focused next.

Eight novel molecules were generated from fluvastatin as the scaffold (Fig. 3.5D). When their cytotoxicity was tested against VHL(-) and VHL(+) cells, only GB-407, 412, and 413 maintained it but to a lesser extent than fluvastatin (Fig. 3.5E and Suppl. Fig. S7A). Moreover, GB-412 and 413 were more toxic to VHL(+) than VHL(-), the opposite of fluvastatin. Therefore, the 3,5-dihydroxyheptenoic acid part of statins was shown to be essential, but how it should be modified to increase the efficacy needs to be elucidated. Another consideration is stereochemistry. So far, all fluvastatin experiments were done with a 1:1 racemate of (3R, 5S)- and (3S, 5R)-fluvastatin, of which (3R, 5S)-fluvastatin exerts pharmacological activities at the liver [29,30]. In concert with this report, (3R, 5S)-fluvastatin was about two times more cytotoxic than racemic fluvastatin in both VHL(-) and VHL(+) (Suppl. Fig. S7B). (3S, 5R)-fluvastatin

couldn't be obtained due to a manufacturing issue, but it will be tested and expected to be less cytotoxic than the racemate or (3R, 5S)-fluvastatin.

4.3.7. Animal studies showed statin's promising efficacy against metastases

Statins' efficacy against metastasis was tested using two animal models. The first system was the avian CAM model. Within ten days, simvastatin suppressed primary tumor growth dose-dependently (Fig. 3.6A). Specifically, the ratio of VHL (-) GFP^+ cells to VHL (+) RFP^+ dropped significantly according to flow cytometry, confirming statins' selective inhibition of VHL (-) (Fig. 3.6B). Most importantly, metastasis to distant organs was almost completely diminished in the treatment group that received 5μM simvastatin (Fig. 3.6C). This remarkable therapeutic result was confirmed in a mouse orthotopic implantation model injected with #18 patient-derived primary cells within four weeks (Fig. 3.6D). The nude mice treated with 15 mg/kg, 6 days/week fluvastatin for two weeks had significantly smaller primary tumors and little metastasis than the DMSO control group (Fig. 3.6E, F). Whether fluvastatin shrank or delayed the tumor has to be investigated, but altogether, these results strongly suggest that statins can inhibit RCC metastasis by disrupting VHL (-) metastatic driver.

4.4. DISCUSSION

Statins have a long history as drugs for hypercholesterolemia and have recently also been found to have anti-neoplastic ability. As millions of people take statins, multiple retrospective analyses have been conducted to see the association between statin use and cancer patient outcomes. However, except for a few statins that showed statins improving cancer death rate [31,32], none of these retrospective analyses produced positive correlations [8–10]. Currently, the only clinical trials running are combination studies of statin and immunotherapy, focusing on the immunosuppressive role of statins through LFA-1/ICAM binding on regulatory T cells. For RCC, detailed analyses were done on statins and VHL [15]. Interestingly, they first found the Rho/Rock pathway through HTS to find a synergistic molecule with VHL(-) [33]. However, the MOA was unclear, except that VHL and HIF were relevant.

According to the findings in this chapter, dosage, statin type, and cancer type must be carefully considered when assessing statin's anti-neoplastic efficacy (Fig. 7A). First, the working dosage of statins against cancers is much higher than its cholesterol-lowering dose (0.61μM = 610nM vs. 3.78nM) (Fig. 3.1) [14]. Dosages used in clinical trials are in the cholesterol-lowering range, not reaching the cytotoxic range. Second, older statins with less cholesterol-lowering ability are more efficacious in anti-neoplasia. Fluvastatin was more effective than atorvastatin or rosuvastatin in suppressing VHL(-), though their HMGCR or cholesterol inhibition abilities are completely the opposite (Fig. 3.1, 3.2) [14]. Many trials were done with atorvastatin because it's the most used statin, but it might not be the best choice, considering the potential novel target of statins, to which fluvastatin may bind most (Fig. 3.2). Finally, patients should be stratified based on which type of treatments they had, or which stage their cancers were in. Statins work for more aggressive tumors, at least for renal, breast, prostate, lung, and brain cancers (Fig. 3.3) [19]. This makes sense, considering the recent reports about transdifferentiation, where different tumors diverged into a common type as they prolonged to metastatic transformation (Fig. 3.4) [34,35].

Continuing this project using both medicinal chemistry and *in vivo* approaches will produce interesting and impactful findings about statins' anti-neoplastic ability. Below are some considerations to corroborate the current study.

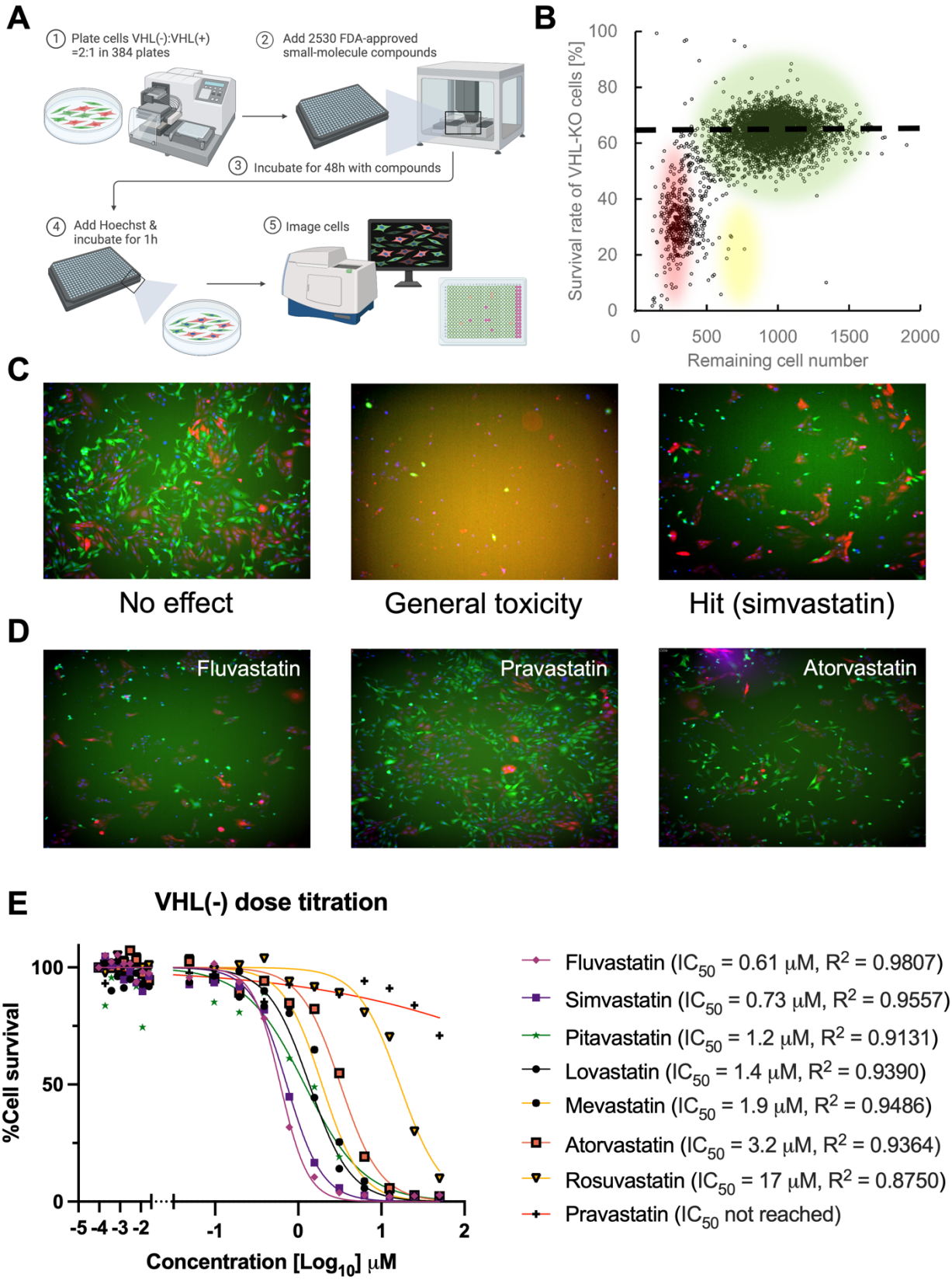
- Fig. 3.1F: tested human RCC lines lack VHL naturally, and wildtype VHL was overexpressed to produce the VHL(-) and VHL(+) pairs like RENCA, but VHL-overexpressed lines remained sensitive to statins. This contradicts the results reported in the literature [15]. The reason is currently being investigated, but it's probably due to the different methods used (MTS for up to six days vs. colony formation assays for up to two weeks). Nonetheless, the same rank order of statins was observed in VHL(-) human RCC lines.
- Fig. 3.2C: complete knockout of HMGCR was lethal in VHL(-). This indicates the necessity of the mevalonate pathway in VHL(-), although the level of HMGCR expression didn't correspond with statin sensitivity. Also, HMGCR knockdown or knockout should be tested in VHL(+), which has a higher basal HMGCR level and thus may be affected by HMGCR depletion, unlike VHL(-).

- Fig. 3.2E: Statins usually only affect synthetic cholesterol but not total cholesterol, whose main source is cholesterol uptake from the environment rather than synthesis. Therefore, VHL(+)'s behaviors were physiologically expected for both synthetic and total cholesterol, whereas VHL(-)'s were not, especially when treated with fluvastatin and simvastatin. This may be due to fluvastatin & simvastatin being too toxic at the concentration used here (0.7uM), and the cell measurement was not accurate due to the altered morphology of dying cells. 0.7uM was chosen because it's fluvastatin's IC50, and the question asked was if statins have different cholesterol-lowering abilities at the same concentration. However, since cholesterol lowering concentration is at a low nM range, fewer statins should have been used to prevent any obvious cell death. Nonetheless, cholesterol is most likely not relevant because 1) complete media is cholesterol-rich due to FBS and 2) squalene didn't rescue VHL(-) from statin killing (Fig. 3.2F).
- Fig. 3.2G-I: The level of each intermediate of the mevalonate pathway should be tested upon treatment with different statins in VHL(-) vs VHL(+) cells, in addition to the rescue experiments. Kaplan-Meier curves indicate the majority of the mevalonate pathway enzymes show the same trend as HMGCR in patient survival, where a lower protein expression was associated with a worse prognosis (Fig. 7B). On the other hand, enzymes in the GGPP arm, farnesyl diphosphate synthase (FDPS1) and geranylgeranyl diphosphate synthase 1 (GGPS1), show a flipped trend, suggesting a separate regulation mechanism might be at a play (Fig. 7C).
- Fig. 3.4: Among all pathways revealed, those upregulated in statin-sensitive lines are most interesting and will be followed through. KEGG and GO gene sets were also used in GSEA but are currently being analyzed. Sequencing results comparing VHL(-) treated with fluvastatin vs. atorvastatin would be interesting and was run already but didn't produce significant results. The experiment will be repeated with proper controls and more sample numbers.
- Suppl. Fig. S7B: Once the other enantiomer arrives, its IC_{50} will be confirmed. One stereochemistry study reported an interesting finding where (3R, 5S)-fluvastatin was most efficacious in binding

against glucocorticoid receptor (GR) [29]. This is worth following because GR is associated with aggressive tumors of various tissues [36–40].

- Fig. 3.6D: Oral administration of statins by gavage should have been employed instead of i.p. injection, as it's more physiologically relevant. Tumor composition, death/proliferation marker, and cholesterol/health markers in blood/normal tissue should be assessed when repeating in vivo experiments with fluvastatin or, even better, with a synthesized molecule that works better *in vitro*.

Despite all these shortcomings, this study sheds light on an interesting biology of statins in metastatic cancer. Thanks to a strong collaboration with medicinal chemists, the next aims of this project include synthesizing novel compounds in addition to repositioning statins. Successful execution of this research will allow the development of novel anti-metastatic reagents either way and will have a huge tangible impact in the clinic.


A
1 Plate cells VHL(-):VHL(+) =2:1 in 384 plates
2 Add 2530 FDA-approved small-molecule compounds
3 Incubate for 48h with compounds
4 Add Hoechst & incubate for 1h
5 Image cells
B
Survival rate of VHL-KO cells [%]
Remaining cell number
C
No effect
General toxicity
Hit (simvastatin)
D
Fluvastatin
Pravastatin
Atorvastatin
E
VHL(-) dose titration
%Cell survival
Concentration [Log10] μM
Fluvastatin (IC50 = 0.61 μM, R2 = 0.9807)
Simvastatin (IC50 = 0.73 μM, R2 = 0.9557)
Pitavastatin (IC50 = 1.2 μM, R2 = 0.9131)
Lovastatin (IC50 = 1.4 μM, R2 = 0.9390)
Mevastatin (IC50 = 1.9 μM, R2 = 0.9486)
Atorvastatin (IC50 = 3.2 μM, R2 = 0.9364)
Rosuvastatin (IC50 = 17 μM, R2 = 0.8750)
Pravastatin (IC50 not reached)

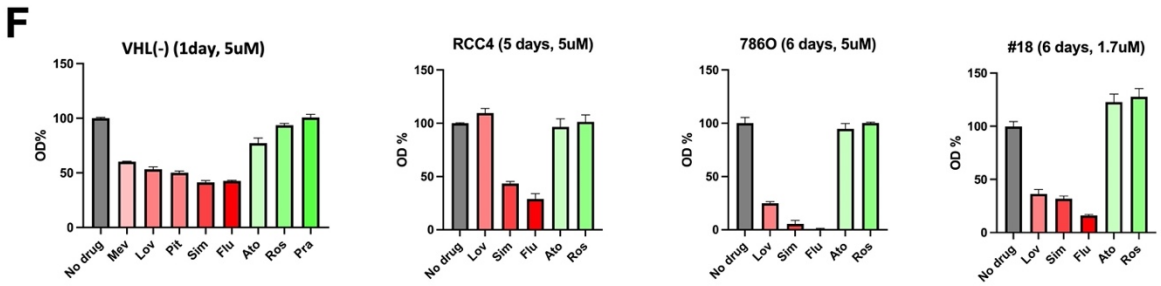


Fig. 4.1 HTP setup and results. (A) Schematic of HTS setup for our ratiometric black box approach. Created with BioRender.com. (B) Summary of the HTS. Green - no effect, red - unspecific toxicity, yellow - green-specific toxicity = hits. (C) Representative pictures of each of the categories shown in (B). Confocal microscopic pictures at 10x magnification and 3-channel fluorescence (GFP, RFP, Hoechst). (D) Representative pictures of statin wells in the HTS. Confocal microscopic pictures at 10x magnification and 3-channel fluorescence (GFP, RFP, Hoechst). (E) Dose titration curves with 8 statins on VHL(-) cells at 48h. (F) MTS results showing the rank order of statin cytotoxicity against VHL(-) cells from mouse and human origins.

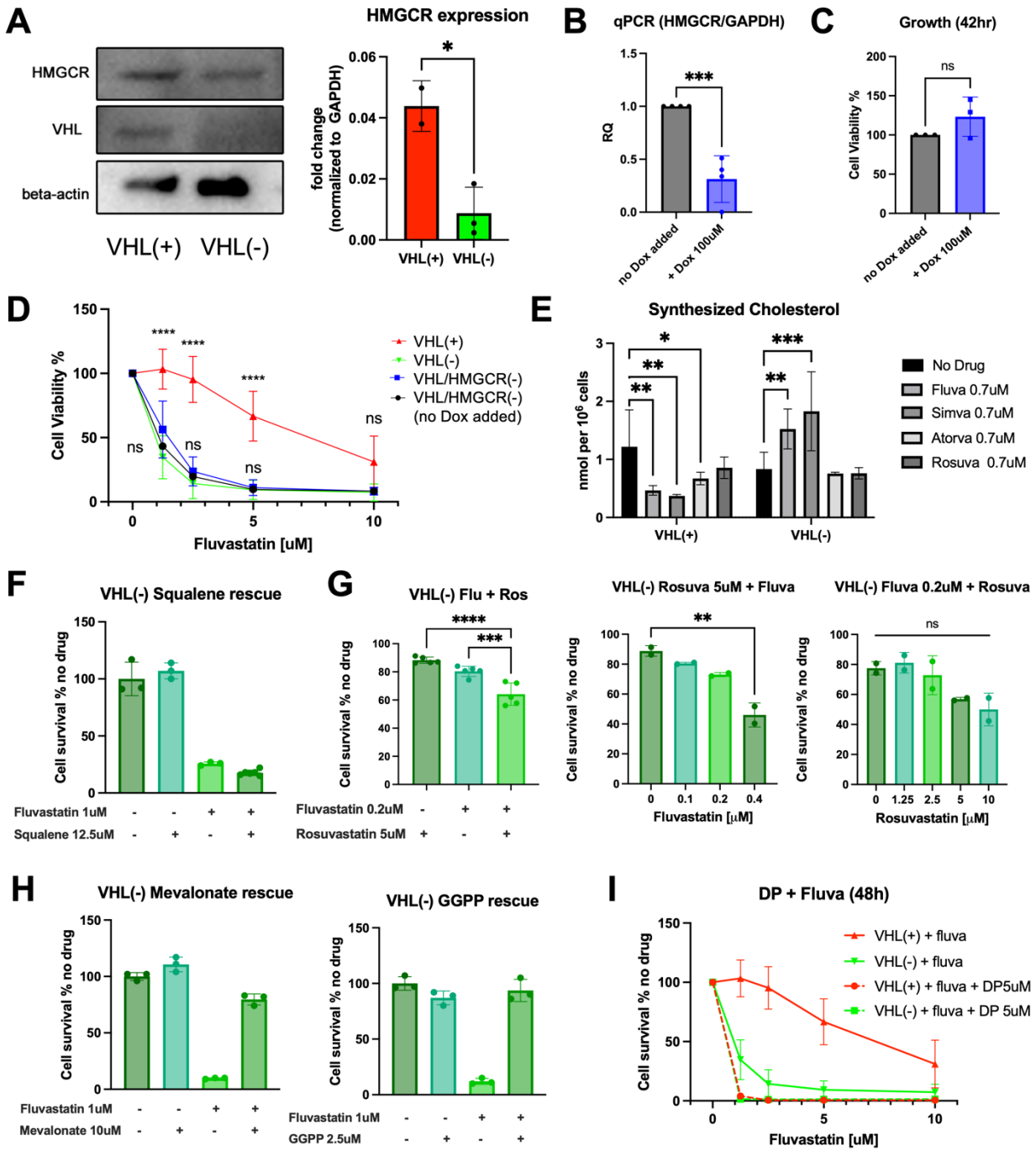


Fig. 4.2 MOA of statins' cytotoxicity. (A) Protein and mRNA expression of HMGCR were measured for VHL(+) and VHL(-) cells. (B) HMGCR expression was measured to confirm the knockdown upon treatment with doxycycline 100μM in the VHL(-)HMGCR(-) line. (C) Cell growth was measured for the VHL(-)HMGCR(-) line with or without 100μM doxycycline. (D) Fluvastatin sensitivity measured by MTS. (E) Synthesized cholesterol level was measured upon treatment with different statins. (F) Rescue

experiment of VHL(-) with co-treatment of fluvastatin and squalene, cholesterol precursor. (G) VHL (-) cell survival was measured with MTS upon co-treatment with fluvastatin and rosuvastatin. 0.2μM fluvastatin and 5μM rosuvastatin were used to assess a synergistic effect (left). Each drug was titrated and tested as well (middle, right). (H) Rescue experiment of VHL(-) with co-treatment of fluvastatin and mevalonate or GGPP, intermediates of the mevalonate pathway. (I) Cell survival assays with MTS upon co-treatment of dipyridamole and fluvastatin to assess the interplay between the mevalonate pathway and dipyridamole.

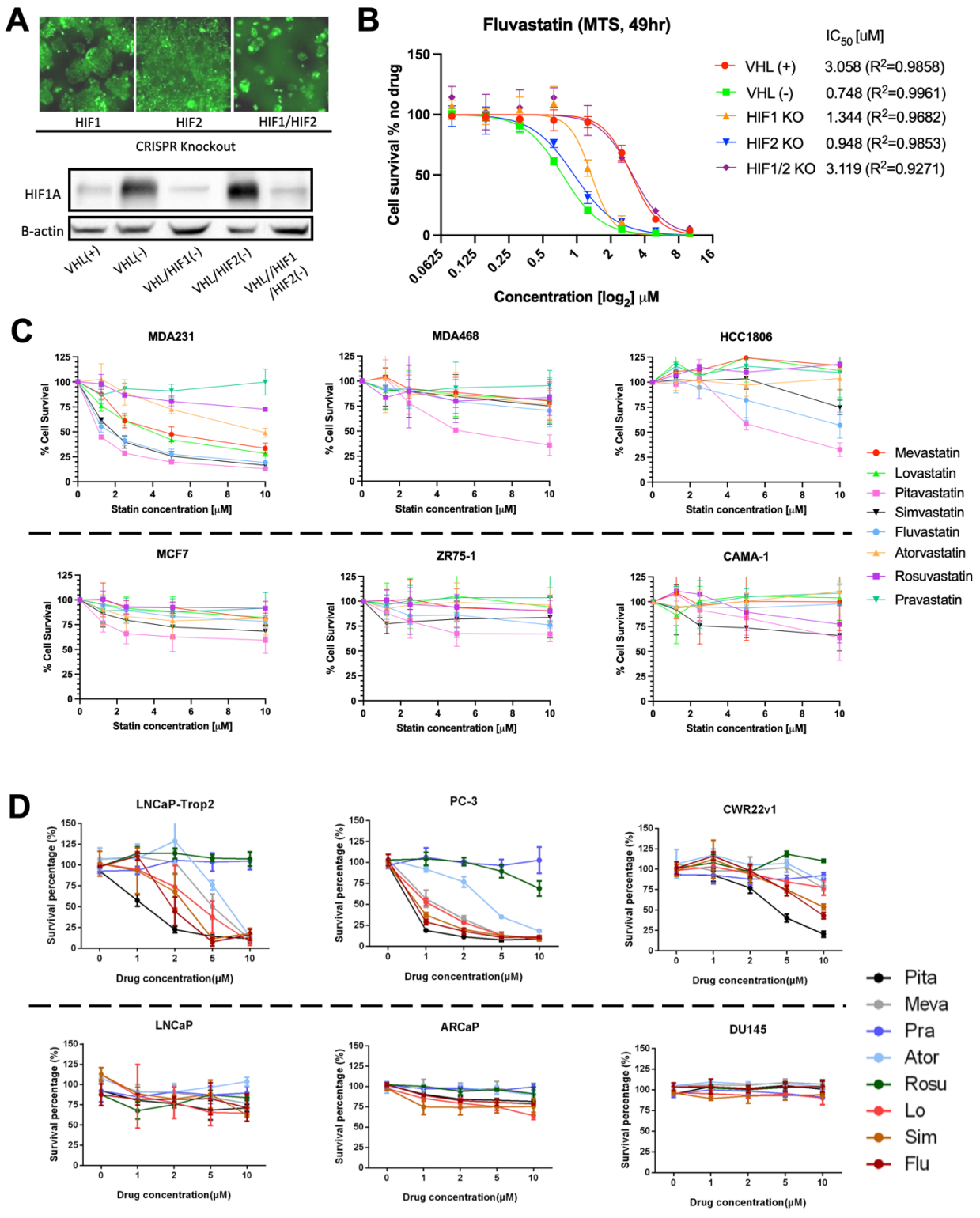


Fig. 4.3 HIF, EMT, and statin sensitivity in pan-tissue metastatic cancer. (A) (top) 10x images of VHL (-) lines with an additional knockout of HIF1, HIF2, or both, taken with a fluorescent microscope. (bottom)

Western blot assessing HIF1A expression in VHL (+), (-), and the 3 HIF-knockout lines. (B) Dose-response curve of the above 5 cell lines with fluvastatin in 20-step titration from 95.4pM to 50μM. (C) Cell survival assays were assessed with MTS in 3 TNBC (top) and 3 non-TNBC lines (bottom) with statin treatment. (D) Cell survival assays were assessed with MTS in 3 NEPC or CRPC (top) and 3 adenocarcinoma prostate cancer lines (bottom) with statin treatment.

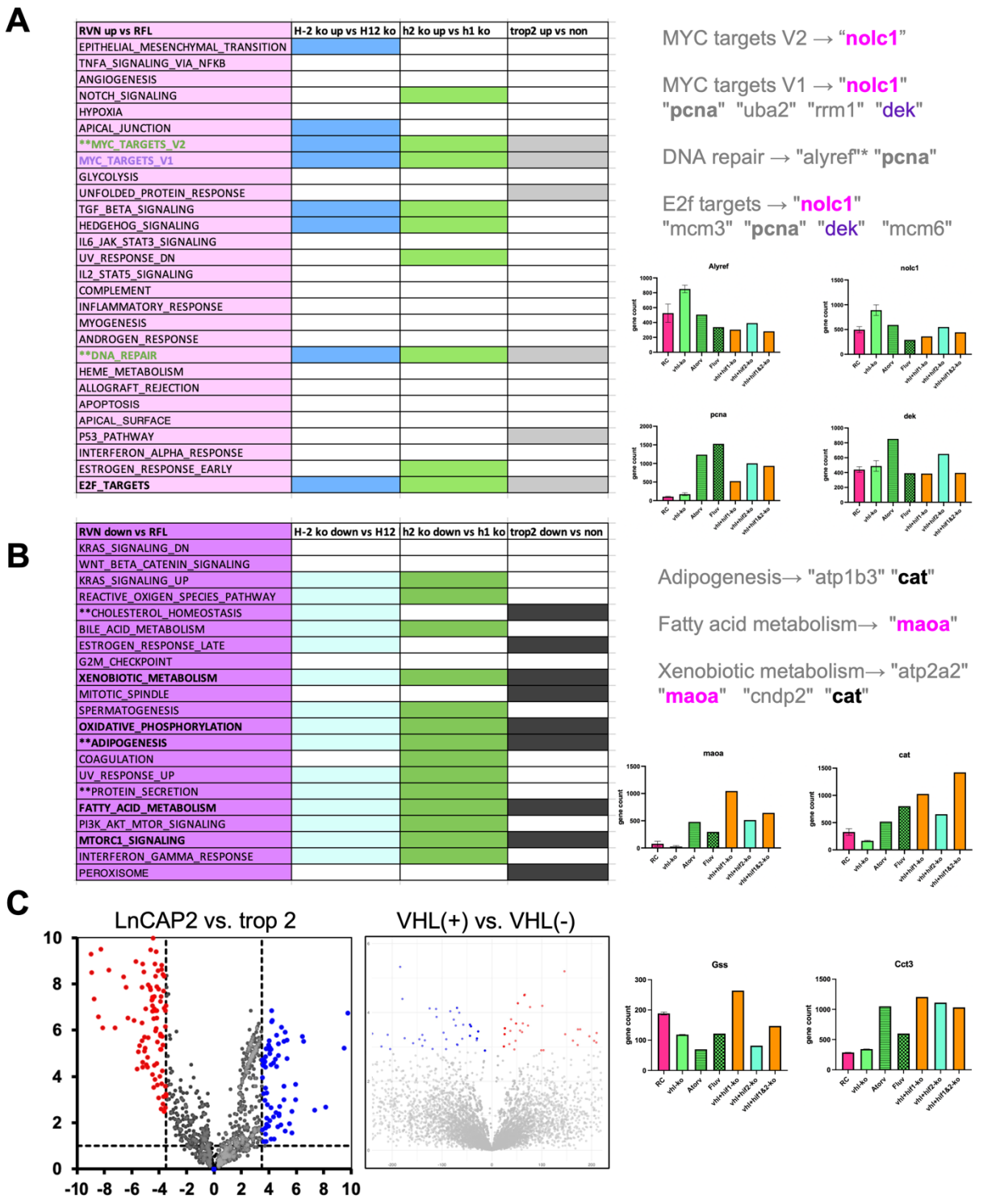


Fig. 4.4 Bioinformatical analyses to find common genes in statin-sensitive lines. (A) (left) The summary table of GSEA results for four comparisons to find common pathways upregulated in the statin-sensitive lines. (right) Common genes upregulated in the sensitive lines in each pathway are listed. Individual gene

expression was extracted and plotted. (B) Same as above, except for looking for downregulated pathways and genes. (C) Volcano plots comparing LnCaP vs. LnCaP-trop 2 and VHL(+) vs. VHL(-). The only common genes between these comparisons were GSS (down in sensitive lines) and CCT3 (up in sensitive).

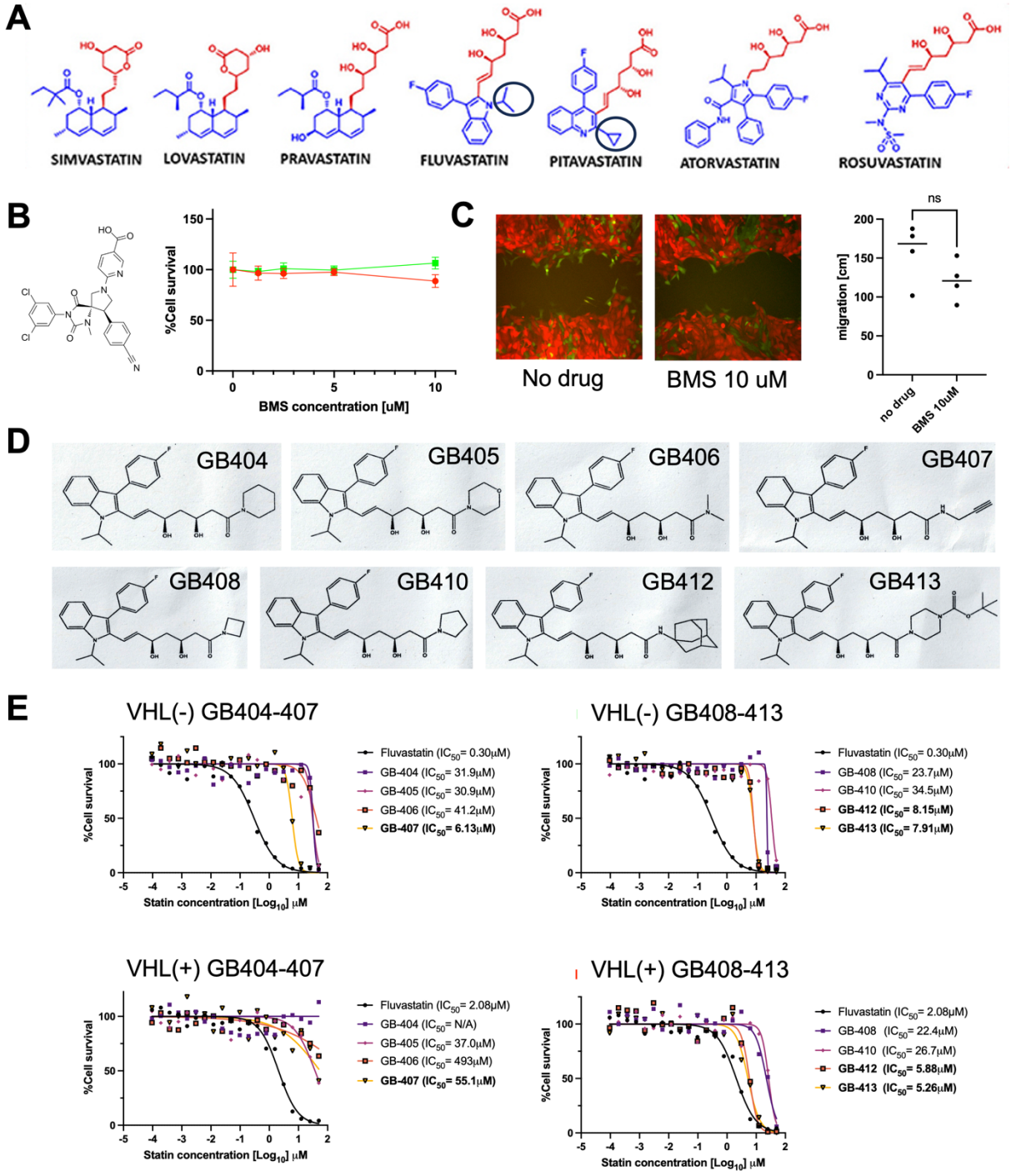


Fig. 4.5 SAR-based analyses of statins' cytotoxicity. (A) Chemical structures of statins adapted from [41]. Blue – the indole ring; Red – the 3,5-dihydroxyheptenoic acid chain; Black circle – the structural similarity of fluvastatin and pitavastatin, which may explain their efficacy higher than other statins. (B) Chemical structure of the LFA-1 inhibitor, BMS-688521, and its cytotoxicity assay measured by MTS at 48h. (C) 2D migration assays were measured with a fluorescent microscope. Migration of VHL(+) (RFP) was plotted for no drug vs. 10μM BMS-688521 treatment. (D) Chemical structure of the eight fluvastatin derivatives. (E) 20-step dose titration ranging from 95.4pM to 50μM was used to determine the IC_{50} of the fluvastatin derivatives compared to fluvastatin. Top vs. bottom: VHL(-) vs. VHL(+). Left: fluvastatin & GB404 – 407. Right: fluvastatin & the rest of the derivatives.

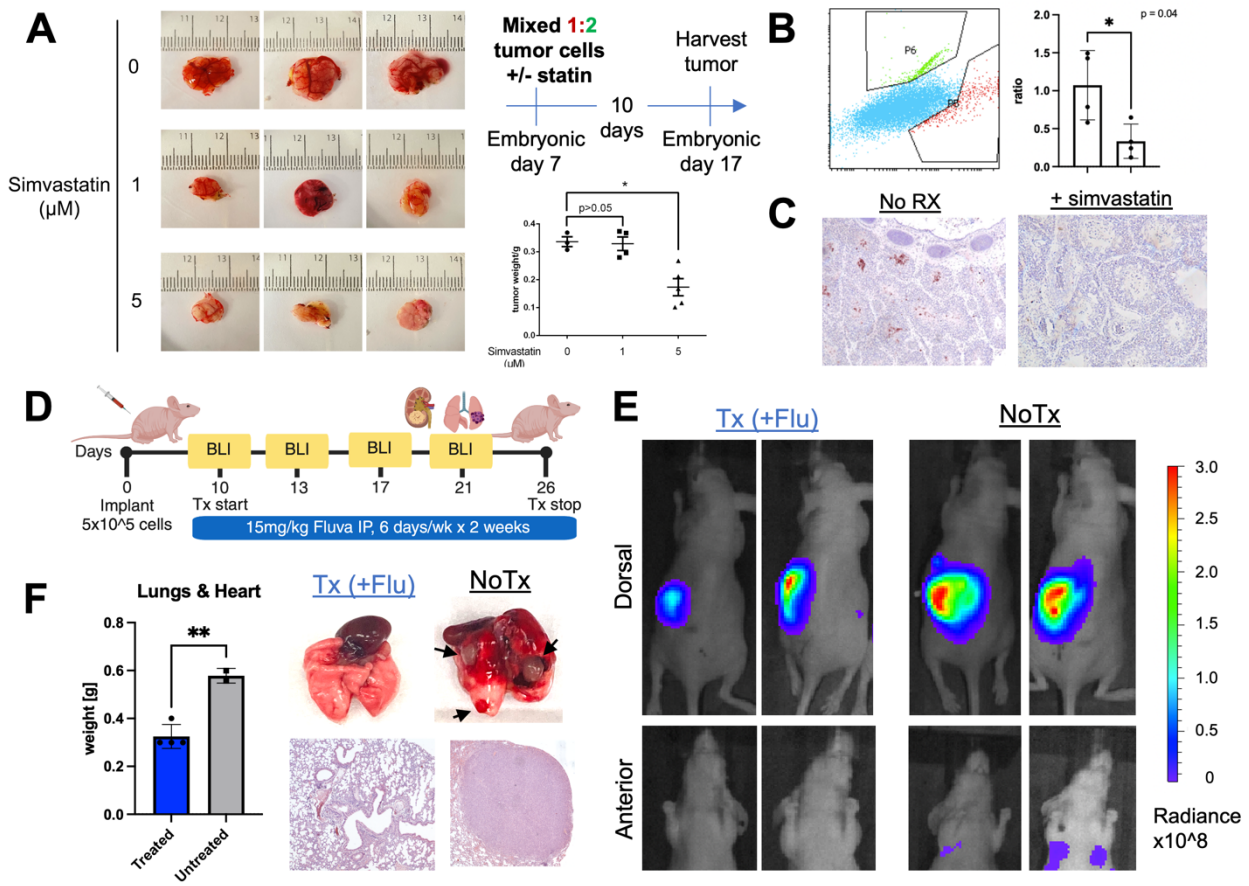


Fig. 4.6 Therapeutic studies in two animal models. (A) CAM tumors from 1:2 mix implantation with different doses of simvastatin after 10 days. Gross view, timeline, and weight measurement are shown. (B) Cell composition analysis of CAM tumors using flow cytometry. Visualization of GFP/RFP cells after gating out dead or doublet cells (left) and quantification of GFP (VHL-): RFP (VHL+) ratio (right) is shown. (C) IHC pictures of chick embryo lungs on day 10 stained for FLAG, which indicates the presence of the implanted VHL(-) or VHL(+) cells. (D) Schematic of mouse orthotopic implantation model in Nu mice. (E) BLI images for firefly luciferase in mice on day 26 post-implantation for dorsal and anterior views. (F) Lung & heart weight was measured at dissection (left). Goss view and H&E staining of a representative lung + heart from each group are shown (right).

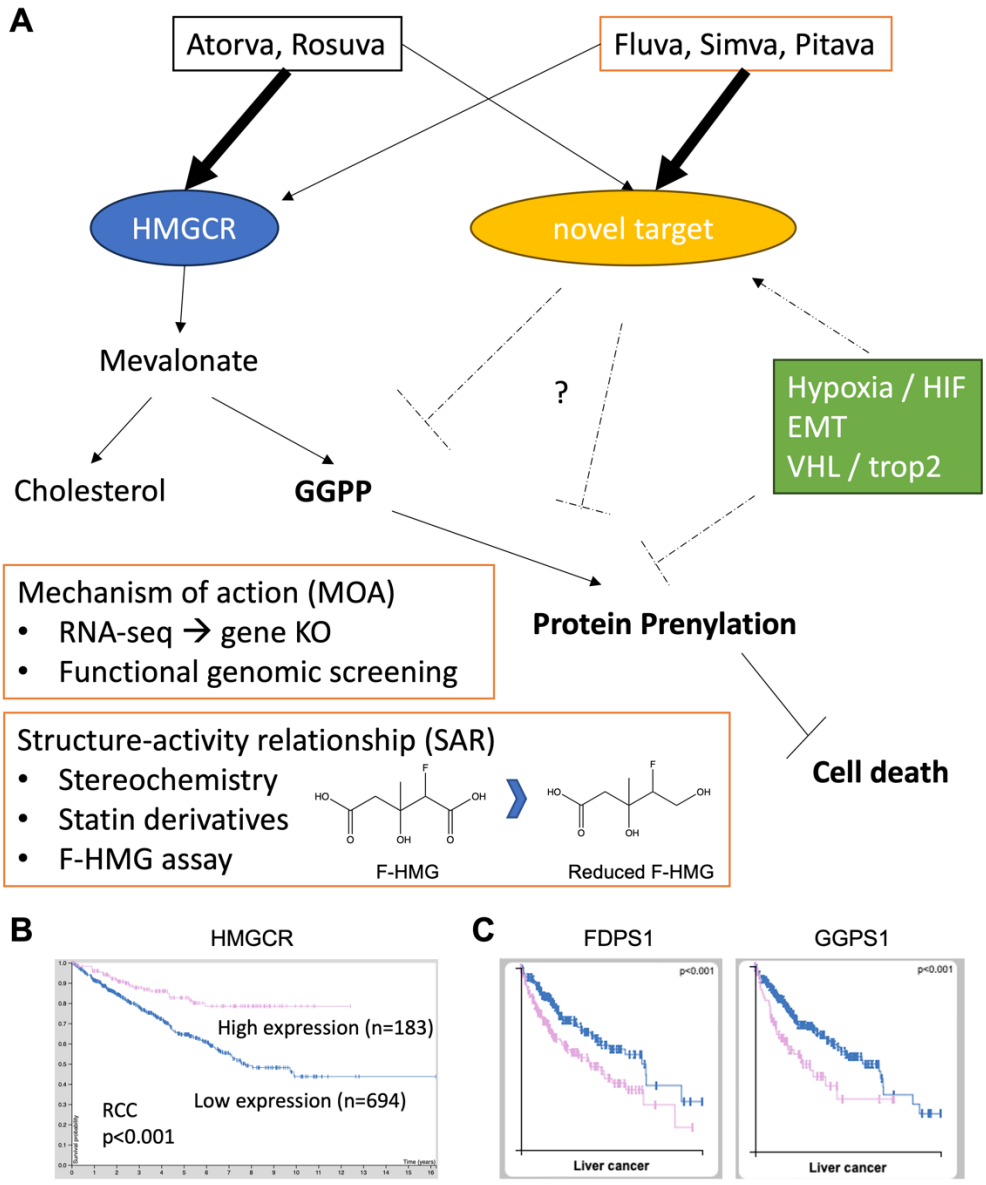
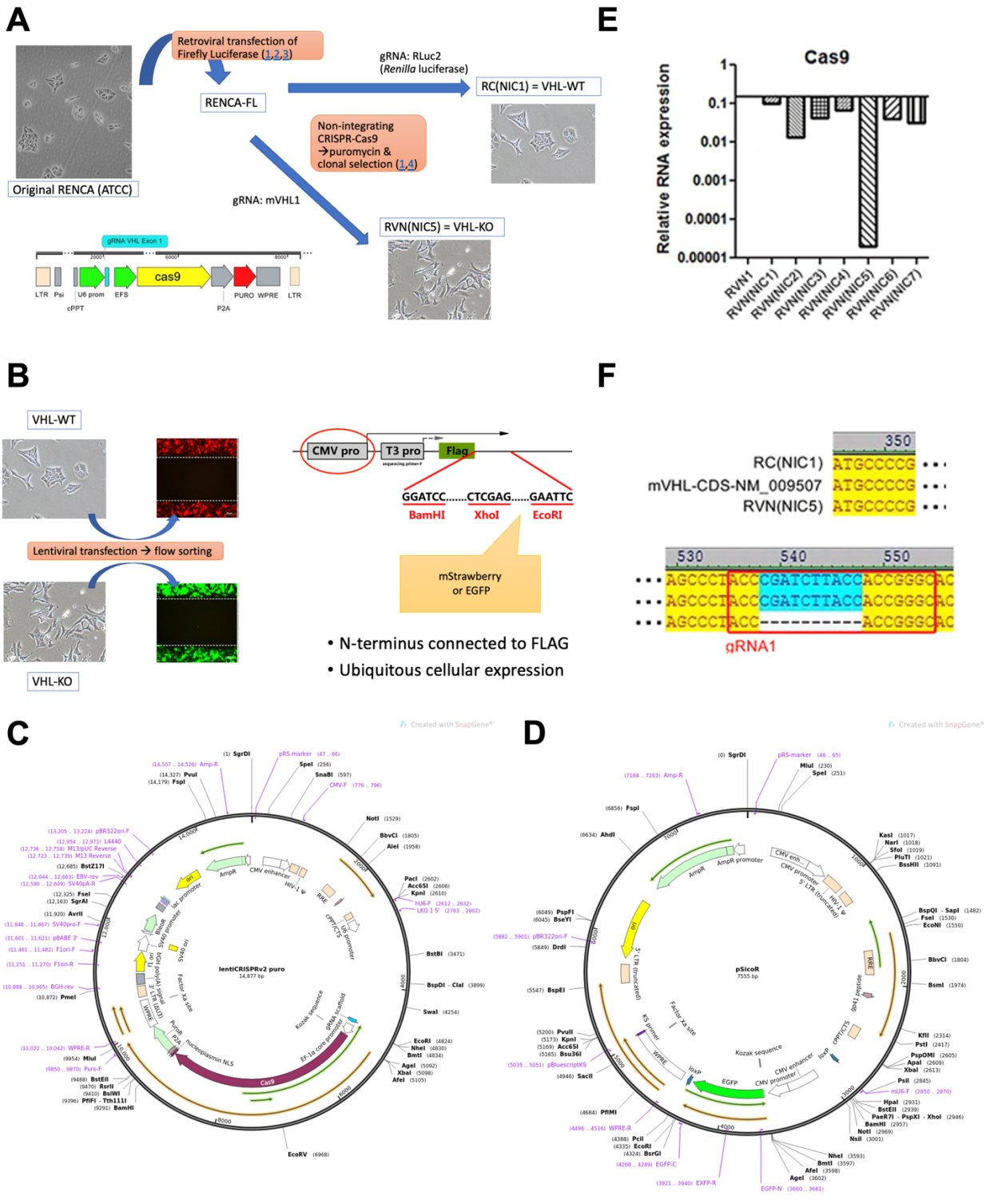


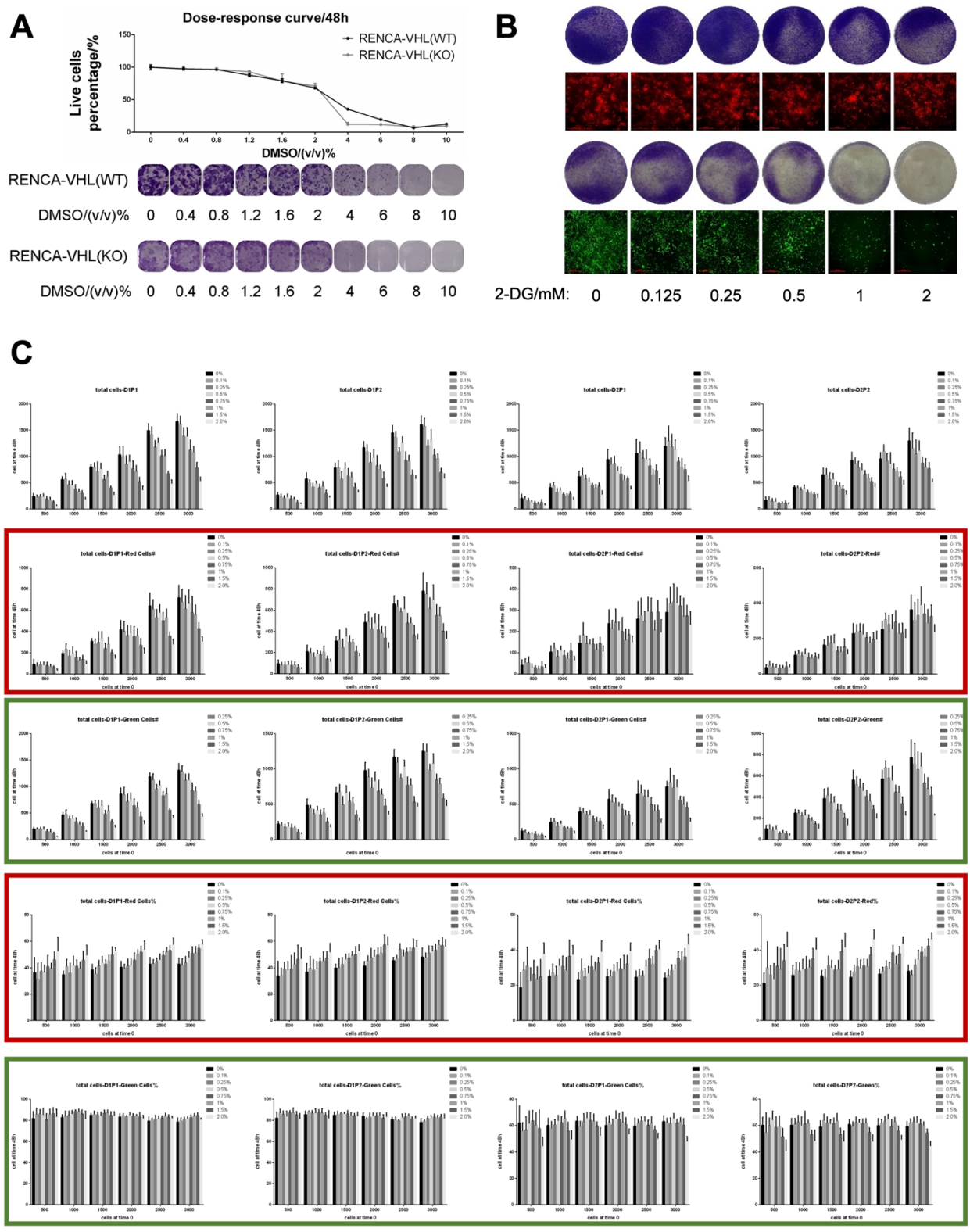
Fig. 4.7 Schematic of working hypothesis about MOA. (A) Our hypothesis is that effective statins bind to a novel, unknown target distinctive from HMGCR. According to the rescue experiments, the mevalonate pathway is involved in cytotoxicity, but the relationship between the pathway and the novel target remains elusive. The common vulnerability of these metastatic tumors, which makes them sensitive to statins, will be investigated with a focus on hypoxia, EMT, and pathways related to VHL and trop2. (B-C) Survival curves of RCC patients stratified by HMGCR protein expression and liver cancer patients stratified by FDPS1 or GGPS1 protein expressions [42,43].

4.5. SUPPORTING MATERIALS



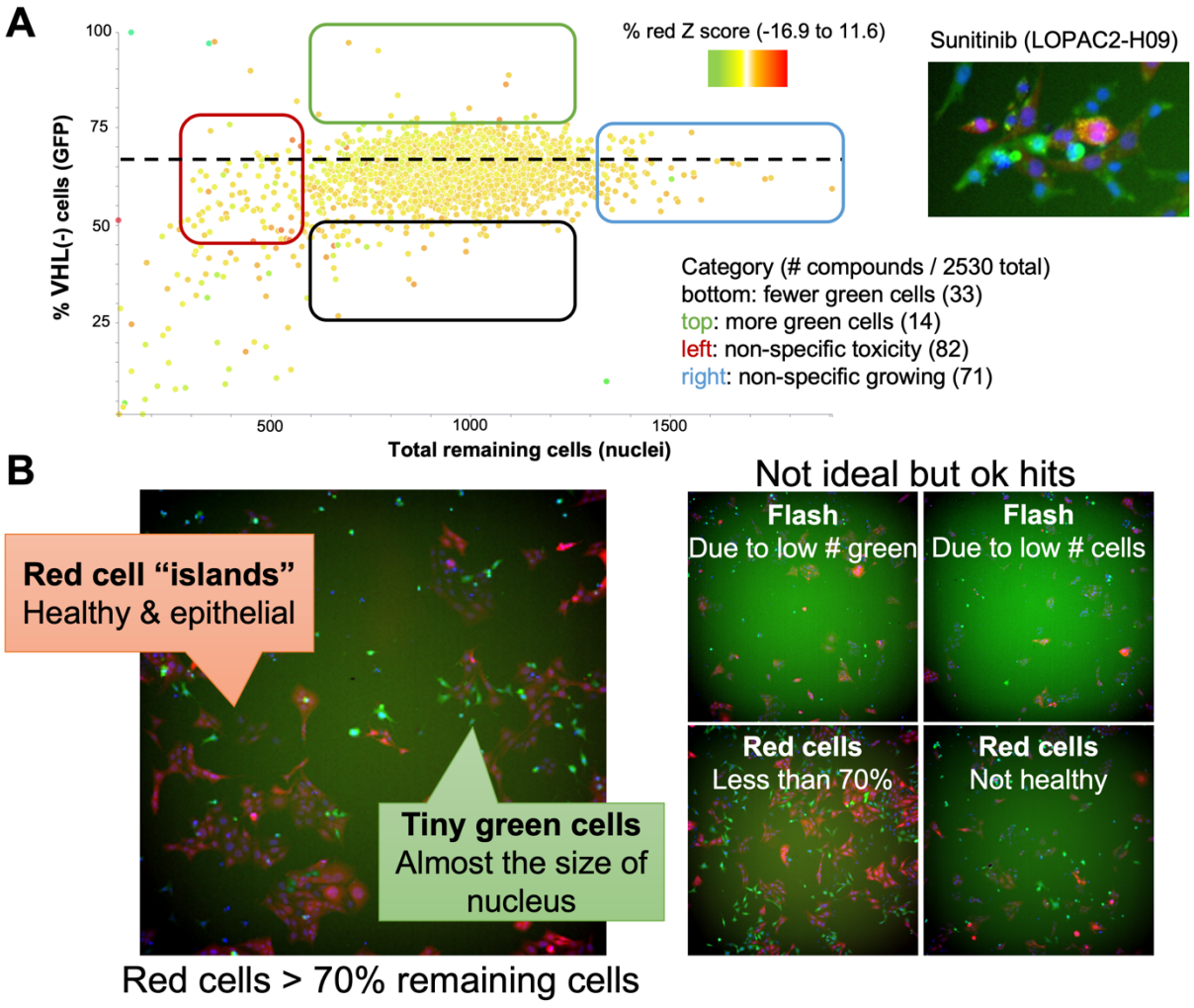
Suppl. Fig. S1 Detailed cell line information. (A, B) Schematic of how VHL(+) & VHL(-) cell lines were

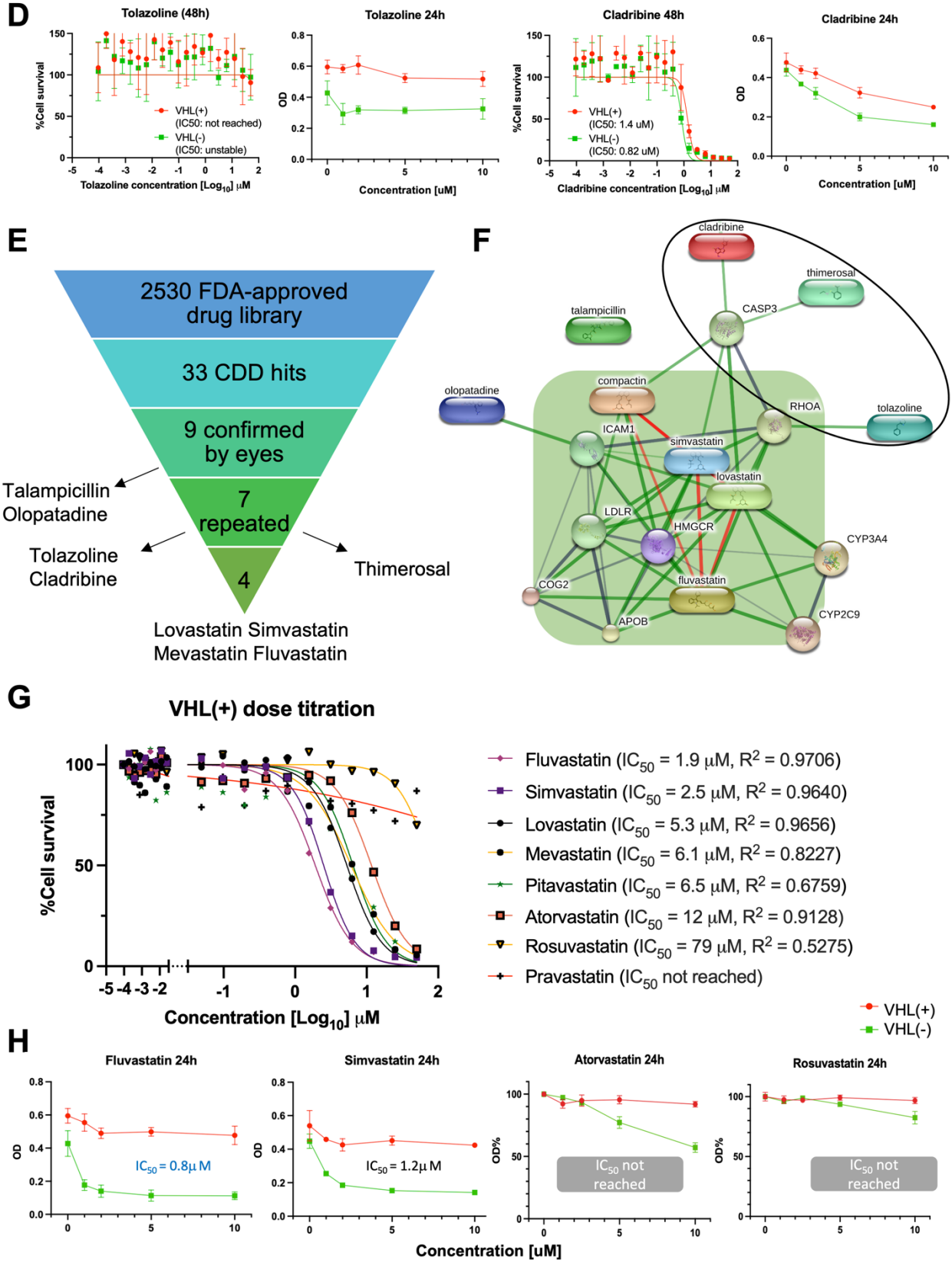
generated from RENCA, murine RCC line. See Materials & Methods for description. (C) CRISPR plasmid map used for panel A. https://www.addgene.org/98290/ (D) Lentiviral plasmid map used for panel B. https://www.addgene.org/11579/ (E) The resulting cells have low expression of Cas9, allowing stable growth of these cells in immunocompetent mice. Adapted from [3]. (F) The sequencing result confirms the knockout of VHL in RVN(NIC5)=VHL-KO cells. Also adapted from [3].



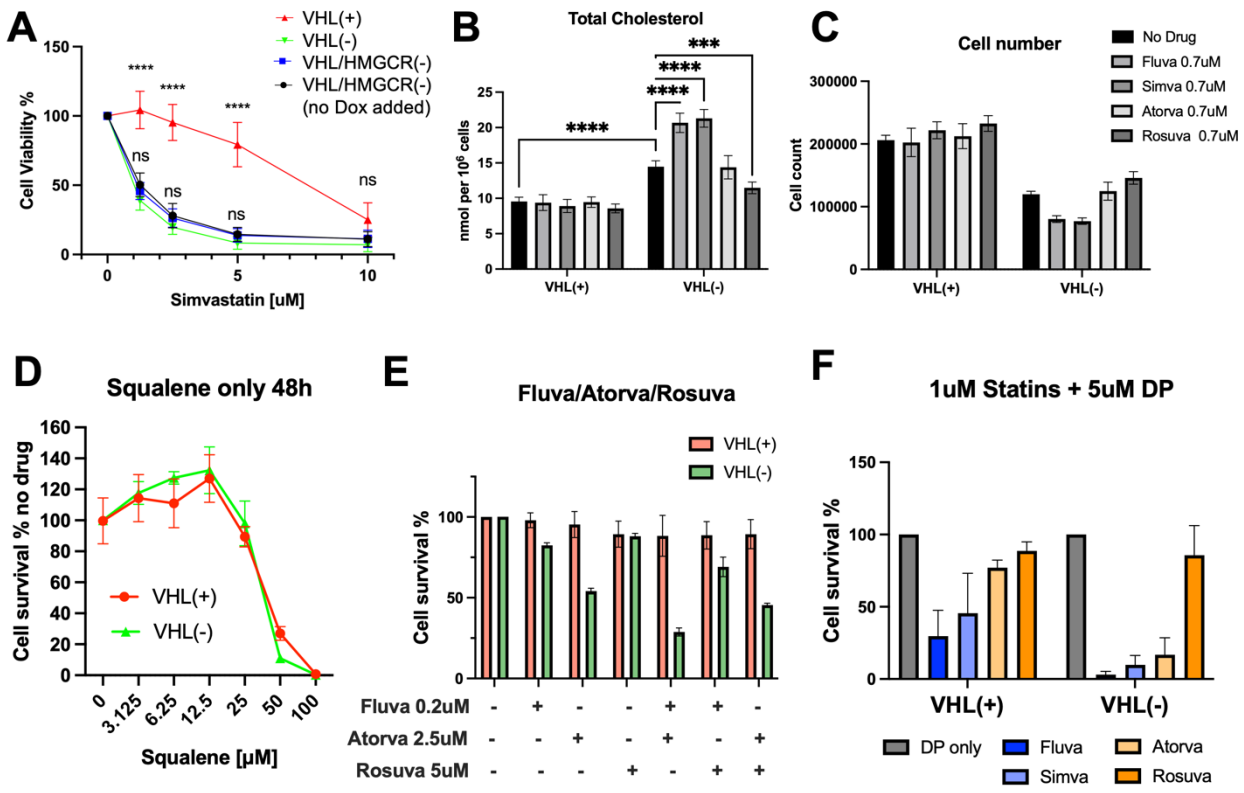
Suppl. Fig. S2 HTS optimization. (A) DMSO dose-response curve to determine the DMSO concentration to be used in HTS as negative control. (B) Images of 2DG dose titration to determine the 2DG concentration

to be used in the HTS as the positive control. (C) Optimization of cell number, DMSO concentration, and analysis module conducted for two days with two plates /day, totaling four plates. (top) total cell number measured by Hoechst count. (2^{nd} and 3^{rd} rows) RFP VHL(+) and GFP VHL(-) measured with module 1, respectively. (4^{th} and 5^{th} rows) RFP VHL(+) and GFP VHL(-) measured with module 2, respectively.

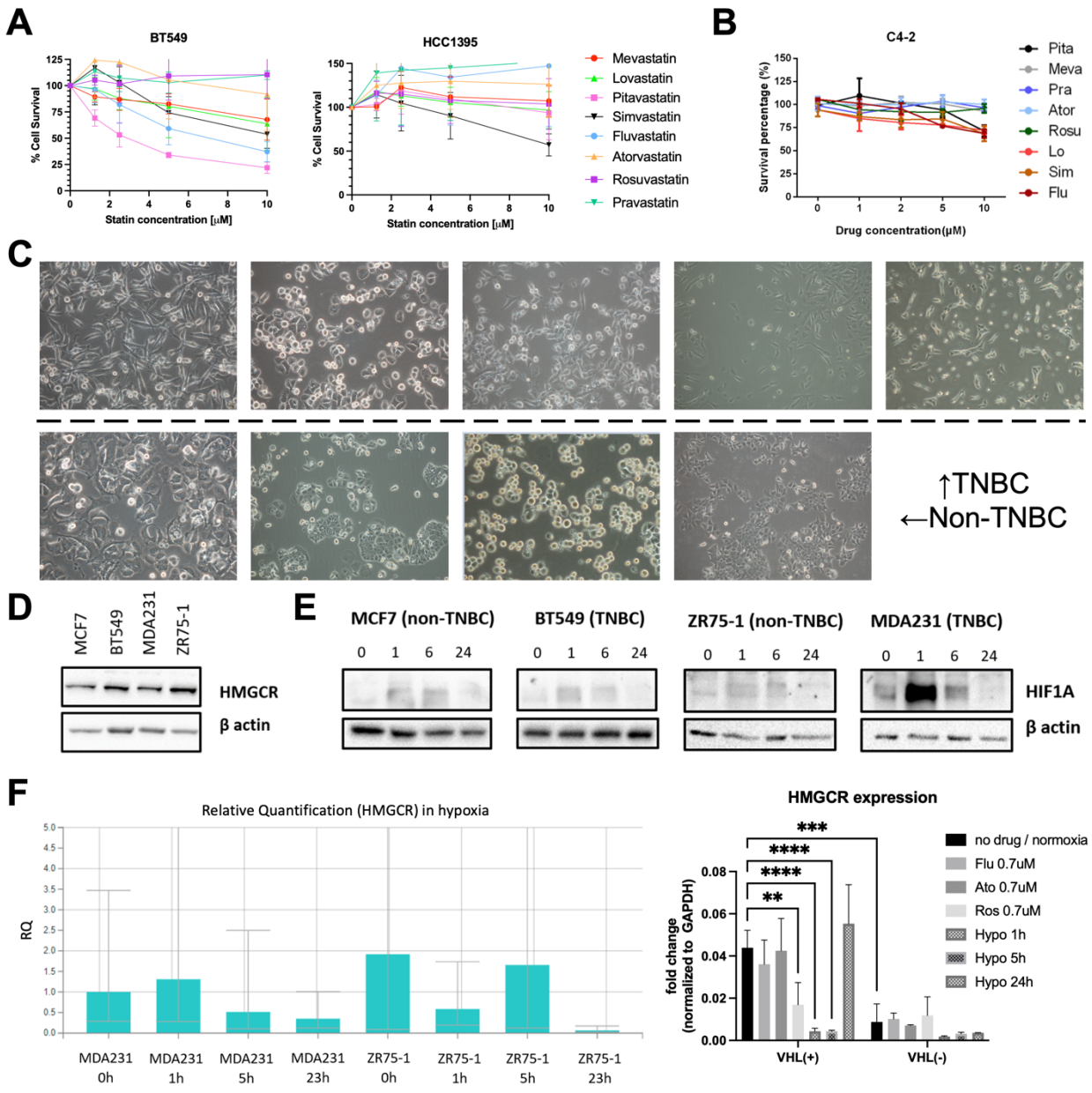

A
% red Z score (-16.9 to 11.6)
Sunitinib (LOPAC2-H09)
% VHL(-) cells (GFP)
100
75
50
25
500
1000
1500
Total remaining cells (nuclei)
Category (# compounds / 2530 total)
bottom: fewer green cells (33)
top: more green cells (14)
left: non-specific toxicity (82)
right: non-specific growing (71)
B
Red cell "islands"
Healthy & epithelial
Tiny green cells
Almost the size of nucleus
Red cells > 70% remaining cells
Not ideal but ok hits
Flash
Due to low # green
Flash
Due to low # cells
Red cells
Less than 70%
Red cells
Not healthy
C
Mevastatin
Lovastatin
Tolazoline
Cladribine
Talampicillin
Olopatadine
Thimerosal


D
Tolazoline (48h)
%Cell survival
VHL(+)
(IC50: not reached)
VHL(-)
(IC50: unstable)
Tolazoline concentration [Log10] μM
Tolazoline 24h
OD
Concentration [uM]
Cladribine 48h
%Cell survival
VHL(+)
(IC50: 1.4 uM)
VHL(-)
(IC50: 0.82 uM)
Cladribine concentration [Log10] μM
Cladribine 24h
OD
Concentration [uM]
E
2530 FDA-approved drug library
33 CDD hits
9 confirmed by eyes
7 repeated
4
Talampicillin
Olopatadine
Tolazoline
Cladribine
Thimerosal
Lovastatin Simvastatin
Mevastatin Fluvastatin
F
cladribine
thimerosal
talampicillin
CASP3
olopatadine
compactin
RHOA
tolazoline
ICAM1
simvastatin
lovastatin
LDLR
HMGCR
CYP3A4
COG2
fluvastatin
APOB
CYP2C9
G
VHL(+) dose titration
%Cell survival
Concentration [Log10] μM
Fluvastatin (IC50 = 1.9 μM, R2 = 0.9706)
Simvastatin (IC50 = 2.5 μM, R2 = 0.9640)
Lovastatin (IC50 = 5.3 μM, R2 = 0.9656)
Mevastatin (IC50 = 6.1 μM, R2 = 0.8227)
Pitavastatin (IC50 = 6.5 μM, R2 = 0.6759)
Atorvastatin (IC50 = 12 μM, R2 = 0.9128)
Rosuvastatin (IC50 = 79 μM, R2 = 0.5275)
Pravastatin (IC50 not reached)
H
VHL(+)
VHL(-)
Fluvastatin 24h
OD
IC50 = 0.8μM
Simvastatin 24h
OD
IC50 = 1.2μM
Atorvastatin 24h
OD%
IC50 not reached
Rosuvastatin 24h
OD%
IC50 not reached
Concentration [uM]

Suppl. Fig. S3 Detailed HTS analyses. (A) Visualization of HTS (11 plates x 384 wells: LOPAC 1-4, NIHII1-3, NPW1-4) on CDD Vault. Each dot represents one of the 2530 compounds screened for their total remaining cell number (x-axis, nuclei count) and % VHL(-) cells (y-axis, GFP count). The dot color represents the Z-score of % VHL(+) cells measured by RFP. Initial hits were defined by "total cell number between 600 &1200" & "%green between 25% and 50%" (bottom, black square). 33 compounds satisfying these criteria were identified as initial hits. Other categories that might be interesting in future research are also highlighted but will not be discussed further in this manuscript. Top (green) = VHL(+)-specific toxicities, 14 compounds, "total cell number between 600 & 1200" & "%green more than 76.5%." Left (red) = non-specific toxicities, 82 compounds, "total cell number under 590" & "%green between 45% and 76%." Right (blue) = non-specific growing, 71 compounds, "total cell number over 1320" & "%green between 50% and 76%." The top (green) groups include VHL (+) specific toxicity, as well as the "dots" group, including sunitinib, which later turned out to be auto-fluorescent. (B) Representative images of the ideal and ok hits. A few characteristics of each are denoted in the figure. (C) 7 out of the 9 hits that were confirmed by eyes and moved onto hit picks are shown. The other two (fluvastatin and simvastatin) are shown in Fig. 3.1C and D. (D) 20-step dose-titration and MTS results are shown for the two compounds (tolazoline and cladribine) that failed at the final validation stage. (E) Summary of the HTS analysis. Out of the 2,530 FDA-approved compounds, 33 were determined hits by CDD Vault, 9 by eyes, 7 by hit picks (talampicillin and olopatadine failed), and 4 by dosage titration (tolazoline and cladribine failed, whereas thimerosal was not available from the vendor for bigger vials). All 4 final hits were statins. (F) STITCH analysis of the 9 hits confirmed by eyes and shown in panel C. STITCH is a database of known and predicted interactions between chemicals and proteins. The interactions include direct (physical) and indirect (functional) associations stemming from computational prediction, knowledge transfer between organisms, and interactions aggregated from other primary databases (http://stitch.embl.de). Statins and related pathways are highlighted in green. Non-statin hits that didn't fail at the next step are circled, showing stronger connections to statins than those that failed at hit-picks (talampicillin and olopatadine). (G) 20-step dose titration of statins on VHL(+) cells. (H) Cell survival assays by MTS at 24h.



Suppl. Fig. S4 Optimization and validation of MOA of statins' cytotoxicity. (A) Simvastatin sensitivity was measured by MTS for the VHL(-)HMGCR(-) line with or without 100μM doxycycline treatment and compared to VHL(-) and VHL(+) cells. (B, C) The total cholesterol level was measured upon treatment with different statins. Total cholesterol was normalized to 10^6 cells and plotted along with the cell numbers for reference. (D) MTS measured squalene toxicity to determine the amount to be used in the rescue experiments. (E) VHL (-) cell survival was measured with MTS upon different combinations of co-treatment of 0.2μM fluvastatin, 2.5μM atorvastatin, and 5μM rosuvastatin. (F) Cell survival assays with MTS upon co-treatment of dipyridamole and different statins in VHL(+) and VHL(-) cells.



Suppl. Fig. S5 Additional TNBC/NEPC data and preliminary results on the relationship between HMGCR and hypoxia. (A) Cell survival assays were assessed with MTS for two additional breast cancer lines: 1 TNBC and 1 non-TNBC. (B) Cell survival assays were assessed with MTS in one additional CRPC line. (C) Morphology of the breast cancer lines used in this study. All were taken with 20x magnification. Top: TNBC (MDA-MB-231, MDA-MB-468, HCC1806, BT549, HCC1395). Bottom: non-TNBC (MCF-7, ZR 75-1, CAMA-1, BT474). BT474's MTS data is excluded because more optimization is needed to accommodate its slow growth. (D) Western blot of basal HMGCR expression in four breast cancer lines.

(E, F) Western blot and qPCR of HMGCR expression in breast cancer and RCC lines under normoxia (basal expression) and various lengths of hypoxia (1h, 5h, 24h) or 0.7μM statin treatment (RCC only). GAPDH was used for qPCR normalization. Protein expression is depicted relative to β-actin as a positive control.

A

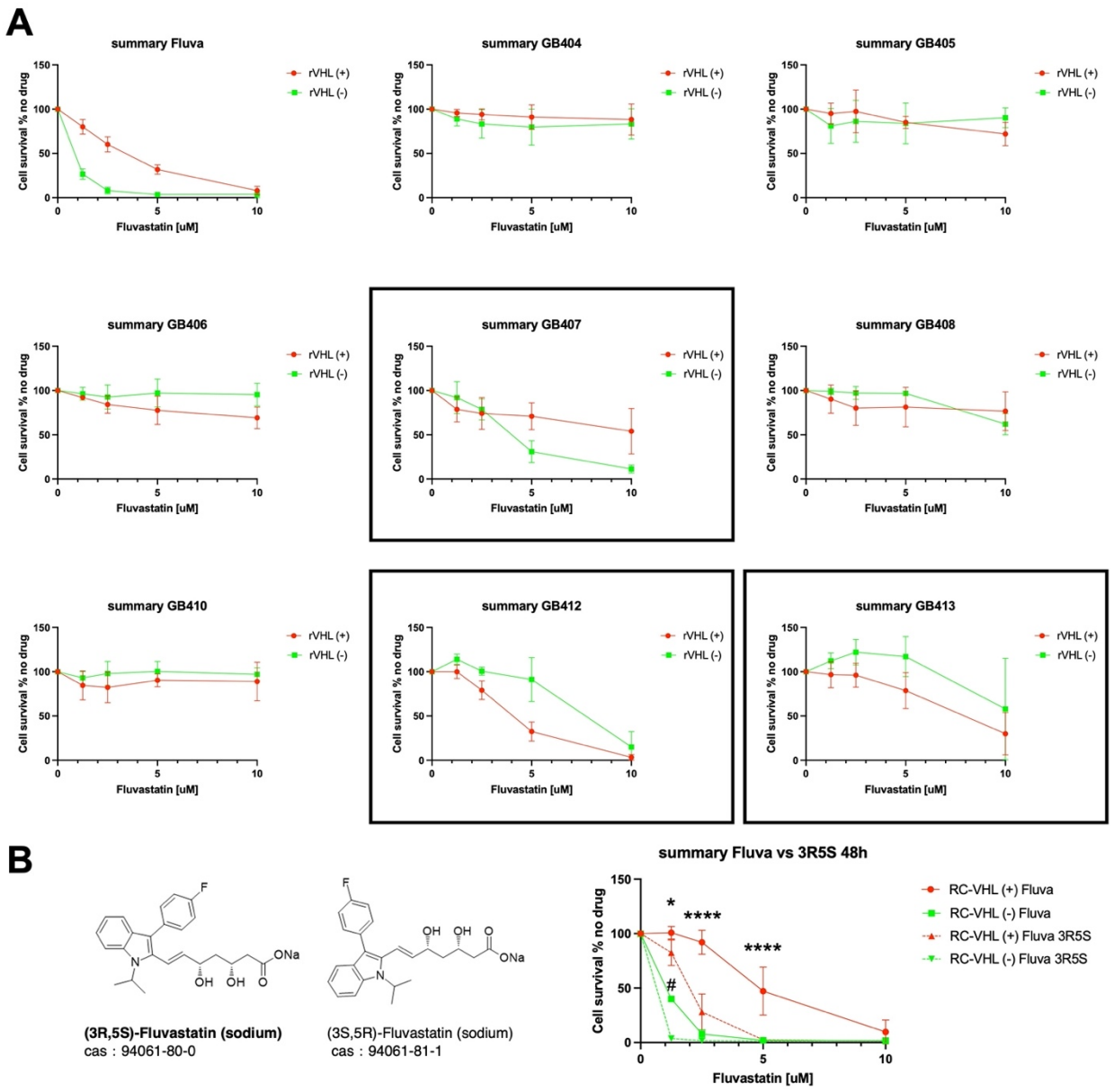
REACTOME_AUF1_HNRNP_D0_BINDS_AND_DESTABILIZES_MRNA		
REACTOME_DNA_REPLICATION_PRE_INITIATION	mcm3	
REACTOME_REGULATION_OF_MRNA_STABILITY_BY_PROTEINS_THAT_BIND_AU_RICH_ELEMENTS		
REACTOME_THE_ROLE_OF_GTSE1_IN_G2_M_PROGRESSION_AFTER_G2_CHECKPOINT		
REACTOME_MITOTIC_METAPHASE_AND_ANAPHASE	anapc5	
REACTOME_SWITCHING_OF_ORIGINS_TO_A_POST_REPLICATIVE_STATE	mcm3	
REACTOME_ORC1_REMOVAL_FROM_CHROMATIN	mcm3	
REACTOME_NERVOUS_SYSTEM_DEVELOPMENT		
REACTOME_MAPK_FAMILY_SIGNALING_CASCADES		
REACTOME_SIGNALING_BY_HEDGEHOG		
REACTOME_DEVELOPMENTAL_BIOLOGY		
REACTOME_MITOTIC_G1_PHASE_AND_G1_S_TRANSITION	mcm3	
REACTOME_RHO_GTPASE_CYCLE	vim	
REACTOME_SIGNALING_BY_RECEPTOR_TYROSINE_KINASES		
REACTOME_SELECTIVE_AUTOPHAGY	vim	
REACTOME_RHO_GTPASES_ACTIVATE_FORMINS		
REACTOME_METABOLISM_OF_NUCLEOTIDES	rrm2	rrm1
REACTOME_APOPTOSIS	vim	
REACTOME_RESOLUTION_OF_SISTER_CHROMATID_COHESION		
REACTOME_PROGRAMMED_CELL_DEATH	vim	
REACTOME_HEDGEHOG_OFF_STATE		
REACTOME_INTERFERON_SIGNALING		
REACTOME_MRNA_SPLICING	alyref	
REACTOME_G2_M_CHECKPOINTS		
REACTOME_NUCLEAR_ENVELOPE_NE_REASSEMBLY		

B

REACTOME_THE_CITRIC_ACID_TCA_CYCLE_AND_RESPIRATORY_ELECTRON_TRANS	mt-nd4							
REACTOME_RESPIRATORY_ELECTRON_TRANSPORT_ATP_SYNTHESIS_BY_CHEMIOS	mt-nd4							
REACTOME_RESPIRATORY_ELECTRON_TRANSPORT	mt-nd4							
REACTOME_METABOLISM_OF_LIPIDS	dbi	asah1	oxct1					
REACTOME_MHC_CLASS_II_ANTIGEN_PRESENTATION	ctsb							
REACTOME_TRANSPORT_TO_THE_GOLGI_AND_SUBSEQUENT_MODIFICATION	tmed7	ctsz	mia2	man2a2	tuba4a	lman1		
REACTOME_ASPARAGINE_N_LINKED_GLYCOSYLATION	tmed7	ctsz	mia2	man2a2	tuba4a	lman1	ctsa	pdia3
REACTOME_FATTY_ACID_METABOLISM	dbi							
REACTOME_NEUTROPHIL_DEGRANULATION	ctsb	asah1	gns	fth1	cat			
REACTOME_INTRA_GOLGI_AND_RETROGRADE_GOLGI_TO_ER_TRAFFIC	tmed7							
REACTOME_PHASE_II_CONJUGATION_OF_COMPOUNDS	cndp2	mgst1						
REACTOME_MEMBRANE_TRAFFICKING	myo6	scarb2	gns	fth1				
REACTOME_TRANS_GOLGI_NETWORK_VESICLE_BUDDING	fth1							
REACTOME_CELLULAR_RESPONSE_TO_CHEMICAL_STRESS	mt-co1							
REACTOME_VESICLE_MEDIATED_TRANSPORT	myo6	scarb2	gns	fth1				
REACTOME_BIOLOGICAL_OXIDATIONS	cndp2	mgst1	maoa					

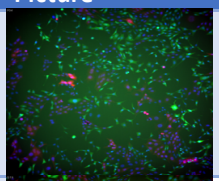
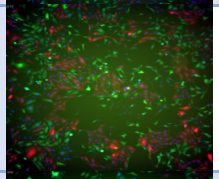
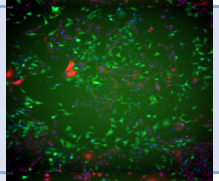
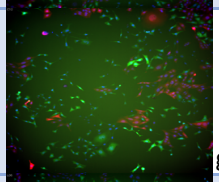
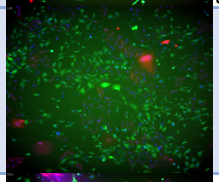
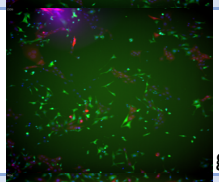
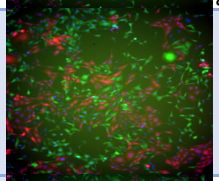
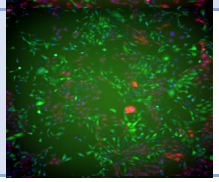
Key
missing from **trop2 vs non**
missing from **RVN vs RC**
missing from **H2 vs H12**

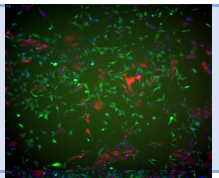
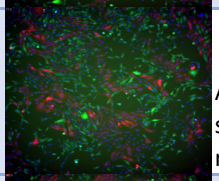
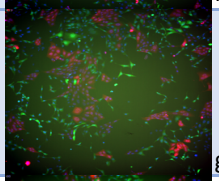
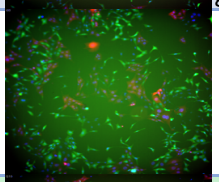
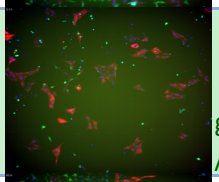
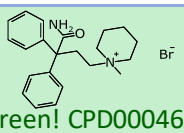
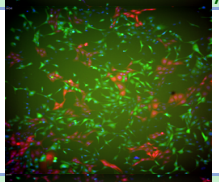
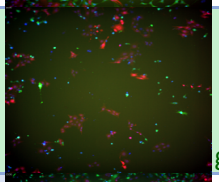
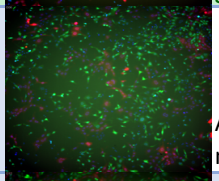
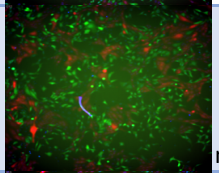
Suppl. Fig. S6 GSEA analyses with Reactome gene sets. (A) The summary table of GSEA results for four comparisons to find common pathways upregulated in the statin-sensitive lines. Genes that showed up multiple times are in blue. (B) Same as above, except for looking for downregulated pathways and genes.

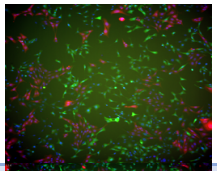
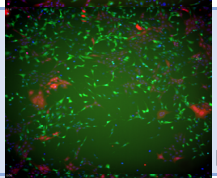
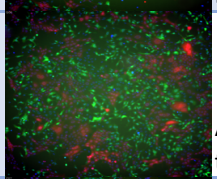
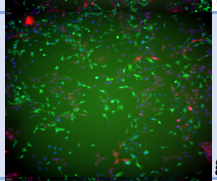
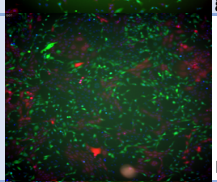
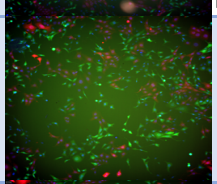
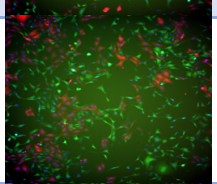
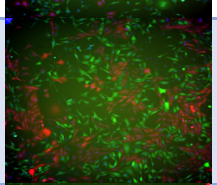
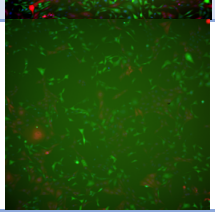


Suppl. Fig. S7 Additional cytotoxicity data of fluvastatin derivatives and enantiomers. (A) Cell survival was measured with MTS to assess the cytotoxicity of the eight fluvastatin derivatives in VHL(+) and VHL(-) cells. The boxes show the compounds with any toxicity. (B) Chemical structures of fluvastatin enantiomers (3R, 5S) and (3S, 5R) are shown. Of those, (3R, 5S)-fluvastatin was tested for its cytotoxicity against VHL(+) and VHL(-) cells by MTS at 48h and compared to racemic fluvastatin.

Suppl. Table: The HTS had dozens of compounds targeting the mevalonate pathway. Their name, target, plate & well info, and the resulting well pictures are summarized below. Green indicates potential hits.

Name	Target	Plate	Well	Picture	Toxicity
Alendronate sodium	FPP	NPW-2	P04		
Ibandronate sodium	FPP synthetase	NPW-3	G19		
Ibandronate sodium	FPP synthetase	LOPAC-4	M08		
Zoledronic acid monohydrate	FPP synthetase	LOPAC-3	C12		general
Atorvastatin	HMG-CoA reductase	NPW-4	L05		
Atorvastatin	HMG-CoA reductase	LOPAC-1	O09		general
Lesinopril(?)	HMG-CoA reductase	NPW-1	N04		
Pravastatin	HMG-CoA reductase	NPW-4	P11		

Aurothioglucose	RAC	LOPAC-3	I11		
NKIL-EHop-016	RAC	NKIL-1	P18		A was general toxicity, showing D, no effect (G also no effect)
NKIL-NSC 23766	RAC	NKIL-2	M13		green! At D, not A or G
(-)-Perillic acid	RAS	LOPAC-4	I03		
SAM001246642	RAS	LOPAC-3	G10		 green! CPD000469284 /Fenpiverinium
SAM001246643	RAS	NIHII-1	M04		
SAM001246644	RAS	NPW-2	B06		green! … Mevastatin
GSK 429286 A	Rho/Rock	NKIL-1	O06		A, maybe green (D also, but not G)
HA-1077 Fasudil	Rho/Rock	NKIL-1	O12		none, even at A

Rhodblock6	Rho/Rock	LOPAC-1	N15		
RKI-1447	Rho/Rock	NKIL-1	L14		D, maybe green (G also)
Thiazovivin	Rho/Rock	NKIL-1	G06		A, maybe green but can't tell (D also, not G)
Y27632	Rho/Rock	LOPAC-2	C07		general
Y27632	Rho/Rock	NKIL-1	G07		none, even at A
Liranaftate	Squalene	NPW-3	A16		
Naftifine hydrochloride	Squalene	NPW-4	E08		
Tolnaftate	Squalene	NPW-1	M21		
LOPAC-Sandoz 58-035	Acyl-CoA:cholesterol acyltransferase (ACAT)	LOPAC-1	K15		

4.6. REFERENCES

1. General Info - Molecular Screening Shared Resource Available online: https://mssr.cnsi.ucla.edu/general-info/ (accessed on 8 December 2023).

2. Schokrpur, S.; Hu, J.; Moughon, D.L.; Liu, P.; Lin, L.C.; Hermann, K.; Mangul, S.; Guan, W.; Pellegrini, M.; Xu, H.; et al. CRISPR-Mediated VHL Knockout Generates an Improved Model for Metastatic Renal Cell Carcinoma. *Sci Rep-uk* **2016**, *6*, 29032, doi:10.1038/srep29032.

3. Hu, J.; Schokrpur, S.; Archang, M.; Hermann, K.; Sharrow, A.C.; Khanna, P.; Novak, J.; Signoretti, S.; Bhatt, R.S.; Knudsen, B.S.; et al. A Non-Integrating Lentiviral Approach Overcomes Cas9-Induced Immune Rejection to Establish an Immunocompetent Metastatic Renal Cancer Model. *Mol Ther - Methods Clin Dev* **2018**, *9*, 203–210, doi:10.1016/j.omtm.2018.02.009.

4. Mok, S.; Koya, R.C.; Tsui, C.; Xu, J.; Robert, L.; Wu, L.; Graeber, T.G.; West, B.L.; Bollag, G.; Ribas, A. Inhibition of CSF-1 Receptor Improves the Antitumor Efficacy of Adoptive Cell Transfer Immunotherapy. *Cancer Res.* **2014**, *74*, 153–161, doi:10.1158/0008-5472.can-13-1816.

5. Koya, R.C.; Mok, S.; Comin-Anduix, B.; Chodon, T.; Radu, C.G.; Nishimura, M.I.; Witte, O.N.; Ribas, A. Kinetic Phases of Distribution and Tumor Targeting by T Cell Receptor Engineered Lymphocytes Inducing Robust Antitumor Responses. *Proc. Natl. Acad. Sci.* **2010**, *107*, 14286–14291, doi:10.1073/pnas.1008300107.

6. Hu, J.; Tan, P.; Ishihara, M.; Bayley, N.A.; Schokrpur, S.; Reynoso, J.G.; Zhang, Y.; Lim, R.J.; Dumitras, C.; Yang, L.; et al. Tumor Heterogeneity in VHL Drives Metastasis in Clear Cell Renal Cell Carcinoma. *Signal Transduct. Target. Ther.* **2023**, *8*, 155, doi:10.1038/s41392-023-01362-2.

7. Lv, X.; Li, J.; Zhang, C.; Hu, T.; Li, S.; He, S.; Yan, H.; Tan, Y.; Lei, M.; Wen, M.; et al. The Role of Hypoxia-Inducible Factors in Tumor Angiogenesis and Cell Metabolism. *Genes Dis.* **2017**, *4*, 19–24, doi:10.1016/j.gendis.2016.11.003.

8. Longo, J.; Leeuwen, J.E. van; Elbaz, M.; Branchard, E.; Penn, L.Z. Statins as Anticancer Agents in the Era of Precision Medicine. *Clin Cancer Res* **2020**, *26*, 5791–5800, doi:10.1158/1078-0432.ccr-20-1967.

9. Jiang, W.; Hu, J.-W.; He, X.-R.; Jin, W.-L.; He, X.-Y. Statins: A Repurposed Drug to Fight Cancer. *J Exp Clin Canc Res* **2021**, *40*, 241, doi:10.1186/s13046-021-02041-2.

10. Liu, C.; Chen, H.; Hu, B.; Shi, J.; Chen, Y.; Huang, K. New Insights into the Therapeutic Potentials of Statins in Cancer. *Front. Pharmacol.* **2023**, *14*, 1188926, doi:10.3389/fphar.2023.1188926.

11. Manzoni, M.; Rollini, M. Biosynthesis and Biotechnological Production of Statins by Filamentous Fungi and Application of These Cholesterol-Lowering Drugs. *Appl. Microbiol. Biotechnol.* **2002**, *58*, 555–564, doi:10.1007/s00253-002-0932-9.

12. Furberg, C.D.; Pitt, B. Withdrawal of Cerivastatin from the World Market. *Trials* **2001**, *2*, 205, doi:10.1186/cvm-2-5-205.

13. Luo, J.; Seeger, J.D.; Donneyong, M.; Gagne, J.J.; Avorn, J.; Kesselheim, A.S. Effect of Generic Competition on Atorvastatin Prescribing and Patients' Out-of-Pocket Spending. *JAMA Intern. Med.* **2016**, *176*, 1317, doi:10.1001/jamainternmed.2016.3384.

14. McTaggart, F.; Buckett, L.; Davidson, R.; Holdgate, G.; McCormick, A.; Schneck, D.; Smith, G.; Warwick, M. Preclinical and Clinical Pharmacology of Rosuvastatin, a New 3-Hydroxy- 3-Methylglutaryl Coenzyme A Reductase Inhibitor11CRESTOR Is a Trademark, the Property of AstraZeneca PLC. Research Discussed in This Article Was Supported by AstraZeneca. *Am. J. Cardiol.* **2001**, *87*, 28–32, doi:10.1016/s0002-9149(01)01454-0.

15. Thompson, J.M.; Alvarez, A.; Singha, M.K.; Pavesic, M.W.; Nguyen, Q.H.; Nelson, L.J.; Fruman, D.A.; Razorenova, O.V. Targeting the Mevalonate Pathway Suppresses VHL-Deficient CC-RCC through a HIF-Dependent Mechanism. *Mol Cancer Ther* **2018**, *17*, molcanther.1076.2017, doi:10.1158/1535-7163.mct-17-1076.

16. Holdgate, G.A.; Ward, W.H.J.; McTaggart, F. Molecular Mechanism for Inhibition of 3-Hydroxy-3-Methylglutaryl CoA (HMG-CoA) Reductase by Rosuvastatin. *Biochem. Soc. Trans.* **2003**, *31*, 528–531, doi:10.1042/bst0310528.

17. Parihar, S.P.; Guler, R.; Brombacher, F. Statins: A Viable Candidate for Host-Directed Therapy against Infectious Diseases. *Nat. Rev. Immunol.* **2019**, *19*, 104–117, doi:10.1038/s41577-018-0094-3.

18. Mullen, P.J.; Yu, R.; Longo, J.; Archer, M.C.; Penn, L.Z. The Interplay between Cell Signalling and the Mevalonate Pathway in Cancer. *Nat. Rev. Cancer* **2016**, *16*, 718–731, doi:10.1038/nrc.2016.76.

19. Warita, K.; Warita, T.; Beckwitt, C.H.; Schurdak, M.E.; Vazquez, A.; Wells, A.; Oltvai, Z.N. Statin-Induced Mevalonate Pathway Inhibition Attenuates the Growth of Mesenchymal-like Cancer Cells That Lack Functional E-Cadherin Mediated Cell Cohesion. *Sci. Rep.* **2014**, *4*, 7593, doi:10.1038/srep07593.

20. Hanahan, D. Hallmarks of Cancer: New Dimensions. *Cancer Discov.* **2022**, *12*, 31–46, doi:10.1158/2159-8290.cd-21-1059.

21. Yao, H.; He, G.; Yan, S.; Chen, C.; Song, L.; Rosol, T.J.; Deng, X. Triple-Negative Breast Cancer: Is There a Treatment on the Horizon? *Oncotarget* **2016**, *8*, 1913–1924, doi:10.18632/oncotarget.12284.

22. Yamada, Y.; Beltran, H. Clinical and Biological Features of Neuroendocrine Prostate Cancer. *Curr. Oncol. Rep.* **2021**, *23*, 15, doi:10.1007/s11912-020-01003-9.

23. Goard, C.A.; Chan-Seng-Yue, M.; Mullen, P.J.; Quiroga, A.D.; Wasylishen, A.R.; Clendening, J.W.; Sendorek, D.H.S.; Haider, S.; Lehner, R.; Boutros, P.C.; et al. Identifying Molecular Features That Distinguish Fluvastatin-Sensitive Breast Tumor Cells. *Breast Cancer Res. Treat.* **2014**, *143*, 301–312, doi:10.1007/s10549-013-2800-y.

24. O'Grady, S.; Crown, J.; Duffy, M.J. Statins Inhibit Proliferation and Induce Apoptosis in Triple-Negative Breast Cancer Cells. *Méd. Oncol. (Northwood, Lond., Engl.)* **2022**, *39*, 142, doi:10.1007/s12032-022-01733-9.

25. Brown, M.; Hart, C.; Tawadros, T.; Ramani, V.; Sangar, V.; Lau, M.; Clarke, N. The Differential Effects of Statins on the Metastatic Behaviour of Prostate Cancer. *Br. J. Cancer* **2012**, *106*, 1689–1696, doi:10.1038/bjc.2012.138.

26. Han, H.; Park, C.K.; Choi, Y.-D.; Cho, N.H.; Lee, J.; Cho, K.S. Androgen-Independent Prostate Cancer Is Sensitive to CDC42-PAK7 Kinase Inhibition. *Biomedicines* **2022**, *11*, 101, doi:10.3390/biomedicines11010101.

27. Weitz-Schmidt, G.; Welzenbach, K.; Brinkmann, V.; Kamata, T.; Kallen, J.; Bruns, C.; Cottens, S.; Takada, Y.; Hommel, U. Statins Selectively Inhibit Leukocyte Function Antigen-1 by Binding to a Novel Regulatory Integrin Site. *Nat. Med.* **2001**, *7*, 687–692, doi:10.1038/89058.

28. Walling, B.L.; Kim, M. LFA-1 in T Cell Migration and Differentiation. *Front. Immunol.* **2018**, *9*, 952, doi:10.3389/fimmu.2018.00952.

29. Korhonova, M.; Doricakova, A.; Dvorak, Z. Optical Isomers of Atorvastatin, Rosuvastatin and Fluvastatin Enantiospecifically Activate Pregnane X Receptor PXR and Induce CYP2A6, CYP2B6 and CYP3A4 in Human Hepatocytes. *PLoS ONE* **2015**, *10*, e0137720, doi:10.1371/journal.pone.0137720.

30. Fluvastatin: Uses, Interactions, Mechanism of Action | DrugBank Online Available online: https://go.drugbank.com/drugs/DB01095 (accessed on 30 November 2023).

31. Beckwitt, C.H.; Brufsky, A.; Oltvai, Z.N.; Wells, A. Statin Drugs to Reduce Breast Cancer Recurrence and Mortality. *Breast Cancer Res* **2018**, *20*, 144, doi:10.1186/s13058-018-1066-z.

32. Barbalata, C.I.; Tefas, L.R.; Achim, M.; Tomuta, I.; Porfire, A.S. Statins in Risk-Reduction and Treatment of Cancer. *World J Clin Oncol* **2020**, *11*, 573–588, doi:10.5306/wjco.v11.i8.573.

33. Thompson, J.M.; Nguyen, Q.H.; Singh, M.; Pavesic, M.W.; Nesterenko, I.; Nelson, L.J.; Liao, A.C.; Razorenova, O.V. Rho-Associated Kinase 1 Inhibition Is Synthetically Lethal with von Hippel-Lindau Deficiency in Clear Cell Renal Cell Carcinoma. *Oncogene* **2017**, *36*, 1080–1089, doi:10.1038/onc.2016.272.

34. Tsoi, J.; Robert, L.; Paraiso, K.; Galvan, C.; Sheu, K.M.; Lay, J.; Wong, D.J.L.; Atefi, M.; Shirazi, R.; Wang, X.; et al. Multi-Stage Differentiation Defines Melanoma Subtypes with Differential Vulnerability to Drug-Induced Iron-Dependent Oxidative Stress. *Cancer Cell* **2018**, *33*, 890-904.e5, doi:10.1016/j.ccell.2018.03.017.

35. Chen, C.-C.; Tran, W.; Song, K.; Sugimoto, T.; Obusan, M.B.; Wang, L.; Sheu, K.M.; Cheng, D.; Ta, L.; Varuzhanyan, G.; et al. Temporal Evolution Reveals Bifurcated Lineages in Aggressive Neuroendocrine Small Cell Prostate Cancer Trans-Differentiation. *Cancer Cell* **2023**, doi:10.1016/j.ccell.2023.10.009.

36. Prekovic, S.; Schuurman, K.; Mayayo-Peralta, I.; Manjón, A.G.; Buijs, M.; Yavuz, S.; Wellenstein, M.D.; Barrera, A.; Monkhorst, K.; Huber, A.; et al. Glucocorticoid Receptor Triggers a Reversible Drug-Tolerant Dormancy State with Acquired Therapeutic Vulnerabilities in Lung Cancer. *Nat. Commun.* **2021**, *12*, 4360, doi:10.1038/s41467-021-24537-3.

37. Khadka, S.; Druffner, S.R.; Duncan, B.C.; Busada, J.T. Glucocorticoid Regulation of Cancer Development and Progression. *Front. Endocrinol.* **2023**, *14*, 1161768, doi:10.3389/fendo.2023.1161768.

38. Pufall, M.A. Glucocorticoid Signaling, From Molecules to Mice to Man. *Adv. Exp. Med. Biol.* **2015**, *872*, 315–333, doi:10.1007/978-1-4939-2895-8_14.

39. Clarisse, D.; Bosscher, K.D. How the Glucocorticoid Receptor Contributes to Platinum-Based Therapy Resistance in Solid Cancer. *Nat. Commun.* **2021**, *12*, 4959, doi:10.1038/s41467-021-24847-6.

40. Dwyer, A.R.; Kerkvliet, C.P.; Truong, T.H.; Hagen, K.M.; Krutilina, R.I.; Parke, D.N.; Oakley, R.H.; Liddle, C.; Cidlowski, J.A.; Seagroves, T.N.; et al. Glucocorticoid Receptors Drive Breast Cancer Cell Migration and Metabolic Reprogramming via PDK4. *Endocrinology* **2023**, *164*, bqad083, doi:10.1210/endocr/bqad083.

41. Bello, E.D.; Zwergel, C.; Mai, A.; Valente, S. The Innovative Potential of Statins in Cancer: New Targets for New Therapies. *Front. Chem.* **2020**, *8*, 516, doi:10.3389/fchem.2020.00516.

42. UALCAN Available online: https://ualcan.path.uab.edu/ (accessed on 11 December 2023).

43. The Human Protein Atlas Available online: https://www.proteinatlas.org/ (accessed on 11 December 2023).

Chapter 5. Conclusion and Future Prospects

A lucid unmet need in the clinic is the lack of an effective treatment for metastatic ccRCC, primarily due to a poor understanding of the mechanism of metastasis and a lack of suitable animal models. Recently, our lab published a groundbreaking work characterizing a novel, VHL heterogeneity-mediated cooperative metastasis, where VHL(-) cancer cells are the metastatic driver and induce aggressive transformation of the VHL(+) counterparts [1]. Based on this work, this dissertation aimed to 1) establish a sustainable *in vivo* model alternative to the mouse orthotopic implantation model and 2) develop a novel small-molecule inhibitor of metastasis by targeting the metastatic driver, VHL(-) cancer cells.

For the first aim, Chapter 2 showed the usefulness of the CAM model in further verifying the novel concept of cooperative metastasis in clinical cases. We have achieved a critical objective in establishing CAM PDXs, maintaining the heterogeneity and architecture observed in patient tumors. Some preliminary results show promises in PET/CT imaging, PDX propagation in CAM, and incorporation of autologous immune cells to build even more clinically relevant models (Fig. 2.7). If successful, these humanized CAM PDXs can serve as renewable sources of tumor specimen and as an extremely valuable resource to test and personalize therapeutic strategy for ccRCC patients in the.

Chapter 3 continued to show the usefulness of CAM as a tumor model applicable to pan-tissue urological cancers. Though not included here, CAM was able to establish ovarian cancers from mouse and human origins as well [2]. An extremely interesting path to follow would be whether cooperative metastasis occurs in other tumor types. For that, CAM assays using the mixed population of LnCaP and LnCaP-trop2 are being conducted and will answer the question fairly soon. Exosomes were also shown to be an integral part of pro-metastatic intratumoral communication (Fig. 3.3). CAM helped us quickly test the hypothesis that exosomes derived from VHL(-) were enough to promote metastasis of VHL(+), even when VHL(-) cells were not present (Fig. 3.4). These findings about exosomes are all useful to deepen our understanding about cooperative metastasis and expand novel therapeutic avenues.

For the second aim (small-molecule inhibitor of metastasis), Chapter 4 illustrated many preliminary yet interesting data about statins' specific cytotoxicity against VHL(-). Fluvastatin and other effective statins were suggested to bind to a novel target that still works through the GGPP arm of the mevalonate pathway. RAS may be the key (Suppl. Table), so the geranylation of RAS in VHL(-) and VHL(+) cells with or without statin treatment would be interesting to check. MOA determination was originally planned with high-throughput cDNA library screening, which can efficiently and comprehensively accelerate the determination process. However, VHL(-) cells were unsuitable for transfection with extremely low efficiency (Fig. 5A). This caused extra labor and time to create new cell lines from human kidney cancer cell lines. #18 patient line had a little better transfection efficiency, but it was still low at 3%, far below sufficient for the cDNA screening requiring at least 60% (Fig. 5B, C). We are currently investigating ways to improve the transfection efficiency, but meanwhile, we took a low throughput but more targeted approach.

Though out of the scope of this dissertation, the HTS revealed compounds with interesting characteristics other than green-killing, such as red-killing, yellow dots, general toxicity, and general growth (Suppl. Fig. S3A). STITCH analyses of these compounds may suggest important pathways to follow up (Fig. 5D). In addition to the FDA-approved drug library of 2,530 compounds, HTS was also run on a much bigger library of 185,571 compounds, including lead-like and unique UCLA libraries. Data has not been mined yet, except for the NKIL (kinase) libraries, due to the data size and a lack of a comprehensive image analysis scheme (Fig. 5E). Optimization of image analysis will take place soon to utilize the unused screening results.

One thing to highlight from both aims is that our approach can be applied to multiple cancer types. As our colleagues recently suggested, tumors develop from normal cells to early-, transitional-, and eventually late-stage along a shared lineage trajectory, termed transdifferentiation [3–5]. Fluvastatin, simvastatin, and pitavastatin work on VHL(-) RCC, TNBC, and NEPC, all highly aggressive and difficult to treat tumors. Therefore, finding a common, targetable vulnerability of these tumors through the MOA study will have an even bigger impact and imply the possibility of a metastasis inhibitor effective across different aggressive tumor types.

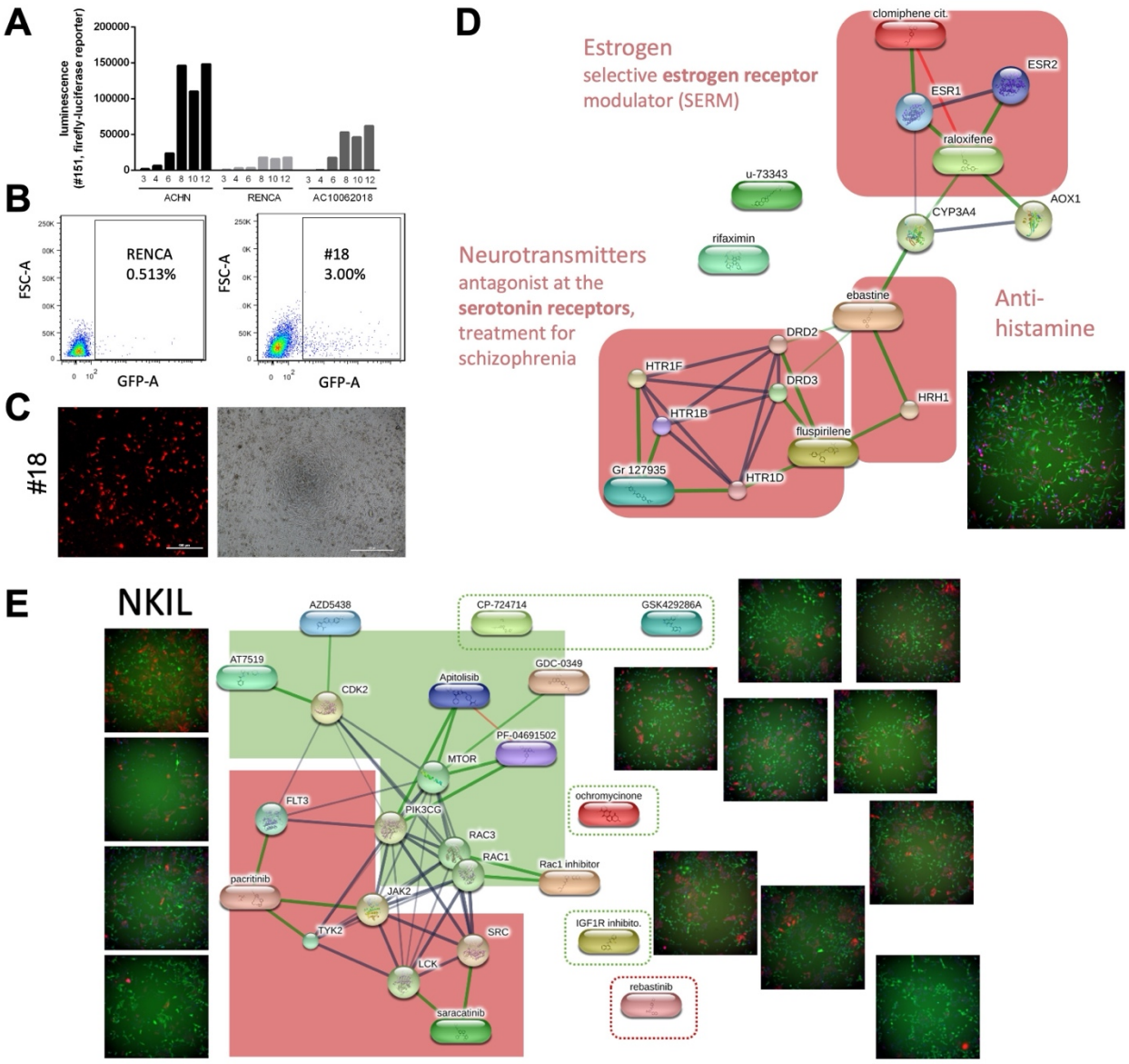


Fig. 5 Future directions. (A-C) Transfection efficiency was tested using luciferase assay (A), flow cytometry (B), and fluorescent microscope (C). (D-E) STITCH pathway analysis and representative images of VHL(+)-specific inhibitors from the repurposing libraries (D) and VHL(-)/VHL(+) inhibitors from NKIL libraries included in the expanded screening (E).

REFERENCES

1. Hu, J.; Tan, P.; Ishihara, M.; Bayley, N.A.; Schokrpur, S.; Reynoso, J.G.; Zhang, Y.; Lim, R.J.; Dumitras, C.; Yang, L.; et al. Tumor Heterogeneity in VHL Drives Metastasis in Clear Cell Renal Cell Carcinoma. *Signal Transduct. Target. Ther.* **2023**, *8*, 155, doi:10.1038/s41392-023-01362-2.

2. Sharrow, A.C.; Ishihara, M.; Hu, J.; Kim, I.H.; Wu, L. Using the Chicken Chorioallantoic Membrane In Vivo Model to Study Gynecological and Urological Cancers. *J. Vis. Exp.* **2020**, doi:10.3791/60651.

3. Park, J.W.; Lee, J.K.; Sheu, K.M.; Wang, L.; Balanis, N.G.; Nguyen, K.; Smith, B.A.; Cheng, C.; Tsai, B.L.; Cheng, D.; et al. Reprogramming Normal Human Epithelial Tissues to a Common, Lethal Neuroendocrine Cancer Lineage. *Science* **2018**, *362*, 91–95, doi:10.1126/science.aat5749.

4. Tsoi, J.; Robert, L.; Paraiso, K.; Galvan, C.; Sheu, K.M.; Lay, J.; Wong, D.J.L.; Atefi, M.; Shirazi, R.; Wang, X.; et al. Multi-Stage Differentiation Defines Melanoma Subtypes with Differential Vulnerability to Drug-Induced Iron-Dependent Oxidative Stress. *Cancer Cell* **2018**, *33*, 890-904.e5, doi:10.1016/j.ccell.2018.03.017.

5. Chen, C.-C.; Tran, W.; Song, K.; Sugimoto, T.; Obusan, M.B.; Wang, L.; Sheu, K.M.; Cheng, D.; Ta, L.; Varuzhanyan, G.; et al. Temporal Evolution Reveals Bifurcated Lineages in Aggressive Neuroendocrine Small Cell Prostate Cancer Trans-Differentiation. *Cancer Cell* **2023**, doi:10.1016/j.ccell.2023.10.009.